UNIVERSITÉ DE MONTRÉAL

CONDUCTING POLYMERS AND NATURAL MOLECULAR MATERIALS FOR BIOELECTRONICS AND ENERGY STORAGE

PRAJWAL KUMAR

DÉPARTEMENT DE GÉNIE CHIMIQUE

ÉCOLE POLYTECHNIQUE DE MONTRÉAL

THÈSE PRÉSENTÉE EN VUE DE L'OBTENTION

DU DIPLÔME DE PHILOSOPHIAE DOCTOR

(GÉNIE CHIMIQUE)

DÉCEMBRE 2016

UNIVERSITÉ DE MONTRÉAL

ÉCOLE POLYTECHNIQUE DE MONTRÉAL

Cette thèse intitulée:

CONDUCTING POLYMERS AND NATURAL MOLECULAR MATERIALS FOR BIOELECTRONICS AND ENERGY STORAGE

présentée par : KUMAR Prajwal

en vue de l'obtention du diplôme de : Philosophiae Doctor

a été dûment acceptée par le jury d'examen constitué de :

M. BUSCHMANN Michael, Ph. D., président

M. CICOIRA Fabio, Ph. D., membre et directeur de recherche

Mme SANTATO Clara, Doctorat, membre et codirectrice de recherche

M. KÉNA-COHEN Stéphane, Ph. D., membre

M. CHAN Julian, Ph. D., membre externe

ACKNOWLEDGEMENTS

I am grateful for all the support and guidance I have received over the last 4 years at Polytechnique Montreal. First and foremost, I am immensely grateful to my advisor, Fabio Cicoira, for giving me the opportunity to work in his research group. Without your continuous support and encouragement, Fabio, it would have not been possible to reach this stage. It was truly a pleasure to work with you. I am very thankful to my co-supervisor Clara Santato, not only for her research advices but also for her moral support. Her patience and laboratory space were invaluable. My next acknowledgement goes to a visiting professor, specializes in the field of electrochemistry, Dr Francesca Soavi. I am indebted for her guidance, which helped me to improve the knowledge of electrochemistry. I am grateful to Dr. Alessandro Pezzella for the time spent together during his visit to our laboratory and demonstration of his vast experience of melanin synthesis. I gratefully acknowledge funding from Natural Sciences and Engineering Research Council of Canada (NSERC) and the Groupe de Recherche en Sciences et Technologies Biomédicales (GRSTB). My special gratitude goes to Daniel Pilon, Christophe Clément, Alireza H. Mesgar, Yves Drolet, Francis Boutet, Marie-Hélène Bernier, Robert Delisle and Josianne Lefebvre for their technical assistance during four years. Throughout all the time I spent at Polytechnique Montreal, my friends and colleagues helped me to build such a memorable and enjoyable experience. I have to mention many, especially Irina, Shiming, Gaia, Zhihui, Fanny, Guido, Xiang, Eduardo, Tian, Xu, Elizabeth, Hao, Jonathan, Julia, Dilek, Francis, Frédéric, Colleen, Tania, Samik, Laurie, Amel, Dominic, Arvindh, Sampath, Suchakra, Tanushree, Gabriel, Mengjiao, Xinhe, Xiaojie. It was pleasure to work with you. Also thanks to Polytechnique Montreal for academic and administrative services.

Finally, through all this I have had the unflagging support of my family: my mom and dad, Niriksha my sister and my brothers. Thank you for making me smiling, laughing and relaxed.

RÉSUMÉ

La découverte de la conduction électronique dans les matériaux organiques, dans les années 70, est à l'origine du développement des technologies optoélectroniques organiques. La remarquable propriété que présentent les semiconducteurs organiques de conduire les ions, en plus des porteurs de charge électroniques, a permis l'émergence d'un nouveau domaine de l'optoélectronique organique, c'est à dire la bioélectronique. La bioélectronique organique ouvre de nouvelles opportunités d'interface entre l'électronique organique et la biologie, avec la promesse d'applications dans des domaines aussi variés que les biocapteurs, la livraison de médicament, l'enregistrement et la stimulation neural. Combiner un transport ionique et électronique dans les semiconducteurs organiques utilisés pour les transistors représente une tentative intéressante pour parvenir à des dispositifs bioélectroniques efficaces. Ces dispositifs opèrent à faible polarisation de l'électrode de grille, grâce à la formation d'une double couche électrique au niveau de l'interface électrode/électrolyte. Les capacitances de double couches résultantes ont des valeurs qui dépassent de plusieurs ordres de grandeurs celles typiques des interfaces métal/diélectrique, en raison de la faible épaisseur (ca. 3nm) des doubles couches électriques. Par conséquent, les capacitances de double couche peuvent mener à de plus fortes modulations en courant pour des différences de potentiel de grille plus faibles (~1 V), compatibles avec les milieux aqueux.

Le cœur de cette thèse de doctorat est dévoué à une meilleure compréhension des mécanismes d'opération d'une classe importante de dispositifs bioélectroniques organiques, c'est-à-dire les transistors électrochimiques organiques (OECTs), dans le but d'optimiser leurs performances et de concevoir de nouveaux dispositifs bioélectroniques. Les OECTs sont formés d'un canal en polymère conducteur ainsi que d'une électrode de grille mis en contact avec le canal au travers d'un électrolyte. L'application d'une différence de potentiel électrique au niveau de la grille entraîne l'inclusion d'ions de l'électrolyte à l'intérieur de la couche mince en polymère en qui changent sa conducitvité initiale. Dans cette thèse, nous nous sommes concentrés sur le poly(3,4-éthylènedioxythiophène) dopé avec du poly(styrène sulfonate) (PEDOT:PSS) en tant que matériau actif dans le canal de OECTs.

Nous avons utilisé différentes épaisseurs de canal ainsi que deux électrolytes différents : le bromure de cétyltriméthyl-ammonium (CTAB), un surfactant apte à former des micelles, et du

NaCl. Les rapports ON/OFF les plus élevés ont été obtenus pour de transistors utilisant de faibles épaisseurs (~ 50 nm) de la couche mince et le CTAB comme électrolyte. La voltammétrie cyclique suggère qu'une réaction rédox entre les molécules d'oxygène dissoutes dans l'électrolyte et le PEDOT:PSS mène à de faibles ratios ON/OFF quand le NaCl est utilisé comme électrolyte. La voltammétrie cyclique et la spectroscopie d'impédance électrochimique révèlent que le dopage/dédopage du canal devient plus lent à des épaisseurs relativement élevés de la couche mince et en présence d'ions de plus grande taille.

Les caractéristiques de l'électrode de grille ont des effets significatifs sur le comportement des OECTs. Dans cette thèse, du carbone activé (AC) avec une importante surface spécifique a été utilisé comme matériau pour l'électrode de grille dans les OECTs basés sur le PEDOT:PSS. L'utilisation d'électrodes de grille en AC de grande surface, a mené à une importante modulation en courant drain-source dans les OECTs et à la limitation des réactions électrochimiques indésirables.

La biocompatibilité et la biodégradabilité des matériaux utilisés en bioélectronique organique sont essentiels. Ces propriétés sont importantes même pour des dispositifs alimentant les dispositifs bioélectroniques. La mélanine est un biopigment abondant en nature et doté d'activité redox. Ce biopigment peut être mis en forme à température ambiante et est donc un matériau extrêmement intéressant pour le développement de dispositifs de stockage de l'énergie biocompatibles et « verts ». L'eumélanine est une des formes de la mélanine qui est particulièrement étudiée par les chercheurs en science de matériaux. Celle-ci se retrouve dans de nombreuses parties du corps humain, dont la peau, les cheveux, l'oreille interne et le cerveau. L'eumélanine réalise de nombreuses fonctions dans le corps humain comme l'absorption dans une large bande du spectre UV-visible ou encore la chélation métallique. Dans cette thèse, nous rapportons les propriétés de stockage d'énergie électrochimique de la part d'électrodes basées sur l'eumélanine, en configuration supercondensateur. L'eumélanine est formée de monomères faits de 5,6-dihydroxyindole (DHI) et d'acide 5,6-dihydroxyindole carboxylique (DHICA), présents sous différentes formes redox (hydroxyquinone, semiquinone et quinone). La synergie entre l'activité redox des monomères et la capacité de plusieurs de leurs fonctionnalités à lier des cations de façon réversible permet l'utilisation de l'eumélanine dans des dispositifs de stockage

d'énergie fonctionnant en mode pseudocapacitif. En partant de la démonstration des supercondensateurs basés sur l'eumélanine, nous avons utilisé une approche non-conventionnelle pour fabriquer des micro-condensateurs flexibles sur substrats plastiques.

ABSTRACT

The discovery of electronic conduction in carbon-based materials, in the 1970s, is the basis of the development of organic optoelectronics technologies. The remarkable property of organic semiconductors to conduct ions, in addition to electronic charge carriers, has recently offered a new emerging direction in organic optoelectronics, called organic bioelectronics. Organic bioelectronics opens the opportunity to interface organic electronics with biology with promising applications such as biosensing, drug delivery, neural recording and stimulation. Combining ionic and electronic transport in organic semiconductors into transistor architectures represents an interesting attempt to achieve efficient bioelectronics devices. These devices operate at low gate biases, due to the formation of electrical double layers at electrode/electrolyte interfaces. The resultant double layer capacitances are a few orders of magnitude higher compared to capacitances typical of metal/dielectric interfaces, due to the low thickness (ca. 3 nm) of the electrical double layers, which consequently leads to higher current modulations at lower gate voltage (~1 V).

The core of this Ph.D. thesis is devoted to a better understanding of the operational mechanism of an important class of organic bioelectronics devices, i.e. organic electrochemical transistors (OECTs), to optimize their performance and to design novel bioelectronics devices. OECTs consist of a conducting polymer channel and a gate electrode in contact with an electrolyte. The application of a gate electrical bias triggers the inclusion of electrolyte ions into the polymer film thus changing its initial conductivity. In this thesis we focus on poly(3,4-ethylenedioxythiophene) doped with polystyrenesulfonate (PEDOT:PSS) as the active material in OECTs.

We employed various channel thicknesses and two different electrolytes: the micelle-forming surfactant cetyltrimethyl ammonium bromide (CTAB) and NaCl. The highest transistor ON/OFF ratios were achieved at low film thicknesses (~ 50 nm), using CTAB as the electrolyte. Cyclic voltammetry suggested that a redox reaction between molecular oxygen dissolved in the electrolytes and PEDOT:PSS leads to low ON/OFF ratios when NaCl was used as the electrolyte. Cyclic voltammetry and electrochemical impedance spectroscopy revealed that doping/dedoping of the channel becomes slower at relatively high film thickness and in the presence of bulky ions.

The characteristics of the gate electrode have significant effects on the behavior of OECTs. In this thesis, high specific surface area activated carbon (AC) was used as gate electrode material in

OECTs based PEDOT:PSS. The use of high surface area carbon gate electrodes led to the high drain-source current modulation in OECT and limited undesirable electrochemical processes.

The biocompatibility and biodegradability property of the materials used in organic bioelectronics is of course of primary importance. These features are important even for devices powering the bioelectronics devices. Melanin is a redox active biopigment abundant in nature. The biopigment can be processed at room temperature and, as such, it is an extremely attractive material for environmentally and human friendly energy storage solutions. A form of melanin highly investigated by materials scientists is eumelanin, found in many parts of the human body including skin, hair, inner ear and brain. Eumelanin has many functions in the human body, such as strong broad-band UV-visible absorption and metal chelation. In this thesis, we report the ion storage property of eumelanin-based electrodes assembled in supercapacitors. Eumelanin is based on 5,6-dihydroxyindole (DHI) and 5,6-dihydroxyindole carboxylic acid (DHICA) building blocks, present in different redox forms (hydroxyquinone, semiquinone and quinone). The synergy between the redox activity of the building blocks and the capability of several of their functionalities to reversibly bind cations constitutes the foundation for the use of melanin in pseudocapacitive energy storage systems. Capitalizing on the demonstration of eumelanin-based supercapacitors, we used an unconventional patterning approach to fabricate binder-free flexible micro-supercapacitors on plastic substrates.

TABLE OF CONTENTS

LIST OF TABLES

LIST OF FIGURES

LIST OF SYMBOLS

AC	Activated carbons
ADH	Alcohol dehydrogenase
Al	Aluminum
Ag	Silver
AgCl	Silver chloride
Ar	Argon
Au	Gold
CE	Counter electrode
CMC	Critical micellar concentration
CTAB	cetyltrimethylammonium bromide
D	Drain
DBSA	Dodecyl benzene sulfonic acid
EG	Electrolyte-gated
EG-OFET	Electrolyte gated field effect transistors
EIS	Electrochemical Impedance Spectroscopy
FET	Field-effect transistor
GO_x	Glucose oxidase
H_2O_2	Hydrogen peroxide
IL	Ionic liquid
KCl	Potassium chloride
NaCl	Sodium chloride
OECTs	Organic electrochemical transistors
OFETs	Organic field-effect transistors
OLEDs	Organic light-emitting diodes
OTFTs	Organic thin-film transistors
P3HT	Poly(3-hexylthiophene)
PBS	Phosphate-buffered saline
PDMS	Poly(dimethylsiloxane)

PEDOT:PSS	Poly(3,4-ethylenedioxythiophene):polystyrenesulfonate
PET	Polyethylene terephthalate
PLGA	Poly(L-lactide-co-glycolide)
PSS	Polystyrenesulfonate
Pt	Platinum
RE	Reference electrode
RIE	Reactive ion etching
S	Source
WE	Working electrode

LIST OF ABBREVIATIONS

A_{ch}	Channel area
A_g	Gate area
c_{ch}	Channel capacitance per unit area
c_g	Gate capacitance per unit area
C	Capacitance
D	Thickness or distance between electrodes
e^-	Electron
E	Stored energy
G	Conductance of the channel
I	Drain-source current at $V_g \neq 0$ V
I_0	Drain-source current at $V_g = 0$ V
I_{ds}	Source-drain current
I_{on}	ON-state current
I_{off}	OFF-state current
I_{gs}	Gate-source current
l	Drift length
L	Length
M^+	Cations
P	Power
t	Time
u	Drift velocity
V_{cell}	Cell voltage
V_{ds}	Drain-source voltage
V_{gs}	Gate-source voltage
V_{sol}	Solution voltage
W	Width

LIST OF APPENDICES

CHAPTER 1 INTRODUCTION

This chapter constitutes an overview of organic electronics (OE) materials and devices, with particular attention given to organic bioelectronics and supercapacitors based on organic polymers. The chapter includes the identification of the scientific problems studied in the thesis as well as its general and specific objectives and motivation.

1.1 Overview

The history of organic electronics begins with the discovery of conducting polymers in 1976, by Heeger, MacDiarmid, and Shirakawa, who were awarded the Nobel Prize in Chemistry in 2000.[1] The discovery that π-conjugated organic molecules and polymers can be electrically conductive generate a great deal of enthusiasm in the scientific community and led to the rise of organic electronics.[2,3]

Organic semiconductors have captured the interest of the research community because of their unique properties, such as electro- and photoluminescence, ease of processing by several techniques (e.g. evaporation, spin coating, printing) and compatibility with a variety of substrates, including mechanically flexible ones. In 1987, Tang et al. demonstrated Tris-(8-hydroxyquinoline) aluminum (Alq_3) based organic electroluminescent diodes.[4] In 1989, R. Friend's group demonstrated the successful use of poly(p-phenylene vinylene) (PPV) for efficient electroluminescent devices.[5] The first organic transistor was fabricated with polythiophene semiconducting thin films.[6] Since then, tremendous developments have taken place in organic electronics for a variety of applications, such as organic light-emitting diodes (OLED), organic field-effect transistors (OFET), and organic photovoltaics (OPV).[4,5,7-13] Some organic electronics products have been on the market for more than a decade. In 1997, Pioneer Corporation released the first commercial OLED product, a passive matrix OLED (PMOLED) display for car audio displays. A decade later, in 2007, Samsung Mobile Display released the first commercial active matrix OLED (AMOLED) display. Although various prototypes of white OLEDs for lighting have been demonstrated over the years, it was not until 2010 that OSRAM Opto Semiconductor released the first commercial white OLED lighting panel. Heliatek has been

commercializing OPV since 2006. Organic transistors find application in backplanes for flexible displays currently developed by Plastic Logic.[14]

1.2 π - conjugated systems

The polymer polyethylene, where each carbon is bonded to two carbons and to two hydrogen atoms through four sigma (σ) bonds, is an insulator (Figure 1.1). On the other hand, polyacetylene, which contains alternating single (σ) and double (σ and π) carbon-carbon bonds, shows a certain electrical conductivity. This sequence of alternating σ and π bonds is called conjugation. Each carbon atom in the backbone of a conjugated polymer is sp^2 hybridized. When polymerization of acetylene occurs, the singly occupied 2s orbital and two of the three singly occupied 2p orbitals ($2p_x$ and $2p_y$) of the carbon atom combine and form three sp^2 hybrid orbitals with equal energy. (Figure 1.2) These three hybridized orbitals are capable to form σ bonds to three neighboring atoms. The electrons involved in these bonds are strongly localized. The remaining $2p_z$ orbital is located perpendicularly to the plan of the three sp^2 hybrid orbitals. When the $2p_z$ orbitals of two adjacent carbon atoms overlap sideways, they combine leading to two molecular orbitals: one π (bonding) and one π* (anti-bonding) orbital. The π bonding molecular orbital is lower energy than the atomic orbitals and anti-bonding π* molecular orbital is higher energy than the atomic orbitals. The energy difference between the highest occupied molecular orbital (HOMO) of π-orbital and the lowest unoccupied molecular orbital (LUMO) of π* orbital is known as energy gap or band gap. In a conjugated polymer containing *n* sp^2 hybridized carbon atoms, there are a total of *n* $2p_z$ atomic orbitals that combine to create *n* molecular orbitals. The π electrons are delocalized along the entire backbone and the polymer can be seen as a one-dimensional metal. This means that the electrons in the π-bonds can be found between any of the carbon atoms and can thus move along the polymer chain. The delocalization of the π-electrons along the carbon backbone is the key to enable facile charge carrier transport within the polymer chain, thus making the polymer conductive.

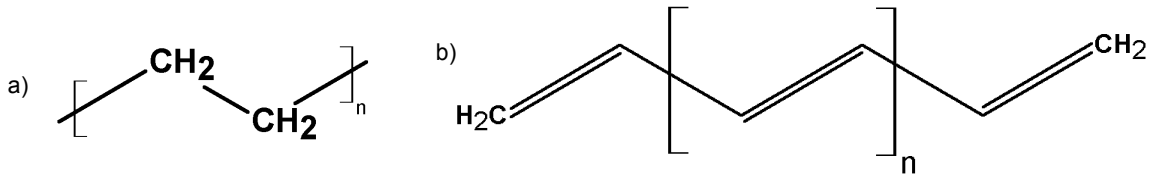

Figure 1.1 Chemical structure of a) polyethylene and b) polyacetylene.

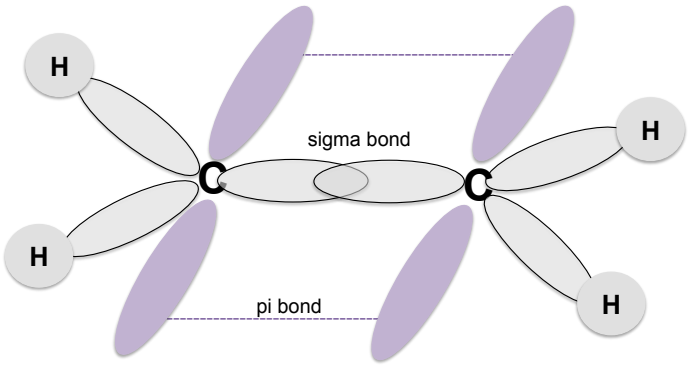

Figure 1.2 Schematic representation of sp^2 hybridized orbitals of ethylene molecule. The sp^2 hybrid orbitals are shown in light gray color, and the non hybridized p_z orbitals in light violet. The p_z orbitals extend in and out of the plane of the molecule.

A low concentration of mobile charge carriers characterizes conjugated organic polymers in their intrinsic state. However, the electrical behavior of these materials can go from insulating to semiconducting and conducting. Highly-conducting polymers can be achieved by chemical doping, e.g. by chemical oxidation or reduction. For example, when polyacetylene is oxidized by AsF_5, the conductivity increases from 10^{-5} S/cm to 200 S cm^{-1}.[1,5,16]

1.3 Organic electronic materials

Organic semiconductors can be of two types: conjugated polymers and conjugated small-molecules. On the other hand, conjugated polymers showing metallic conductivity are known as conducting polymers. Several semiconducting and conducting polymers, such as polythiophenes (Figure 1.3a), have excellent solubility in a variety of organic solvents, therefore thin films can be readily prepared by spin coating, dip-coating, drop-casting, screen printing, or inkjet printing. Small-molecule organic semiconductors can be soluble or insoluble in common organic solvents.

Insoluble small-molecule organic semiconductors are often deposited by thermal evaporation. The most common examples of organic small-molecule semiconductors deposited by thermal evaporation are pentacene, sexithiophene and phthalocyanines (Figure 1.4). In most cases, thin films of small-molecule organic semiconductors have a polycrystalline structure and are characterized by polymorphism.

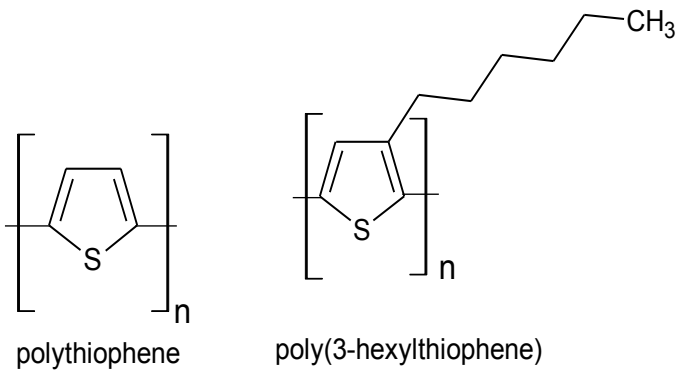

Figure 1.3 Molecular structure of two relevant conjugated polymers in organic electronics.[9] Reprinted with permission. Copyright © 2010, Royal Society of Chemistry.

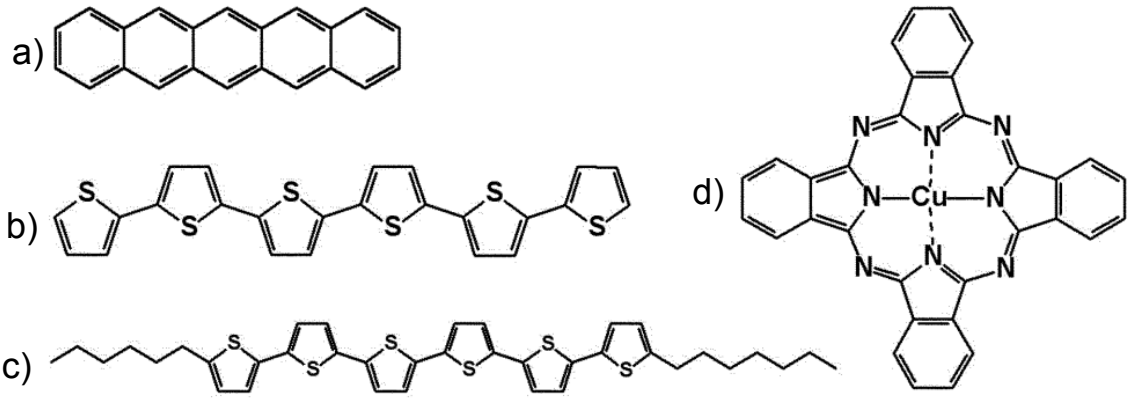

Figure 1.4 Molecular structure of relevant conjugated small-molecule organic semiconductors. (a) Pentacene. (b) Sexithiophene (6T). (c) Dihexylsexithiophene (DH6T, Hex-6T-Hex). (d) Copper phthalocyanine.[9] Reprinted with permission. Copyright © 2010, Royal Society of Chemistry.

The bandgap of organic semiconductors can be tailored by controlling the conjugation length. The longer the extension of the conjugation in the molecule, the smaller is the energy gap between the levels associated to the HOMO and LUMO of the molecule. The strength of the intermolecular π-π stacking interactions establishes the width of the bands (such that from molecular energy levels, energy bands will form for the material), in turn strongly affecting the efficiency of charge carrier transport. The most commonly used conjugated polymers are polyaniline, polypyrrole, polycarbazole, polythiophene, and their derivatives, with applications covering a broad spectrum of optoelectronics solutions as well as chemical and biological sensing (Figure 1.5).

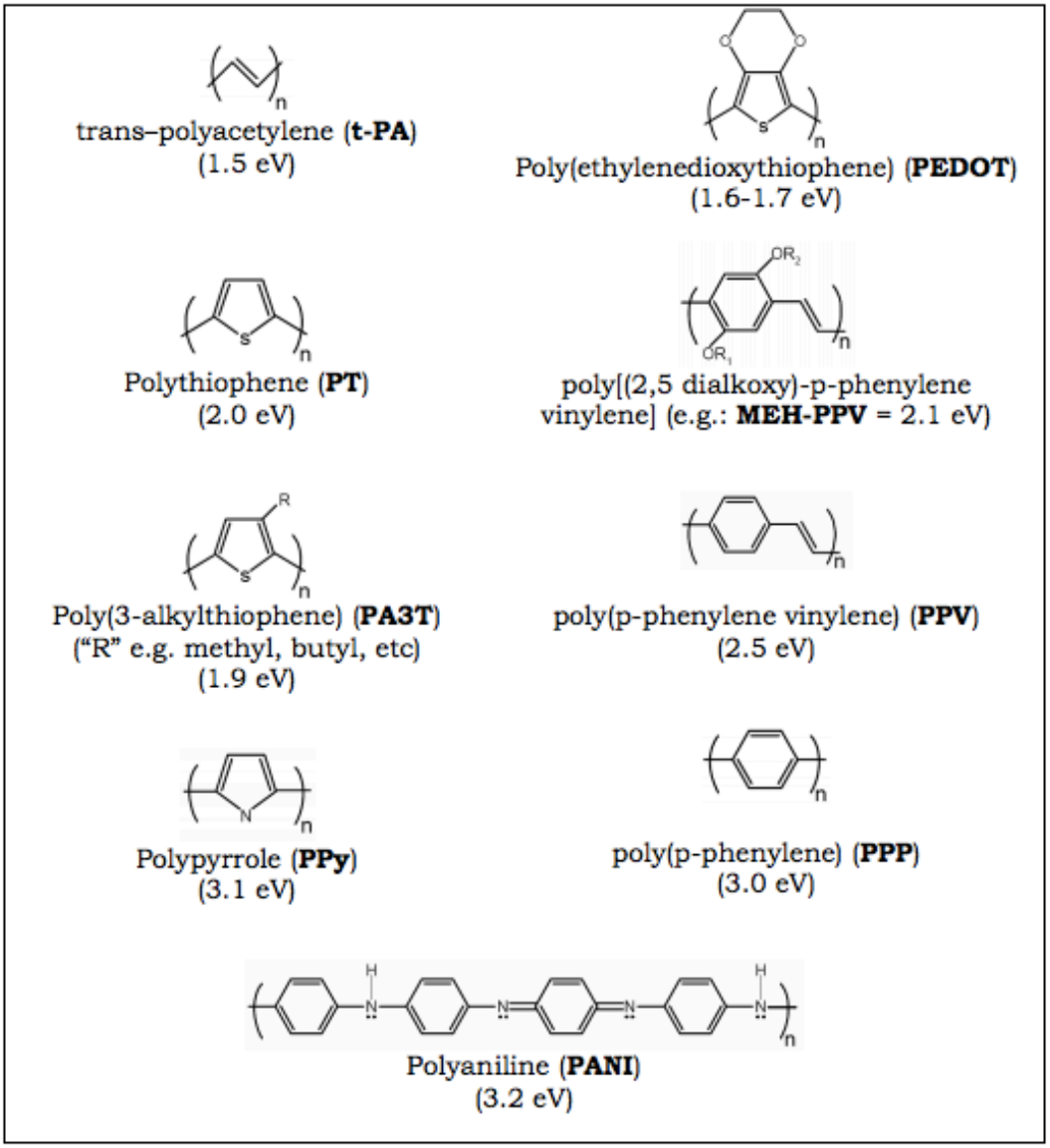

Figure 1.5 The molecular structure of a few technologically relevant conjugated polymers and their electronic band gap.[17]

1.4 Organic electronics devices

1.4.1 Organic light-emitting diodes (OLEDs)

OLED constitute an exciting solution for emissive display technologies and solid state lighting.[18,19] The main advantages of these electroluminescent devices are: low power consumption, fast switching speed and color tunability.

The phenomenon of light generation by electrical excitation was first discovered in anthracene single crystals in the 1960s.[20] In 1987, C.W. Tang and S.V. Slyke developed the first OLED at Eastman Kodak.[21] In 1990 R. Friend's group at Cambridge developed a poly(*p*-phenlenevinylene) (PPV) based OLED.[5] The light emission was in the green-yellow part of the spectrum and the efficiency of about 0.05%. After this early work, there has been increasing research activity in the field of OLED. Enormous progress has been made in the improvement of color gamut, luminescence efficiency and device reliability, mainly motivated by the use of this technology in displays.

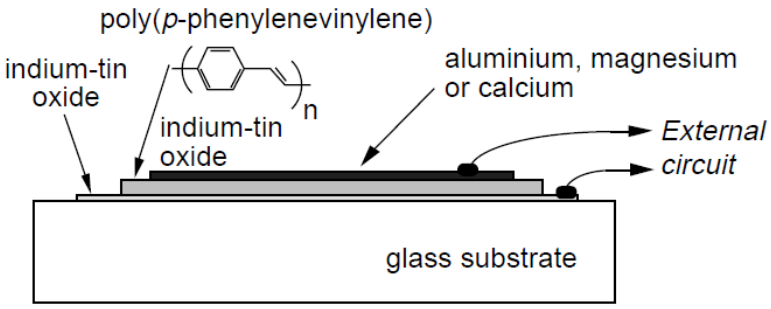

Figure 1.6 Structure of one of the first reported single-layer organic light-emitting diode.[5] Reprinted with permission. Copyright © 1999, Rights Managed by Nature Publishing Group.

An OLED consists of one or more semiconducting organic thin films sandwiched between two electrodes, one of which must be transparent to extract the light. (Figure 1.6) Indium tin oxide (ITO) is commonly utilized as the transparent anode, and a low work function metal (for example Al, Mg) is utilized as the cathode (to inject the electrons). OLEDs are typically fabricated by sequentially depositing organic thin films onto the transparent substrate and the metal cathode, the latter by evaporation through a shadow-mask. The organic films can have several functions in

addition to emission, such as facilitating hole and electron injection (injection layers) and transport (transport layers). As an example, in the case of a three-layer OLED structure, hole and electron transport layers are used to facilitate charge transport from the electrodes to the emissive layer. By applying a positive potential to the anode (forward bias), the injection of holes occurs from the anode into the HOMO of hole transport layer, while electrons are injected from the cathode into the LUMO. The holes or electrons can cross the heterojunction interface to form electron-hole pairs (excitons) in the emissive layer. These excitons can decay radiatively or non-radiatively. The radiative decay leads to electroluminescence.

1.4.2 Organic photovoltaics

Photovoltaic devices convert sunlight into electricity. The photovoltaic effect was discovered in 1839 by Becquerel.[22] In 1883, Fritts developed the first solar cell, based on selenium.[23] In 1954, Chaplin et al. from Bell Laboratories found that silicon doped with certain impurities was sensitive to light.[24] Since then, there have been rapid advances in the power conversion efficiency and reliability of solar cells, including those based on organic semiconductors.

The structure of organic solar cells comprises the active layer, which consists of an electron donor and an electron acceptor, typically a polymer blend, sandwiched between two electrodes (Figure 1.7a).[25] The working mechanism of an organic solar cell involves the following steps: i) capture of photons, which leads to the formation of electron-hole pairs (excitons) of donor and acceptor films, ii) the excitons diffuse to the donor/ acceptor (D/A) interface, 3) carriers (electrons and holes) are generated by the exciton dissociation at the D/A interface, and 4) electrons and holes are moved to and collected at the cathode and anode which generates a current flowing to an external circuit (Figure 1.7c).

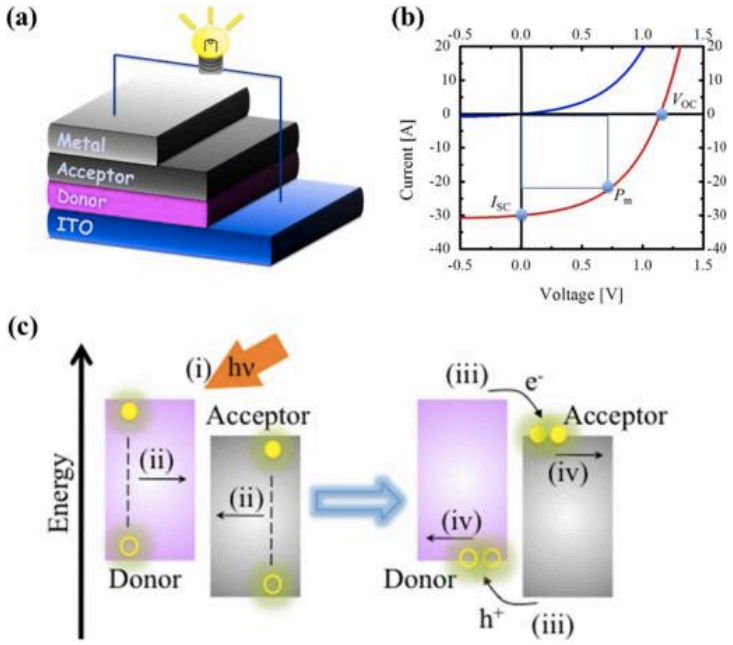

Figure 1.7 Schematic illustration of an OPV cell (a) I–V characteristics of a PV cell under dark (blue) and illumination (red) conditions (b) Schematic illustration of photocurrent generation processes for the OPV cells (c) [25] Reprinted with permission. Copyright © 2013 by Sou Ryuzaki and Jun Onoe.

The power conversion efficiency of a photovoltaic device (η) is defined as the ratio of the maximum electrical power (P_m) to the incident optical power (P_0), and η can be calculated from the following equations:

$$\eta = \frac{P_m}{P_0} = \frac{I_{sc}\, V_{oc}\, FF}{P_0} \times 100$$

where, I_{SC}, V_{OC}, and are, respectively, the short-circuit current, the open-circuit voltage (Figure1.7 b). FF is the fill factor is defined as

$$FF = \frac{P_m}{I_{sc}\, V_{oc}}$$

1.4.3 Organic thin film transistors

Since the invention of the transistor by J. Bardeen, W. Brattain and W. Shockley at Bell Laboratories in Murray Hill in 1947, integrated circuits based on silicon transistors have

dramatically impacted our society. Many efforts have been made to improve the scaling by shrinking the transistors size. In 1965 G. Moore, (co-founder of Intel) predicted the number of transistors on a single chip to double every year (Moore's law).[26] He redefined his view in 1975, predicting that doubling would occur approximately every two years. Nowadays it is believed that, almost after 50 years, the Moore's law is reaching its saturation limit. However, Intel's quad-core chips, the third-generation Core i7 found in Mac and Windows PCs, has 1.4 billion transistors on a surface area of 160 square millimeter. Even if the silicon technology continues to revolutionize our world, other materials and technologies (for instance super-thin sheets of carbon graphene, organic electronics) are being developed to introduce new functionalities such as compatibility with flexible substrates and low temperature processing, that silicon chips cannot offer.

Organic transistors have been intensively investigated during the past three decades.[27] [9] Thin films of conjugated organic polymers or small-molecules are used as channel materials. The gate dielectric separates the semiconductor channel from the gate electrode (Figure 1.8), which is used to switch the transistor ''on'' and ''off''. A modulation of the charge carrier density in the transistor channel takes place upon the application of an electrical bias at the gate. An electrical bias applied between the metal source and drain contacts controls the electric current in the transistor channel.

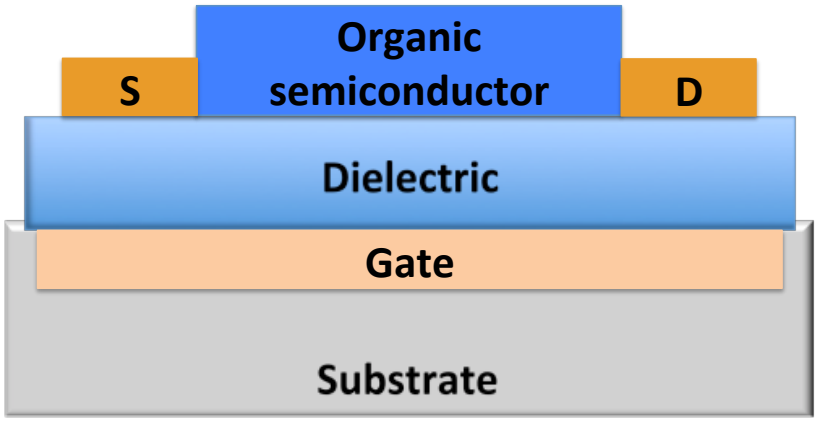

Figure 1.8 Schematic representation of an organic transistor.

Depending on the organic semiconducting material used as the channel material, the majority charge carriers can either be electrons (n-type material) or holes (p-type material). The charge

carrier mobility is one of the parameters used to benchmark the performance of transistors. In the last three decades, the mobility of both p and n-type transistors, based both on small-molecule and polymeric semiconductors, has improved by several orders of magnitude (1-10 cm^2/Vs) (Figure 1.9).[9]

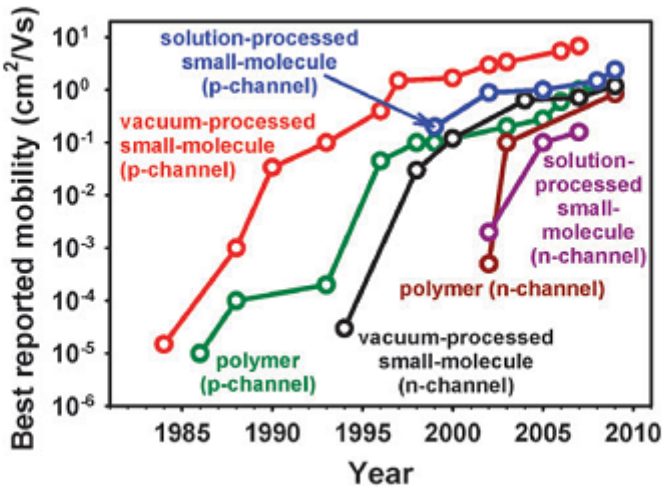

Figure 1.9 Charge carrier mobility of p-channel and n-channel transistors based on small-molecule and polymeric semiconductors. [9] Reprinted with permission. Copyright © 2010, Royal Society of Chemistry.

Organic transistors can be used as sensors. Transistor-based sensors have many attractive features such as high sensitivity and the possibility to be miniaturized by lithographic techniques. The lower temperature of processing (sometimes as low as room temperature) as compared to silicon-based transistors permits to fabricate transistors on flexible polymeric substrates and even on paper. These advantages present the opportunity of low cost fabrication for large area devices such as foldable high-resolution color displays and electronic functionalities on surfaces of arbitrary shape.[9,28]

In an alternative device structure, an electronically insulating but ionically conducting electrolyte replaces the gate dielectric. The resulting device is known as electrolyte-gated transistor (Figure 1.9).[29,30] Electrolyte-gated (EG) transistors were first proposed in the 1950s.[31] In EG transistors, the application of a gate bias leads to the formation of an electrical double layer at the electrolyte/organic semiconductor interface.[32] The thin electrical double layer (few

nanometers) leads to a high capacitance (~10-20 μF/cm^2) according the equation, $C = \frac{\varepsilon A}{D}$ where ε is the permittivity, A is area of the electrode and D is the thickness of the double layer. Therefore, these transistors can be operated at low voltage (<2 V). EG transistors based on metal oxides, conducting polymers, organic semiconductors and carbon nanomaterials have been reported. EG transistors are studied for many different applications, especially in bioelectronics, drug delivery and diagnostics.[33-40]

Since conducting polymers and polycrystalline organic semiconductors cannot be considered completely impermeable to ions, current modulation in EG transistors can actually result from two gating (doping) mechanisms: electrostatic and electrochemical. To understand these mechanisms, we can adopt, initially, a simplified picture of an electrolyte included between two electrodes. When an electrical bias is applied between two electrodes immersed into an electrolyte, electrolyte ions move toward electrodes of opposite charge, driven by the electric field. For a transistor working under an electrostatic regime, with an applied gate bias, an electric double layer forms at the interface between the electrolyte and the channel. The corresponding devices are known as EG organic field-effect transistor (EG-OFET). By application of a gate voltage (V_{gs}), EDL form at the interfaces between the gate and the electrolyte and also between the electrolyte and the channel (Figure 1.10b). This is the electrostatic mechanism. On the other hand, if the ions permeate the channel, an electrochemical dedoping/doping process takes place. This is the electrochemical mechanism of doping. The corresponding devices are known as organic electrochemical transistors (OECT) (Figure 1.10c).

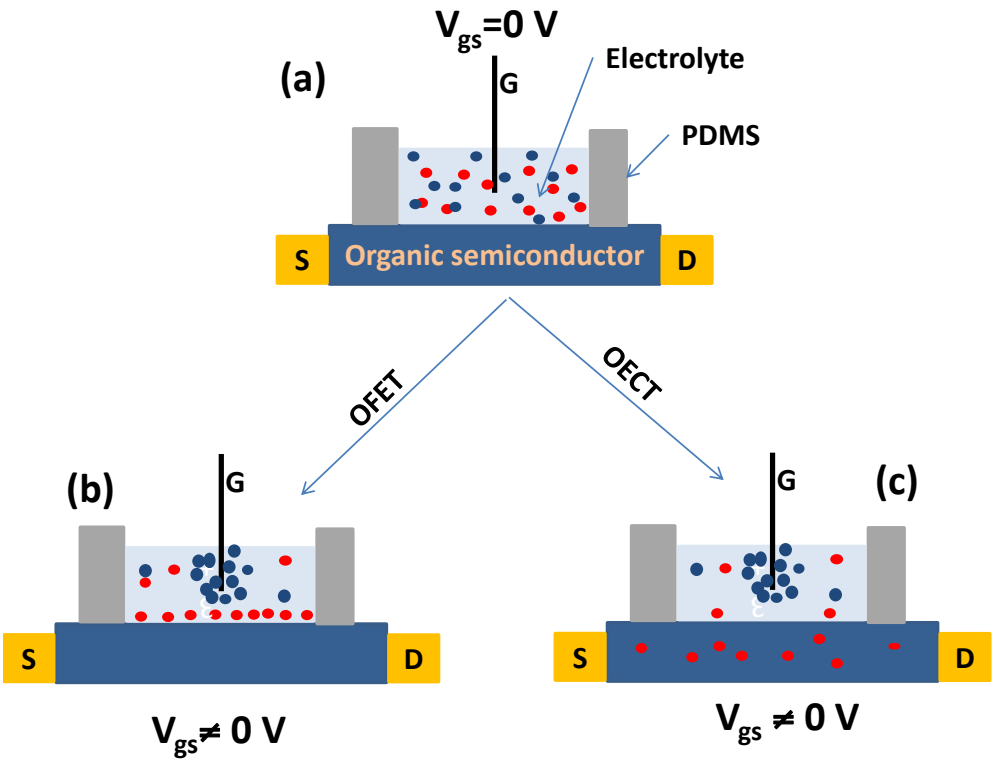

Figure 1.10 Schematic representation of EG transistors and their subcategories, depending on the working mechanism (on the left the mechanism of doping is electrostatic, on the right it is electrochemical).

EG transistors (as all transistor types) can work in accumulation (or enhancement) or depletion mode. Transistors working in accumulation mode are in their OFF state (no or low current flowing between source and drain) when a gate bias (V_{gs}) is not applied and are turned ON upon application of a gate voltage. Transistors working in depletion mode are in the ON state in absence of a gate bias applied and are turned OFF upon application of a gate bias. For a p-type channel working in accumulation mode, upon application of a negative V_{gs}, holes are accumulated in the channel, due to the approach of anions at the interface between the electrolyte and the channel or the intercalation of anions into the channel. For p-type EG transistors working in depletion mode, by application of a positive V_{gs}, cations dedope the channel, decreasing the hole density in the polymer. An analogous behavior (with opposite polarities of the electrical biases applied to the electrodes) is expected for n-type channels.

1.5 Organic bioelectronic devices

Bioelectronics is defined as the study and application of electronics in medicine and biology.[41] Bioelectronics involves interaction between electronic components (for example transistors and electrodes) and biological components such as enzymes, antibodies etc. as well as monitoring of bio-electric signals (e.g. heartbeat, brain or muscular activity). Bioelectronics devices such as biosensors and bioelectrodes have several applications in biological, chemical, health care, and environmental monitoring.[39,42-46]

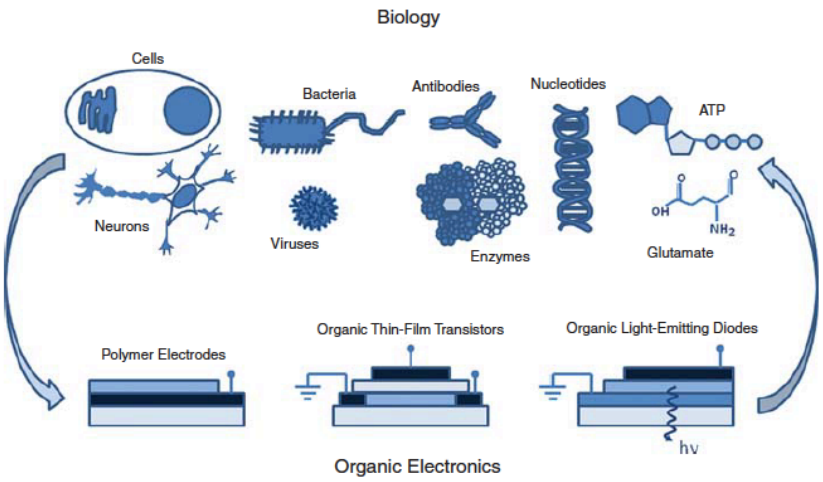

Figure 1.11 Organic bioelectronics: biological moieties, including cells, micro-organisms, proteins, oligonucleotides, and small molecules, can be interfaced with organic electronics devices to yield biosensors, medical diagnostics, tools for biomedical research, and bioelectronic implants that will have a major impact in health care [41]. Reprinted with permission. Copyright © Materials Research Society 2010.

The scope of organic bioelectronics is shown in the schematics (Figure 1.11). Typical recognition elements (analytes) studied in biosensors are: enzymes, nucleic acids, antibodies, whole cells, and receptors collected from blood, urine, saliva, cell culture, food samples, and environmental samples. Transducers and bioreceptors are the main components of the biosensors. Bioreceptors are specific molecules/chemicals, to which the analyte specifically binds. Transducers are devices that translate the specific bioevents into measurable signals.

1.6 Supercapacitors

Supercapacitors (SCs) are promising energy storage devices, since they feature long cycling life, high power density, long shelf life.[47] SCs, also known as electrical double layer capacitors (EDLCs) or ultracapacitors, are intermediate to batteries and pure capacitors. SCs store more energy than capacitors, less energy than batteries, but deliver energy more rapidly than batteries and in a slower manner than capacitors. SCs were discovered in the early 1950s, during experiments on fuel cells and secondary batteries using porous carbon as the electrodes, and were patented in 1957.[48] Initially, SCs employed electrodes in sandwich configuration. Activated carbon coated on aluminum foil was the electrode material (the same for both electrodes), a porous separator was present between them and the electrolyte was liquid or solid. The Japanese company NEC Corporation first commercialized supercapacitors in 1971. At that time, SCs only had limited applications and were mainly used as back-up power supplies for volatile clock chips or computer memories.[49] The capacitance of first-generation SCs was mainly hampered by large internal equivalent series resistance (ESR), owing to the low conductivity of the electrodes and electrolytes. These problems were basically solved with improved electrode materials and the electrolytes by the 1980s. SCs were first used for military applications requiring high power density.[50] During the period from 1975 to 1981, B. E. Conway developed SCs using ruthenium oxide (RuOx) as electrode material.[51,52] This material can store electrostatic charges by the formation of electrical double layers and also generates a kind of “pseudocapacitance”. This means that reversible redox reactions involving electrosorption or intercalation take place at the electrode/electrolyte interface. Sulfuric acid was used as the electrolyte to ensure high specific capacitance (> 700 F/g) and low internal resistance.

The downsizing of SCs into micron scale can enable novel applications in autonomous, wireless microsensors and microelectronics. Photolithography can be used effectively to fabricate micro-supercapacitors (μSCs) in a planar, on-chip geometry. The energy storage and the devices to be powered can be integrated on a single chip, improving scalability and reducing cost.

Based on the working mechanism, supercapacitors are classified into: (i) electrical double layer capacitors (EDLC), in which the electrostatic charge accumulates between the electrode surface and the electrolyte interface, (ii) pseudocapacitors, where fast and reversible redox reactions (Faradaic processes) occur at the electrodes, and (iii) hybrid capacitors in which both processes

take place in a single device.

For EDLC, the capacitance is defined as:

$$C = \frac{\varepsilon_0 \varepsilon_r A}{D}$$

where ε_0 is the permittivity of free space, ε_r is the dielectric constant of the electrolyte, A is the specific surface area of the electrode and D is the distance between the two electrodes. During charging/discharging of supercapacitors, a double layer forms at each of the two electrodes/electrolyte interfaces, so that the system can be treated as two capacitors connected in a series. (Figure 1.12) The cell capacitance (C_{cell}) of a capacitor can be calculated according to:

$$\frac{1}{C_{cell}} = \frac{1}{C_{anode}} + \frac{1}{C_{cathode}}$$

where C_{anode} and $C_{cathode}$ represent the capacitance of the positive and negative electrode, respectively.

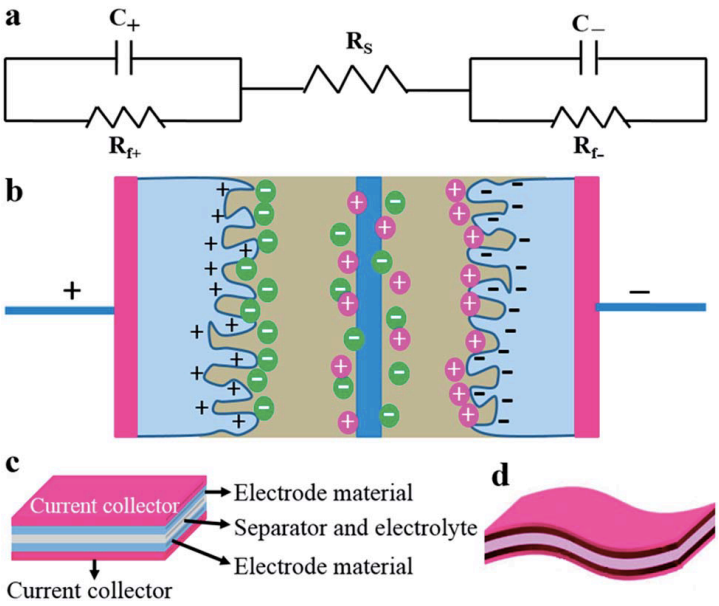

Figure 1.12 (a) Equivalent circuit model for an electrochemical capacitor; b) Schematic representation of a two-electrode supercapacitor; (c) Schematic illustrations of the typical structure of a conventional supercapacitor (d) and its flexible counterpart.[53] Reprinted with permission. Copyright © 2014, Royal Society of Chemistry.

In the case of a symmetric device (with similar anode and cathode electrodes), the capacitance of the complete cell is half of the capacitance of each individual electrode. The specific capacitance of a supercapacitor cell can be calculated by cyclic voltammetry (CV), from the charge integrated from a cyclic voltammogram according to equation:

$$C_{cell} = \frac{Q}{2mV} = \frac{1}{2mV\nu}\int_{V_-}^{V_+} I(V)dV$$

where C_{cell} is the specific capacitance of the cell (F/g), Q is the total charge (C), m (g) is the mass of the active materials in each electrode, ν is the scan rate (V/s), and V_+ and V_- are the electrochemical potentials of the positive and negative electrodes. For the galvanostatic charge discharge (GCD) method, the cell capacitance of a supercapacitor can be calculated from the charge–discharge curves from the following equation:

$$C_{cell} = \frac{I}{mdV/dt}$$

where I is the discharge current, m is the total mass of the active materials in the two electrodes and dV/dt is the slope of the discharge curve. The specific energy density (E, in Wh/kg) can be calculated according to:

$$E = \frac{I}{3600m}\int V.dt$$

The average specific power density (P, expressed in W/ kg) during discharge can be deduced from the specific energy density:

$$P = \frac{E}{\Delta t}$$

The maximum energy (E_{max}, in Wh/ kg) can be calculated according to:

$$E_{max} = \frac{1}{2}C_{cell}V^2$$

where V is the cell voltage or the cut-off voltage. The maximum power (P_{max}, in W/kg) of a supercapacitor is:

$$P_{max} = \frac{V^2}{4\times ESR}$$

where the equivalent series resistance (ESR) is $ESR = \frac{\Delta V}{2I}$, with ΔV the initial drop in voltage upon switching from charging to discharging.

1.7 Problem identification

OECT have attracted much interest for sensing and bioelectronics. However, the operating mechanism of an OECT, depending on doping/dedoping of the conducting polymer channel, is still under investigation. Hence, one of the key points in OECT research is to gain insight on the key parameters affecting the mechanism behind their operation.

Electroactive materials easily available from natural sources and biocompatible are particularly attractive for applications in bioelectronics. Melanin-based biopigments are a broad class of redox-active biopolymers found in living organisms. They are composed of macromolecular aggregates, mostly resembling polymer networks. Melanin-based biopigments exhibit unique optoelectronic properties including efficient photon–phonon conversion, mixed ionic-electronic conduction, redox activity, free radical scavenging, and cation chelation.[54-56] However, the structure-electroactivity relationships of melanin are still largely undiscovered.

1.8 General Objectives

The general objective of this Ph.D. thesis is the design, fabrication, and characterization of PEDOT:PSS organic electrochemical transistors and melanin supercapacitors.

For OECT, a better understanding of the doping/dedoping mechanism will pave the way to novel bioelectronics devices. Important issues that I addressed on OECTs are: i) the effect of the thickness of the channel on OECT modulation, ii) the influence of electrolyte ions on OECT modulation, iii) the influence of atmospheric oxygen on the performance of OECT and iv) influence of the gate material on the OECT performance.

To demonstrate proof of principles of melanin-based devices, I fabricated and characterized flexible melanin-based energy storage devices exploiting the redox activity and the proton transport properties of melanin. Besides the possible technological applications, this investigation

is expected to shed light on structure-electroactivity properties in biocompatible natural materials, well beyond the specific case of melanin.

1.8.1 Motivation

OECTs based on PEDOT:PSS show excellent electrochemical stability and reversibility and are therefore good candidates for applications at the interface with biology. Studying OECT requires a multidisciplinary approach, which includes knowledge in disciplines such as chemistry, device physics and biology.

Shedding light on their fundamental properties, in particular structural and electrochemical, is the premise to use natural materials, featuring desirable properties such as biocompatibility and biodegradability, for OECT or energy storage technological applications.

1.8.2 Specific objectives

To achieve the main objective, the following specific objectives need to be achieved:

I. Exploring the effect of the thickness of the channel of OECT on the device response.

Current modulation in OECT, unlike in field-effect transistors (where the doping is electrostatic and not electrochemical), involves the bulk of the polymer film, rather than the film/dielectric interfaces. Therefore it is important to understand how the thickness of the PEDOT:PSS channel affects the device characteristics. The goal of this study has been to find out how the current modulation varies for thin and thick films. This will shed light into the relationship between thickness of the active material and ON/OFF current ratio. To achieve this objective, we investigated the effect of the PEDOT:PSS channel thickness on OECT modulation using two different electrolytes: the cationic surfactant hexadecyltrimethylammonium bromide, also known as cetyltrimethylammonium bromide (CTAB), and NaCl. We employed cyclic voltammetry (CV) and electrochemical impedance spectroscopy (EIS) to gain insight into the impact of channel thickness, nature of the electrolyte and atmospheric oxygen on device performance.

II. Electrochemical study of the biomacromolecule melanin for application in supercapacitors

The synergy between the redox activity of the building blocks of melanin and the capability of several of their functionalities to reversibly bind electrolyte ions, constitutes the foundation for the use of melanin in pseudocapacitive energy storage systems. The goal of this work, has been to

exploit the energy storage properties of melanin in supercapacitor configuration. Our supercapacitors used melanin on carbon paper electrodes and aqueous electrolytes. Once the supercapacitors behavior was demonstrated, capitalizing on these results, we used an unconventional patterning approach to fabricate binder-free flexible micro-supercapacitors on plastic substrates. This study revealed that melanin can be an extremely attractive material for environmentally and human friendly energy storage solutions, because of its biocompatibility and biodegradability, combined with large availability and room temperature processing.

III. Conducting Polymer Transistors Making Use of Activated Carbon Gate Electrodes

The specific surface area of gate electrodes has an important effect on the performance of OECT, both on the transistor modulation and the gate electrical bias. We introduced the high surface activated carbon (AC) as the gate electrode for OECT. We investigated the performance of OECT based on PEDOT:PSS using AC gate electrodes.

1.9 Organization of the work

This thesis is organized into eight Chapters. Chapter 1 includes an overview of the topics related to the subjects (organic electronics, organic transistors, conducting polymers, organic bioelectronics, supercapacitors), problem identification and objectives of the thesis. Chapter 2 introduces conducting polymers (in particular PEDOT:PSS), the general working mechanism of OECT, a literature survey of OECT, energy storage property of melanin-based supercapacitors. Chapters 3 and 4 correspond to two articles (articles 1 and 2) of which I was the first author. Chapter 5 contains excerpts of an article where two of my colleagues and I contributed equally as first authors (article 3). Chapter 6 is about the “electrochemistry of melanin”.

Article 1: Effect of channel thickness, electrolyte ions, and dissolved oxygen on the performance of organic electrochemical transistors (Published in Applied Physics Letters).

Article 2: Melanin-based flexible supercapacitors (Published in the Journal of Materials Chemistry C).

Excerpts from Article 3: Conducting Polymer Transistors Making Use of Activated Carbon Gate Electrodes (Shared first author article) (Published in ACS Applied Materials and Interfaces).

The following paragraphs describe how these articles contribute to the objectives of the thesis.

In article 1, we investigated the device characteristics of OECT based on thin films of PEDOT:PSS. We employed various channel thicknesses and two different electrolytes: the micelle forming surfactant cetyltrimethyl ammonium bromide (CTAB) and NaCl. The highest ON/OFF ratios were achieved at low film thicknesses using CTAB as the electrolyte. Cyclic voltammetry suggests that a redox reaction between oxygen dissolved in the electrolytes and PEDOT:PSS leads to low ON/OFF ratios, mostly when NaCl is used as the electrolyte. From cyclic voltammetry and electrochemical impedance spectroscopy reveals that doping/ dedoping of the channel becomes slower at high film thickness and in the presence of bulky ions. Article 1 has been published in Applied Physics Letters (2015, 107, 053303(1)- 053303(5)).

In article 2, we used the pseudocapacitive properties of melanin for energy storage systems. We demonstrated supercapacitors and flexible micro-supercapacitors making use of electrodes based on the biocompatible and biodegradable pigment melanin, working in aqueous electrolytes. Melanin-based supercapacitor electrodes are fabricated at room temperature, by easy solution processing, without the need of a high-temperature treatment, unlike the large majority of supercapacitors based on biopolymer-derived electrodes reported to date. In slightly acidic media, a gravimetric specific capacitance as high as 167 F/g was observed for melanin-based electrodes on carbon paper. Further, we demonstrated a binder-free micro-supercapacitor fabricated on flexible polyethylene terephthalate (PET). The microfabrication was performed by unconventional lithography based on ParyleneC patterning. Our flexible micro-supercapacitors showed a power density of 5.24 mW/cm^2 and a specific capacitance of 10.8 F/g.

Article 3 is a shared first author article. My contribution to this article has been included in the thesis. The characteristics of the gate electrode have significant effects on the behavior of OECT, which are intensively investigated for the applications in the booming field of organic bioelectronics. In this work, high specific surface area activated carbon (AC) was used as gate electrode material in OECT based on the conducting polymer PEDOT:PSS. We found that the high specific capacitance of the AC gate electrodes leads to high drain-source current modulation in OECT at low voltage, compared to PEDOT:PSS gate electrodes of comparable geometric area. Article 2 has been published in ACS Applied Materials and Interfaces (2015, 7, 969−973).

Chapter 6 reveals about electrochemistry of eumelanin. In this chapter my research contribution to the electrochemistry of eumelanin are discussed by considering the coauthored articles and supplementary information of Chapter 4.

Chapter 7 is about “General Discussion”. In this chapter some of the similarities and disparities between PEDOT:PSS and melanin molecules were discussed. Also, my research contribution to further understanding of these two molecules was emphasized.

Finally, conclusions are drawn and perspectives on future work are given (Chapter 8).

CHAPTER 2 BIOELECTRONIC MATERIALS, DEVICES AND LITERATURE REVIEW

2.1 PEDOT

Poly(3,4-ethylenedioxythiophene) (PEDOT) was synthesized by Bayer AG in 1988 and today is one of the mostly used conducting polymers (Figure 2.1).[57-59] The reasons behind the widespread use of PEDOT are commercial availability, ease of process, high conductivity, good physical and chemical stability in air, thermal stability, excellent electrochemical stability in the oxidized state and optical transparency in visible region.[58-61]

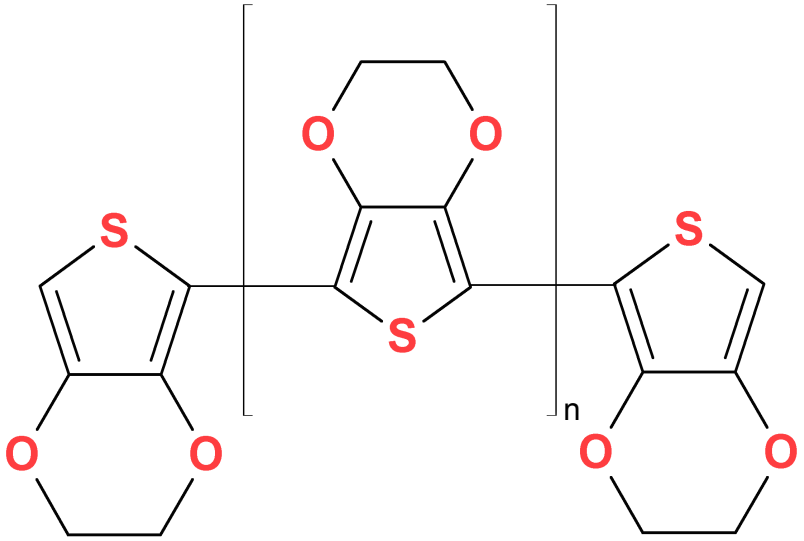

Figure 2.1 Molecular structure of poly(3,4-ethylenedioxythiophene) (PEDOT).

PEDOT and various of its derivatives are used in organic electronics as hole transport layers in OPV, electrodes in LED, transistors and light-emitting electrochemical cells and as channel material in electrochemical transistors. In energy-related applications, PEDOT is used as electrode material for supercapacitors and electrochromic component in “smart” windows and battery (modification of sulphur cathodes in lithium –sulphur batteries).[62-65] Other uses include coatings with anti-static and corrosion protection functions (Figure 2.2).[59,66]

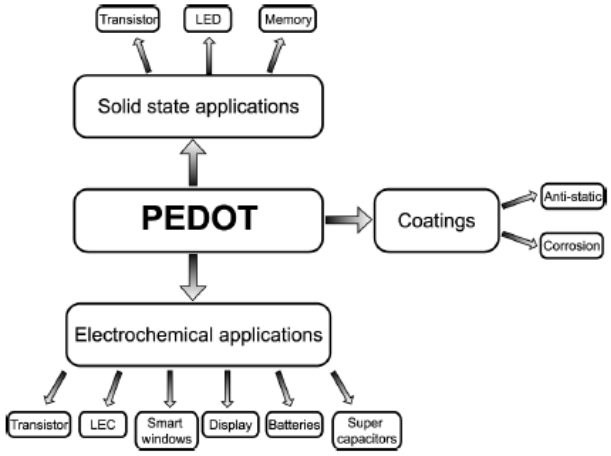

Figure 2.2 Schematic representation of various applications of PEDOT.[67]

PEDOT can be chemically synthesized by the oxidation of the ethylenedioxythiophene monomer (EDOT) in the presence of iron (III) salts as oxidizing agent. The dark blue precipitate of PEDOT in its native state is insoluble in many common solvents and unstable, due to rapid aerial oxidation. The most versatile form of PEDOT for film processing is a polyelectrolyte complex consisting of polymeric cationic PEDOT and a polymeric counter anion.

2.1.1 PEDOT:PSS

The most frequently used counter-ion for PEDOT is polystyrenesulfonic acid (PSS) because PEDOT:PSS forms a stable suspensions in water (Figure 2.3). In an aqueous PEDOT:PSS dispersion, the number of holes on the $PEDOT^{+}$ chains are compensated by polystyrenesulfonate (PSS^{-}) anions on the PSS chains.

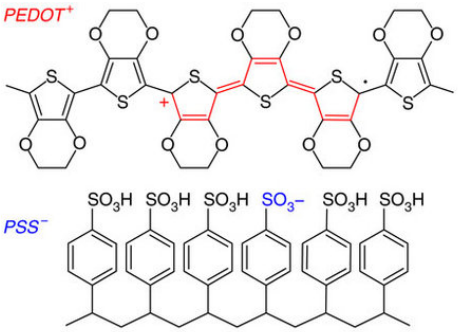

Figure 2.3 Molecular structure of PEDOT:PSS. A hole is indicated on the PEDOT chain in red, in the form of a positive polaron. The acceptor on the PSS chain is indicated in blue.[68] Reprinted with permission. Copyright © 2013, Rights Managed by Nature Publishing group.

PEDOT:PSS dispersions are stable under ambient conditions and can be processed with a wide range of techniques, such as spin casting, doctor blade, spray deposition, inkjet printing and screen printing. PEDOT:PSS has a low band gap of 1.6-1.7 eV; it absorbs strongly in the red part of the visible spectrum, resulting in a deep blue color, which can be gradually modulated by switching from the reduced state (deep blue color) to oxidized state (light blue).

Figure 2.4 shows the chemical synthesis of PEDOT:PSS. The polymerization of EDOT in the presence of the oxidizing agent $Fe_2(SO_4)_3$ and sodium persulfate and polystyrenesulfonic acid results in an aqueous PEDOT:PSS suspension. In PEDOT:PSS, every third or fourth thiophene of PEDOT unit carries a positive charge. The Coulomb interactions between the positively charged $PEDOT^+$ and the negatively charged PSS^- hold the PEDOT and PSS polymer chains together and also result into a high viscosity of the PEDOT:PSS dispersion (up to 80 mPa s at 1.3 wt % solid content in water).

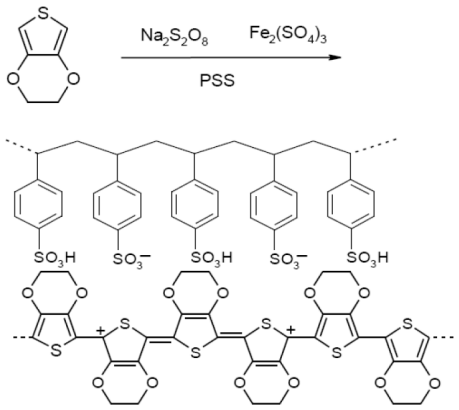

Figure 2.4 Chemical polymerization of ethylenedioxythiophene in the presence of polystyrenesulfonic acid.[61]

2.1.2 Conductivity Enhancement of PEDOT :PSS

The increase of PSS ratio in PEDOT, while making the polymer more stable in ambient conditions and facilitating its processing, reduces its conductivity. The conductivity of PEDOT:PSS depends on film morphology, PEDOT/PSS ratio and conformation of PEDOT chains.[69-72] In order to reach a balance between high conductivity and ease of process, an optimum PEDOT/PSS needs to be maintained. In commercially available Clevios PEDOT:PSS suspensions, the PEDOT/PSS ratio is 1:2.5 (w/w%). However, films processed from pristine suspensions exhibit conductivities as low as 1 Scm^{-1}. The conductivity of PEDOT:PSS films can be increased by 2-3 orders of magnitude by adding small amounts of various compounds to the commercial suspension, like sorbitol, ethylene glycol, glycerol, and dimethyl sulfoxide (DMSO).[73,74] The effect of these compounds, known as secondary dopants or conductivity enhancers, is still under debate. It is known that these compound do not alter the doping level of PEDOT. The increase of the conductivity upon addition of conductivity enhancers is believed to be due to the fact that they alter the film morphology during drying, leading to lower energy barrier for charge carrier transport between individual PEDOT:PSS clusters. Ouyang et al. suggested that addition of solvents to PEDOT:PSS before spin-coating, leads to conformational changes of PEDOT chains from benzoidal to quinoidal structures, i.e. chains of coiled conformation to chains of linear conformation.[75] Kim et al. proposed that conductivity enhancers could induce screening effects, thus reducing the coulombic interactions between $PEDOT^+$ and PSS^- and therefore enhancing the charge carrier hopping rate and conductivity in

PEDOT:PSS films.[73] Pettersson et al. considered that the interaction of dipoles of additives with PEDOT:PSS leads to the reorientation of the PEDOT:PSS.[76] Jonsson et al. proposed that the addition of these agents will lead to the removal of excess insulating PSS^- ultimately improving the conductivity.[77] Similarly, Leo et al. suggested that the depletion of insulating PSS during solvent post treatment leads to efficient contact areas between better oriented PEDOT rich grains and, as a consequence, to the enhancement of pathways for carrier transport.[70] Recently, Ouyang et al. proposed that the polar poly-alcoholic additives weaken the electrostatic interactions between PEDOT and PSS thus leading to phase separation between polymers.[78]

H.C. Stark Inc. commercializes PEDOT:PSS with brand name Clevios™. In this work, Clevios™ PH1000 grade was used for OECTs. The Clevios PH1000 PEDOT:PSS aqueous suspension has a PEDOT:PSS content of 1.1 w/w %, with a PEDOT to PSS ratio of 1:2.5 (i.e.,~ 0.3 w/w % PEDOT and ~ 0.8 w/w % PSS). According to Clevios technical reports, 1:2.5 (w/w) ratio of PEDOT to PSS is the best compromise between high film conductivity and sufficient stability of the dispersion.

2.2 Organic Electrochemical Transistors (OECTs)

As explained in Chapter 1, when electrochemical doping/dedoping takes place upon electrolyte gating, the devices act as OECT. First reported by Wrighton and coworkers in the 1980s, OECT are nowadays used for biological applications because they can be operated in aqueous environment at low voltage, are compatible with flexible substrates and various fabrication techniques and show mixed ionic/electronic conduction that facilitate the interface with biological systems.[39,41,79]

OECT have been investigated for a broad variety of applications including sensors for glucose, dopamine, ions, cells, pH and DNA, in active-matrix physical sensor circuits.[80-82]

In order to achieve the highest performance of OECTs, the device components, i.e., channel, gate and electrolytes are intensively investigated.[83-90]

2.2.1 Working Principle of PEDOT:PSS based OECT

An OECT consists of a conducting polymer channel in contact with an electrolyte where a gate electrode is immersed. Figure 2.5a illustrates the working principle of PEDOT:PSS OECT, which work in depletion mode. In absence of an applied gate bias, upon application of a drain-source voltage, V_{ds}, (Figure 2.5b) holes drift within the transistor channel from drain to source generating a drain-source current, I_{ds}. This corresponds to the transistor ON state. By applying a positive gate-source voltage, V_{gs}, (Figure 2.5c) electrolyte cations, M^+, are incorporated into the channel and dedope it, according to the equation below, thereby decreasing I_{ds} (OFF state).

$$PEDOT^+:PSS^- + M^+ + e^- \longleftrightarrow PEDOT + M^+:PSS^-$$

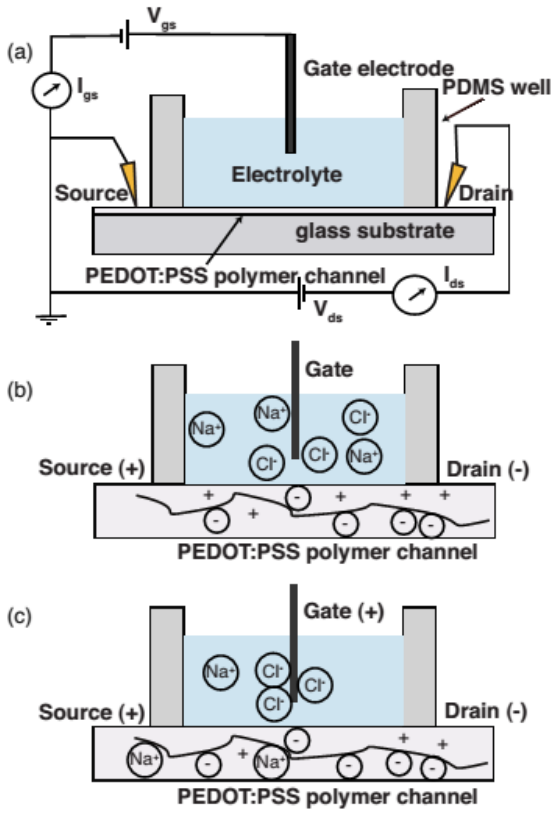

Figure 2.5 (a) Device structure and electrical circuit of a PEDOT:PSS OECT; (b and c) OECT working principle; circles filled with - indicate PSS^- ions and + indicate mobile holes.[91] Reprinted with permission. Rights managed by AIP Publishing LLC.

OECT can work in Faradaic and non-Faradaic regimes, depending on the type of gate material and electrolyte. Under a Faradaic regime, the OECT response is governed by a Nernst-like equation and a non-negligible steady state gate current is measured at the gate electrode. The non-Faradaic regime refers to a capacitive mode of operation. Since the OECT response depends directly on the potential drops occurring at the gate/electrolyte and electrolyte/channel interfaces, the electrolyte solution potential (V_{sol}) determines finally the OECT current modulation.

Based on experimental results, several models have been proposed.[83-85,92] Cicoira et al. investigated the effects of the gate area (A_g) and channel area (A_{ch}) on the performance of PEDOT:PSS OECT, exposed to different concentrations of the analyte hydrogen peroxide. Devices with small gate areas showed lower background signal and higher sensitivity; the minimum and maximum detectable analyte concentrations appeared to be independent on A_{ch}/A_g.[84]

Yaghmazadeh et al. proposed a model to distinguish the operation of OECT as *ion-to-electron converter* and as an *electrochemical sensor* (ECS).[85] The transistor can work as an electrochemical sensor when a redox reaction occurs at the gate electrode, which results in a charge transfer between the analyte in the electrolyte and the gate electrode. For an OECT working as *ion-to-electron converter,* a gate electrode much larger than the channel gives a higher modulation of I_{ds} and hence an optimized value of the transconductance, $(\partial I_{ds})/(\partial V_{gs})$. Likewise, when OECT work as electrochemical sensors, a gate with a smaller area respect to the channel yields higher OECT modulation of I_{ds} and hence a better sensitivity. The explanation relies on the distribution of the potential drop at the gate/electrolyte and electrolyte/channel interfaces (Figure 2.6).

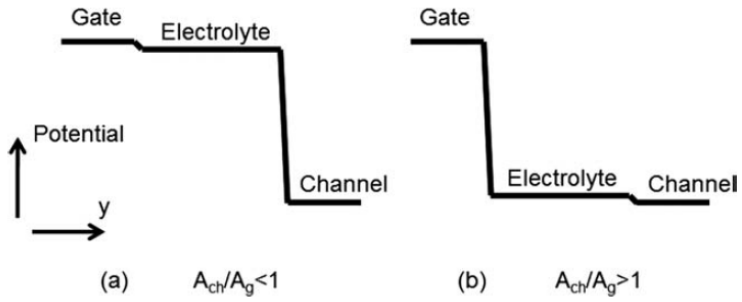

Figure 2.6 Potential distribution between the gate electrode and the channel for two device geometries (a) The transistor with the small gate ($A_{ch}/A_g = 100$) (b) The transistor with the bigger gate ($A_{ch}/A_g = 0.01$).[85] Reprinted with permission. Copyright © 2010 Wiley Periodicals, Inc.

Potential distribution between the gate electrode and the channel for two device geometries (a) The transistor with the small gate ($A_{ch}/A_g = 100$) (b) The transistor with the bigger gate ($A_{ch}/A_g = 0.01$).[85] Reprinted with permission. Copyright © 2010 Wiley Periodicals, Inc.

Successively, the role of the gate material on the OECT response has been analyzed [84,91,93]. Devices operating in a halide ion based electrolyte, as sodium chloride (NaCl), have been used making use of Ag and Pt gate electrodes. Ag and Pt gate electrodes show different responses: using a nonpolarizable Ag electrode, larger current modulations are observed, compared to Pt gate electrodes. (Figure 2.7)

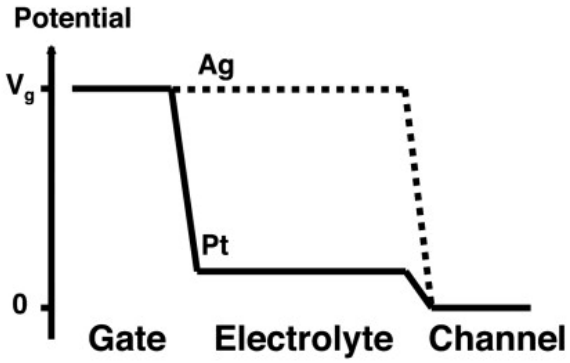

Figure 2.7 Potential distribution between the gate electrode and the channel for Ag and Pt gate electrodes.[91] Reprinted with permission. Rights managed by AIP Publishing LLC.

The electrolyte also has a strong influence on the response of an OECT device.[94] Cicoira et al. reported that using as the electrolyte an aqueous solution of a cationic surfactant hexadecyl trimethyl ammonium bromide or cetyl ammonium bromide (CTAB) above a critical micellar concentration (CMC, about 9×10^{-4} M at room temperature) leads to higher current modulation compared to a conventional NaCl electrolyte. This indicates that positively charged CTAB micelles de-dope PEDOT:PSS more efficiently than dissociated ions. The use of surfactants as electrolytes offers unprecedented opportunities to study the working mechanism of OECTs because they give access to two distinct types of electrolytes, i.e. dissociated CTAB ions below the CMC and CTAB micelles above the CMC. There have been few more approaches to replace the conventional electrolytes of OECT by ionic liquids, solid or gel electrolytes, with the aim to widen their areas of application.[86,94,95]

Current modulation in PEDOT:PSS OECTs relies on bulk doping of the channel, therefore it strongly depends on channel thickness. This is a major difference with respect to OFETs, where current modulation relies on electrostatic doping taking place at the channel/dielectric interface. Hence, the time constant of OECT depends on the ion mobility, rather than charge carrier mobility as in the case of OFETs. For instance, increasing channel thickness will induce higher transconductance, while decreasing the switching speed of the device.[96] Rivnay et. al. investigated the performance of OECTs by tuning the channel thickness from 20 nm to 1 μm. They found a volumetric capacitance of 39 F/cm^3 during the uptake of electrolyte ions by PEDOT:PSS. The obtained value is 100 times more than that of double layer capacitance, which indicates the ion penetration into the channel during the OECTs operation.

There are several reports about OECT biomedical applications including medical diagnostics and bioelectronics implants, for instance electrocardiographic recordings, in vivo electrocortico-graphic (ECoG) arrays to detect epileptic activity, in vitro detect in cardiac cell activity etc.[46,97-102]

2.3 Melanin

Many organic electronics polymers are mixed ionic/electronic conductors. As ionic fluxes are the main vehicle to transport the information in biological systems, devices made of mixed

conductors enable new means of communication between electronics and biology.[103] Melanin is one such kind of polymer. Melanin (from the Greek word melanos, meaning black color) is an abundant biopigment component present in flora and fauna.[104,105] Melanin gained initial attention due to its broad UV-Vis absorption, which is responsible for protection of living organisms from intense UV radiation from sunlight. This function is believed to be related to biological evolution.[106] Melanin-based pigments are present in the skin, hair, middle ear, retina, brain and heart of the human body.[107-109] Melanin has attracted interest due to its functional properties such as thermoregulation, hydration-dependent electrical conduction, anti-oxidant behavior and metal chelation.[54-56,110-115] Different forms of melanin include eumelanin, pheomelanin, and neuromelanin, depending on the biosynthetic path. In humans, the color of the skin, hair and eyes are decisively determined by the amount of brown-black eumelanin and yellow-reddish pheomelanin. Eumelanin is the subclass of melanin most investigated by materials scientists. The heterogeneous macromolecule-structured eumelanin arises in part from the polymerization of L-dopa via 5,6-dihydroxyindole (DHI) and its 2-carboxylated form 5,6-dihydroxyindole-2-carboxylic acid (DHICA). Pheomelanin is derived from the Sulphur-containing cysteinyldopa. Natural melanin is generally derived from the ink sac of cuttlefish. Neuromelanin, found in the substantia nigra of the brain, has been proposed to be a copolymer of eumelanin and pheomelanin. Eumelanin can be produced from the enzymatic oxidation of tyrosine or oxidation of dopa. During the process various precursors of melanin i.e., 3,4-dihydroxy-L-phenylalanine (DOPA), DHI, DHICA can be realized (Figure 2.8)

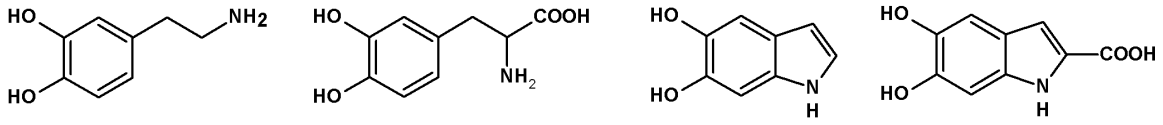

a) b) c) d)

Figure 2.8 Molecular structures of eumelanin precursors: a) dopamine, b) 3,4-dihydroxy-L-phenylalanine (DOPA), c) 5,6-dihydroxyindole (DHI) and d) 5,6-dihydroxyindole carboxylic acid (DHICA).

The macromolecule eumelanin is composed of oligomeric and/or polymeric species of DHI and DHICA, and their various redox forms, namely the ortho-hydroquinone (H_2Q), semiquinone

(SQ), (indole)quinone (Q) and quinone imine (QI) (as the canonical form of Q) (Figure 2.9).

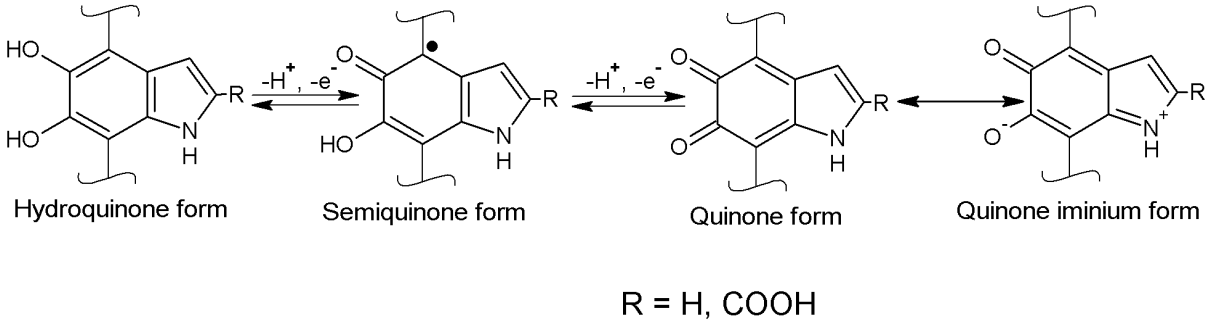

Figure 2.9 Various redox forms of eumelanin building blocks DHI and DHICA.

2.3.1 Melanin Electrochemistry

Horak et al., reported for the first time of electrochemical polymerization of DHI on glassy carbon electrode.[116] Gidanian et al. reported an electrochemical polymerization of DHI in phosphate buffer of pH 7.0.[117] Kim et al., used melanin for sodium-ion battery electrodes.[118] The authors investigated natural melanin (derived from Sepia officinalis), synthetic melanin (derived by auto-oxidation of tyrosine) and electrodeposited melanin (oxidative polymerization of 5,6-dimethoxyindole-2-carboxylic acid). Specific capacities of Na^+ ions loaded melanins measured at constant discharge rate of 10 mA g^{-1} for natural melanin, synthetic melanin, and electrodeposited melanin were 30.4 ± 1.6, 31.1 ± 2.0, and 24.1 ± 2.0 mAh g^{-1}, respectively. Raman Spectroscopy and XPS were used to determine the location of Na^+ ion binding sites of melanin, revealing that catechols, aromatic amines and carboxylate groups are effective binding sites for Na^+.

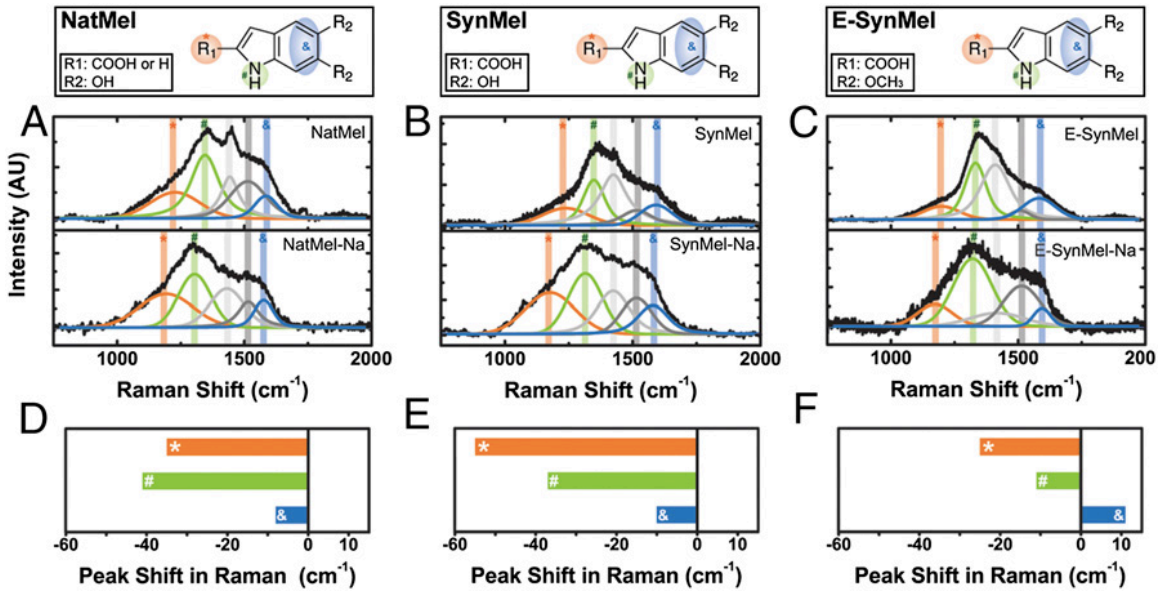

Figure 2.10 Raman spectra of eumelanins. (A) natural melanin and Na-loaded natural melanin; (B) synthetic melanin and Na-loaded synthetic melanin; (C) electrodeposited melanin and Na-loaded electrodeposited melanin. Raw spectra (black lines) are deconvoluted into five bands using a Voigt function.[118] Copyright © (2013) National Academy of Sciences.

Successively, Kim et al., demonstrated melanin as a cathode material for rechargeable electrochemical storage devices.[119] They exploited the reversible redox property of the catechol-quinone system of the melanin (natural melanin) building blocks and their strong affinity towards multivalent ions. The studies were carried out, among others, in presence of the divalent ion Mg^{2+}: a specific capacity of 61.6 ± 0.3 mAh g^{-1} from current density measurements was reported with natural melanin.

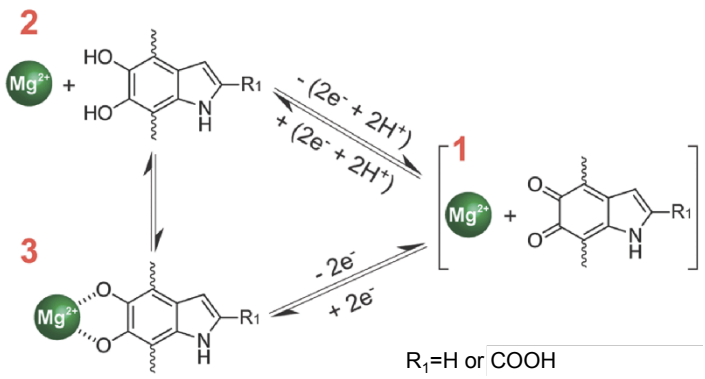

Figure 2.11 The mechanism of Mg^{2+} binding melanin catechols.[119] Reprinted with permission.

In recent studies, Kim et al. proposed that in natural melanin monovalent ions bind to COOH and NH_2 groups whereas multivalent cations bind to catechols.[120] The authors also proposed *porphyrin-like* structures forming from natural melanin through electrochemical Na^+ insertion.

CHAPTER 3 ARTICLE 1: EFFECT OF CHANNEL THICKNESS, ELECTROLYTE IONS AND DISSOLVED OXYGEN ON THE PERFORMANCE OF ORGANIC ELECTROCHEMICAL TRANSISTORS

This article has been published in the journal "Applied Physics Letters" in 2015. This article reports a comparison of organic electrochemical Transistors (OECTs) performance with channel thickness and electrolytes.

3.1 Authors

Prajwal Kumar,[1] Zhihui Yi,[1] Shiming Zhang,[1] Arvindh Sekar,[1] Francesca Soavi,[2] Fabio Cicoira[1a)]

[1]Department of Chemical Engineering, Polytechnique Montréal, C.P. 6079, Succ. Centre Ville, H3C 3A7, Canada. E-mail: fabio.cicoira@polymtl.ca.

[2]Department of Chemistry "Giacomo Ciamician" Università di Bologna, Via Selmi, 2, Bologna, Italy, 40126.

3.2 Abstract

We investigated the device characteristics of organic electrochemical transistors based on thin films of poly(3,4-ethylenedioxythiophene) doped with poly(styrene-sulfonate). We employed various channel thicknesses and two different electrolytes: the micelle forming surfactant cetyltrimethyl ammonium bromide (CTAB) and NaCl. The highest ON/OFF ratios were achieved at low film thicknesses using CTAB as the electrolyte. Cyclic voltammetry suggests that a redox reaction between oxygen dissolved in the electrolytes and PEDOT:PSS leads to low ON/OFF ratios when NaCl is used as the electrolyte. Electrochemical impedance spectroscopy reveals that doping/dedoping of the channel becomes slower at high film thickness and in presence of bulky ions.

3.3 Introduction

Organic conducting polymers lay the foundation for organic bioelectronics.[30,39,45,92,121-123] Poly(3,4-ethylenedioxythiophene) doped with poly(styrene-sulfonate) (PEDOT:PSS) is a well known highly conducting and optically transparent polymer.[70,124] Organic electrochemical transistors (OECTs) based on PEDOT:PSS are exploited in bioelectronics and sensing.[30,99,125,126] OECTs consist of a conducting polymer channel, connected to source and drain electrodes that are in ionic contact with a gate electrode via an electrolyte solution. OECTs based on PEDOT:PSS work in depletion mode: a hole source-drain current (I_{ds}) flows upon application of a drain-source voltage (V_{ds}). When a positive V_{gs} is applied, electrolyte cations enter the channel and dedope it, thus leading to a decrease of I_{ds}. An important figure of merit OECTs is the current modulation, typically expressed in terms of ON/OFF ratio, which depends on processing and composition of the conducting polymer channel,[127] device geometry,[84,85,68,128] gate material[93,129] and nature of the electrolyte.[86,89,130] OECT performance is also affected by the thickness of the conducting polymer channel. As current modulation relies on redox processes, which involve exchange of ions between the electrolyte and the polymer film, the entire film volume is relevant for charge transport. This working mechanism differs from that of organic field effect transistors, where only the very first few monolayers at the gate dielectric/channel interface are relevant for charge carrier transport.[131] Malliaras et al. have recently demonstrated that the transconductance (dI_{ds}/dV_{gs}) and the capacitance of PEDOT:PSS OECTs depends on channel thickness and aspect ratio.[90,96]

Here we investigate the effect of the PEDOT:PSS channel thickness on OECT modulation using two different electrolytes: the cationic surfactant hexadecyltrimethylammonium bromide, also known as cetyltrimethyl ammonium bromide (CTAB) and NaCl. CTAB, beyond its critical micelle concentration (CMC), is known to lead to high current modulation in OECTs and it is therefore a model system to study the doping/dedoping process in OECTs.[89] We employed cyclic voltammetry (CV) and electrochemical impedance spectroscopy (EIS) to gain insight into the impact of channel thickness and nature of the electrolyte on device performance.

3.4 Experimental

The OECT's PEDOT:PSS channels were patterned on a glass substrates using a procedure previously published.[84] The effective channel dimensions (geometric area of about 12 mm2, channel width 2 mm and channel length 8 mm) were defined by the contact region between the film and the electrolyte, confined into a cloning cylinder.[91] Films were deposited by spin coating a mixture containing a PEDOT:PSS suspension (CleviosTM PH 1000, Haraeus GmbH, Germany), the conductivity enhancer ethylene glycol (19.7 v/v %) and dodecylbenzenesulfonic acid (DBSA) (0.3 v/v %).[132] Different speeds (500, 1000, 2000 and 4000 rpm, for 20 seconds) were employed to achieve film thicknesses of about 500, 180, 110, and 50 nm, as measured by a Dektak 150 optical profilometer. The electrical conductivity of PEDOT:PSS films was extracted from the sheet resistance, measured by a four-point probe system.[133] Activated carbon (AC) gate electrodes (geometric area about 25 mm^2) were prepared by drop casting a suspension of AC (Picachem BP9, 28 mg/mL) and Nafion (2.4 mg/mL) in isopropanol, on carbon fiber paper (Spectracarb 2050, 10 mils).[93] Aqueous solutions of 0.01M NaCl and 0.001M CTAB (i.e. above the CMC) were used as the electrolytes. The ionic conductivity of the electrolytes was measured by a Traceable® expanded range conductivity meter. OECT characterization was carried in ambient conditions with an Agilent 2902A source/measure unit controlled via Labview software. Transfer curves were extracted from OECT transient characteristics (Ids *versus* time) measured at different V_{gs}. CV and EIS were carried out in a three-electrode cell, where a PEDOT:PSS film acted as the working electrode (WE), a Pt foil as the counter electrode (CE) an aqueous Ag/AgCl as the reference electrode (RE). The electrolyte solutions were purged with N_2 or air for one hour prior to measurements and during the CV (at reduced flow to prevent the formation of foam in CTAB). A hollow cylindrical well confined the electrolyte on the WE (over an area of 0.64 cm^2).

3.5 Results and Discussions

As channel resistance plays a major role in modulation of OECTs based on PEDOT:PSS, we first measured the electrical conductivity, extracted from the sheet resistance, of PEDOT:PSS at four

different thicknesses (Figure 3.1). The conductivity increases from ~300 S/cm to ~450 S/cm as thickness increases from ~50 nm to ~110 nm. Further increase in thickness to ~180 nm and ~500 nm results in a modest conductivity increase up to ~500 S/cm. Although more investigations are needed to understand this behavior, a possible explanation would be a transition from percolation to bulk-like charge transport occurring in PEDOT:PSS films upon a thickness increase. This would be an analogy to conduction in two-dimensional materials such as graphene.[134] A percolative behavior is characteristic of sparse networks with limited connectivity and few continuous conductive paths. Thus, we hypothesize that, in case of 50 nm thick PEDOT:PSS films, the conductivity is dominated by quasi-two dimensional connection paths between adjacent PEDOT grains, while in thicker films charge carriers are transported in three dimensional PEDOT-PEDOT networks.

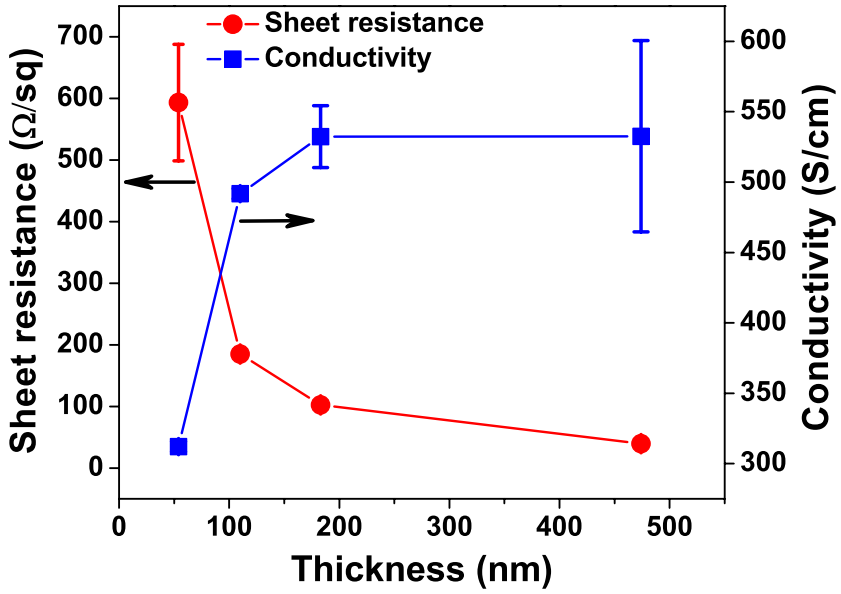

Figure 3.1 Sheet resistance (red circles, left y axis) and electrical conductivity (blue stars, right y axis) of PEDOT:PSS films (geometric area 15x15 mm^2) of different thicknesses (~500, 180, 110, and 50 nm). The error bars correspond the standard deviation of four samples.

The transfer characteristics (-0.4 V $\leq V_{gs} \leq$ 0.6 V and V_{ds} = -0.2 V) of PEDOT:PSS OECTs with different channel thicknesses (Figure 3.2a for NaCl electrolyte and 3.2b for CTAB electrolyte)

show the typical I_{ds} *vs.* V_{gs} behavior of PEDOT:PSS OECTs and reveal that, at a given V_{gs}, $|I_{ds}|$ increases with increasing channel thickness. This trend confirms that the transport of electronic charge carriers takes place in the entire channel volume.

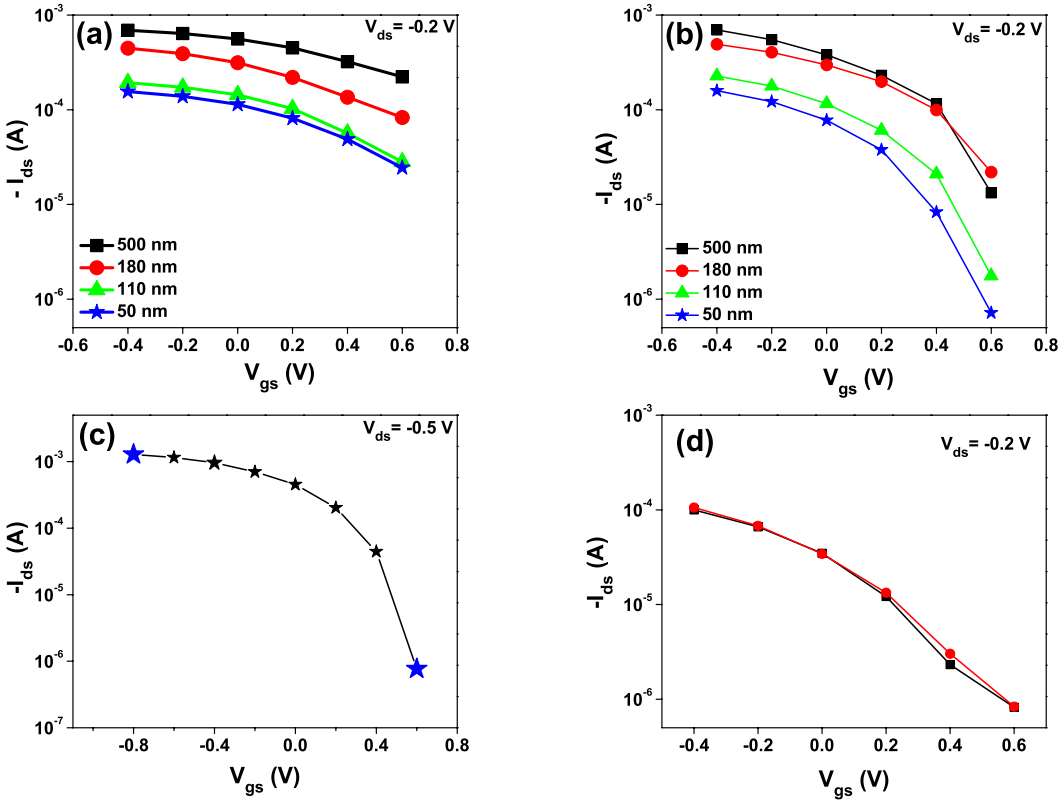

Figure 3.2 Transfer characteristics (-0.4 V ≤ V_{gs} ≤ 0.6 V and V_{ds} = -0.2 V) of PEDOT:PSS OECTs with four different channel thicknesses (~500, 180, 110, 50 nm) using 0.01 M NaCl (a) and 0.001 M CTAB (b) as the electrolyte. OECT based on a 110 nm thick PEDOT:PSS film using 0.001 M CTAB as the electrolyte, showing a high ON/OFF ratio of ~1700 (-0.8 V≤V_{gs}≤0.5 V and V_{ds}=-0.5 V). The blue star represents the ON and OFF currents at V_{gs}=-0.8 and V_{gs}=0.6 V (c). Hysteresis behavior of an OECT based on a 50 nm thick PEDOT:PSS film(d). The black curve corresponds to the forward bias (from V_{gs}=-0.4 to V_{gs}=0.6 with V_{ds}=-0.2 V) and the red curve to the reverse bias. During all OECTs characteristics, gate scan rate of 0.003 V/s was maintained.

The ON/OFF ratios (Table 1) are significantly higher for devices using CTAB as the electrolyte, in agreement with previously published results.[89] Moreover, decreasing the film thickness from ~500 to ~50 nm leads to an increase of the ON/OFF ratio from ~50 to ~220. The same thickness variation only leads to minor changes in devices using NaCl as the electrolyte. ON/OFF ratios as high as ~1700 (at V_{ds}=-0.5 V and -0.8 V $\leq V_{gs} \leq$0.6 V) were achieved with OECTs using a 110 nm thick PEDOT:PSS channel and 0.001 M CTAB as the electrolyte (Figure 3.2c). The devices show negligible hysteresis under our measurements conditions (Figure 3.2d).

Table 3.1 ON/OFF ratios extracted from transfer characteristics (-0.4 V $\leq V_{gs} \leq$ 0.6 V and V_{ds}=-0.2 V) of PEDOT:PSS OECTs with four different channel thickness (~500, 180, 110, 50 nm) using 0.01 M NaCl and 0.001 M CTAB as the electrolytes.

Thickness (nm)	ON/OFF ratio	
	NaCl electrolyte	CTAB electrolyte
470±90	~7.0	~50
180±10	~5.5	~180
110±10	~7	~130
55±5	~7	~220

To further investigate the effects of channel thickness and electrolyte composition on current modulation, we performed CV. Figure 3.3(a) shows CVs of PEDOT:PSS films in CTAB and NaCl. The potential of the WE was swept from 0 V *vs.* Ag/AgCl towards negative potentials (−1 V *vs.* Ag/AgCl) and then towards positive potentials (+0.8 V *vs.* Ag/AgCl) with a scan rate of 5 mV/s. Under N_2 purging, the position of the redox peaks in the two electrolytes does not differ significantly: the typical oxidation wave is observed between −0.4 V and 0.5 V *vs.* Ag/AgCl and

the reduction takes place between −0.4 V and −0.8 V *vs.* Ag/AgCl. The voltammograms are more distorted in CTAB, which suggests a slowed down doping/dedoping process with respect to NaCl, likely related to lower ionic conductivity (~0.1 mS/cm for 0.001M CTAB with respect to ~2.0 mS/cm for 0.01M NaCl), slower migration, and higher steric hindrance. Indeed, the diameter of the positively charged CTA^+ micelle is ~1−4 nm [89,135] and that of Na^+ is ~0.2 nm.

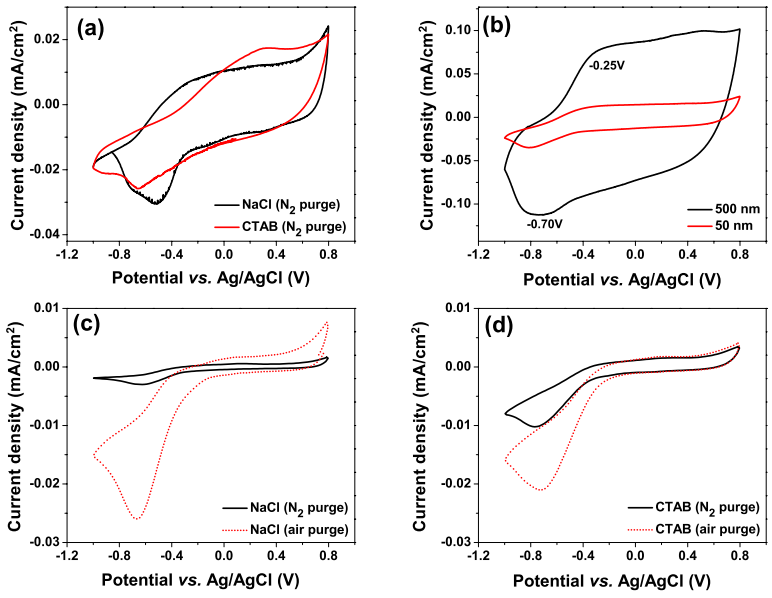

Figure 3.3 Cyclic voltammetry of PEDOT:PSS films (~250 nm thickness) using 0.01M NaCl and 0.001M CTAB as the electrolytes, carried out under N_2 purging (a). Cyclic voltammetry of PEDOT:PSS films (50 nm and ~500 nm thicknesses) using 0.01M NaCl as the electrolyte, carried out under N_2 purging (b). Cyclic voltammetry of PEDOT:PSS films (~50 nm thickness) carried out under N_2 or air purging using 0.01M NaCl (c) and 0.001M CTAB (d) as the electrolyte.

The intensity of the CV current increases with increasing film thickness from ~50 nm to ~500 nm (Figure 3.3(b)). The amount of charge needed to dedope/dope the films (Q) was calculated by integration of the anodic current over time and the film capacitance was calculated from the slope of Q (during doping) *versus* electrode potential (Table II). An increase of the film

capacitance of about a factor of 6 was found upon a thickness increase from 50 nm to 500 nm. These results, in agreement with recent findings by Malliaras *et al.*,[90] are consistent with the dedoping/doping mechanism of PEDOT:PSS films, which involves incorporation/release of electrolyte cations: the CV current depends on the dedoping/doping charge, in turn related to the amount (thickness) of PEDOT:PSS to be dedoped/doped. The values of the volumetric capacitance are higher in thinner films, which points to a more effective dedoping/doping process at lower thicknesses. Although higher values are found for CTAB, the effect of the electrolyte is rather modest.

Table 3.2. Capacitance and amount of dedoping/doping charge (absolute and volumetric values) of PEDOT:PSS films extracted from the anodic voltammetric currents at 5 mV/s in NaCl and CTAB electrolytes. The film volumes are 3.0×10^{-5} cm^3 for the thick film and 3.4×10^{-6} cm^3 for the thin film.

Electrolyte	PEDOT :PSS film thickness (nm)	Charge (C) ($\times10^{-3}$)	Normalized charge (C/cm^3)	Capacitance (F) ($\times10^{-3}$)	Normalized Capacitance (F/cm^3)
0.01 M NaCl	474±90	1.52	50	1.15	38
	54±10	0.25	74	0.2	54
0.001 M CTAB	474±90	1.44	47	1.2	41
	54±10	0.23	66	0.2	55

As OECTs are mostly operated in ambient conditions, we explored the effect of dissolved oxygen on the redox behavior of PEDOT:PSS films (~50 nm thickness) by carrying out CV under air purging (Figures 3.3(c) and 3.3(d), red dotted curves). Voltammograms obtained under air purging indicate an increase of the cathodic current between −0.5 V and −0.8 V *vs.* Ag/AgCl for both electrolytes. This suggests that PEDOT:PSS, once it is electrochemically reduced to the dedoped state, it is readily reoxidized chemically to the doped state by dissolved O_2,[136] with a process similar to that exploited for electrocatalytic oxygen reduction at PEDOT electrodes.[137-141] In OECTs, this effect may hinder the dedoping of PEDOT:PSS that is expected at positive V_{gs}, thus leading to lower ON/OFF ratios. The cathodic current is higher in NaCl than CTAB. This can tentatively be attributed to a lower O_2 solubility, which would result in a more effective dedoping of PEDOT:PSS. We are currently investigating the use of oxygen radical scavenging additives (e.g., tannic acids), in the electrolyte or in the PEDOT:PSS film, to prevent PEDOT:PSS oxidation by environmental O_2.[142]

The doping/dedoping processes in PEDOT:PSS films in NaCl and CTAB were further investigated by EIS (Figure 3.4). The Nyquist plots obtained in NaCl consist of lines almost parallel to the imaginary impedance axis. Those obtained in CTAB are not parallel to the imaginary impedance axis, in particular at high film thickness, thus suggesting a hindered ionic charge transport through the film. For both electrolytes, the uncompensated resistance (which includes ionic contribution from the electrolyte and electronic contribution from PEDOT:PSS) is lower for thicker films. The real component of the impedance of 500 nm-thick films at 10 kHz is ~1.9 kΩ in NaCl and ~4.9 kΩ in CTAB, while that of 50 nm-thick films is ~4.0 kΩ in NaCl and ~9.9 kΩ in CTAB. As the distance between working and reference electrodes was kept constant during all the experiments (i.e., the ionic contribution to the high-frequency real impedance for a given electrolyte remained unchanged), our results indicate that thicker films have lower electronic resistance than thin films. As expected for pseudocapacitve electrodes, the imaginary part of the impedance shows that the capacitive component of the impedance. (i.e., the capacitance at the lowest frequency $C = \frac{1}{Zi2\pi f}$) increases with film thickness. In case of the NaCl electrolyte, the capacitance increases from ~0.12 mF (~35 F/cm^3) to ~0.69 mF (~23 F/cm^3) as the thickness varies from 50 nm to 500 nm. In case of CTAB, for the same thickness variation, the

capacitance increases from ~0.11 mF (~32 F/cm^3) to ~0.42 mF (~35 F/cm^3). The volumetric capacitance is higher for thin films, which supports the trend observed in the CV. Using the capacitance values extracted from CV (Table 3.2) and the high frequency resistance extracted from EIS, we estimated the following time constants ($\tau = RC$) for the doping/dedoping process of PEDOT:PSS films: $\tau \sim 0.8\ s$ in NaCl and $\tau \sim 1.7\ s$ in CTAB for a 50 nm thickness, $\tau \sim 2.4\ s$ in NaCl and $\tau \sim 5.0\ s$ in CTAB for a 500 nm thickness. A similar trend was found for the time constant extracted from transient (I_{ds} *verus* time) OECT measurements. These results confirm that the doping/dedoping process becomes slower at higher film thicknesses and in the presence of bulky ions.

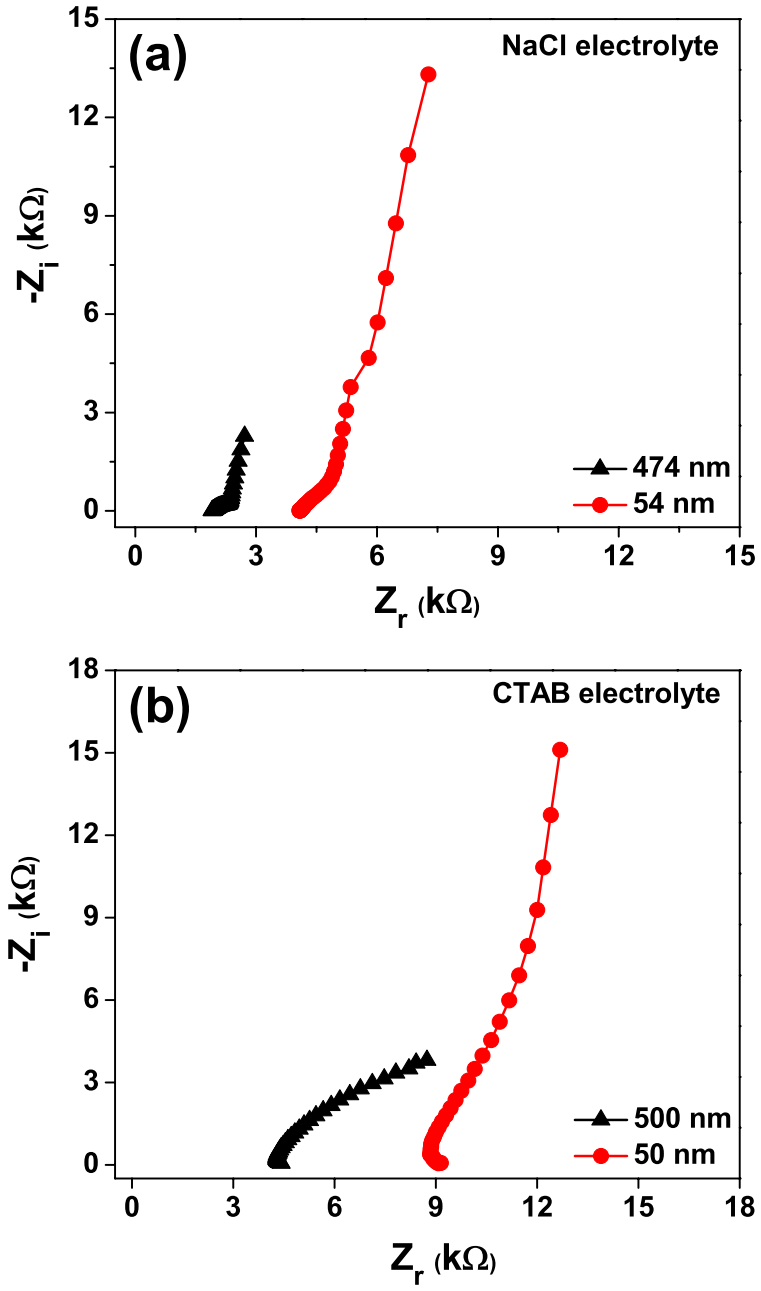

Figure 3.4 Electrochemical impedance spectroscopic analysis (Nyquist plots) of PEDOT:PSS films (thicknesses ~500 nm and ~50 nm) in 0.01 M NaCl (a) and 0.001 M CTAB (b) electrolytes. PEDOT:PSS is used as working electrodes, a Pt foil as counter electrode, and Ag/AgCl as reference. The frequency range is 0.5 kHz to 10^{-4} kHz with an AC amplitude of 5 mV. The PEDOT:PSS films were doped at 0.6 V vs Ag/AgCl for 30 s prior to EIS by chronoamperometry.

3.6 Conclusion

We investigated the effect of channel thickness, electrolyte ions (NaCl and CTAB), and dissolved oxygen on the performance of OECTs based on PEDOT:PSS. We found that (i) higher ON/OFF ratios are achieved when CTAB is used as the electrolyte; (ii) thin PEDOT:PSS films have superior performance as OECT channels, in terms of current modulation, compared to their thicker counterpart, despite their lower electrical conductivity; (iii) the effect of thickness on current modulation is more pronounced when CTAB is used as the electrolyte. Using cyclic voltammetry, we detected a significant effect of dissolved O_2 on the CV current of PEDOT:PSS, particularly in the presence of a NaCl electrolyte. The dissolved oxygen might oxidize PEDOT:PSS during the electrochemical dedoping process, thus leading to a lower ON/OFF ratio. EIS revealed that the doping/dedoping process in PEDOT:PSS becomes slower at higher film thicknesses and in the presence of bulky ions.

3.7 Acknowledgments

The authors are grateful to Professor C. Santato for fruitful discussions and to D. Pilon, for technical support. Funding for this project was provided by an *NSERC Discovery* grant and start-up funds from Polytechnique Montréal awarded to FC. P.K. is grateful to GRSTB for partial salary support. Z.Y. and S.Z. are grateful to NSERC for financial support through Vanier Canada Graduate Scholarships. FS acknowledges financial support from Alma Mater Studiorum-Università di Bologna (researcher mobility program, Italian-Canadian cooperation agreement). This work is supported by CMC Microsystems through the programs MNT financial assistance and CMC Solutions. This work has also benefited from the support of FRQNT and its *regroupement stratégique* program through a grant awarded to RQMP.

CHAPTER 4 ARTICLE 2: MELANIN-BASED FLEXIBLE SUPERCAPACITORS

This article has been published in "Journal of materials chemistry C" in 2016. This article reveals the exploitation of natural pigment melanin as an electrode for energy storage devices.

4.1 Authors

Prajwal Kumar,[a] *Eduardo Di Mauro* [b] *Shiming Zhang,*[a] *Alessandro Pezzella,*[c] *Francesca Soavi,* [d] *Clara Santato* *[b] *and Fabio Cicoira* *[a]

[a] Department of Chemical Engineering
Polytechnique Montréal
C.P. 6079, Succ. Centre-ville, Montréal, Québec, H3C 3A7 Canada
Email: fabio.cicoira@polymtl.ca

[b] Department of Engineering Physics
Polytechnique Montréal
C.P. 6079, Succ. Centre-ville, Montréal, Québec, H3C 3A7 Canada
Email: clara.santato@polymtl.ca

[c] Dipartimento di Scienze Chimiche
Università di Napoli Federico II
Cupa Nuova Cintia, 21, 80126, Napoli, Italy

[d] Dipartimento di Chimica "Giacomo Ciamician"
Università di Bologna
Via Selmi, 2, 40126, Bologna, Italy
Email: francesca.soavi@unibo.it

4.2 Abstract

Biocompatible and biodegradable materials that store electrochemical energy are attractive candidates for applications in bioelectronics and electronics *for everywhere*. Eumelanin is a ubiquitous biopigment in flora and fauna. It exhibits strong broad-band UV-visible absorption, metal chelation as well as good thermal and photo-stability. Eumelanin is based on 5,6-dihydroxyindole (DHI) and 5,6-dihydroxyindole carboxylic acid (DHICA) building blocks, present in different redox forms (hydroxyquinone, semiquinone and quinone). The synergy between the redox activity of the building blocks and the capability of several of their functionalities to reversibly bind cations constitutes the foundation for the use of melanin in pseudocapacitive energy storage systems.

In this work, we report on the energy storage properties of eumelanin in supercapacitor configuration. Initially, a gravimetric specific capacitance as high as 167 F/g (specific capacity of 24 mAh/g) was observed for eumelanin electrodes on carbon paper, in aqueous electrolytes. A maximum power density of up to 20 mW/cm^2 was deduced for the corresponding melanin supercapacitors. Capitalizing on these results, we used an unconventional patterning approach to fabricate binder-free flexible micro-supercapacitors on plastic substrates.

Our results demonstrate that melanin is a valid candidate for future supercapacitor electrodes. The biocompatibility and biodegradability featured by eumelanin, combined with its easy availability and room temperature processing, make it an extremely attractive material for environmentally and human friendly energy storage solutions.

4.3 Introduction

Environmentally and human friendly electronic devices based on natural biocompatible and biodegradable materials are expected to benefit our everyday life, by improving our current capability to handle waste electrical and electronic equipment (WEEE) and boosting the development of smart environments for “ubiquitous sensor networks” and biomedical implants.[143,144]

Micro-supercapacitors are of the utmost importance to address the need for on-board energy supply/storage, e.g. in wearable electronic devices and embedded wireless sensor networks.[145-152] Supercapacitors, with respect to batteries, exhibit higher power density and longer cycle

life.[153] Micro-supercapacitors are mostly fabricated from three classes of materials, i.e. carbon (activated carbon and nanostructured carbon), conducting polymers and metal oxides.[154] Micro-supercapacitors based on natural electrode materials and aqueous electrolytes, exhibiting mechanical flexibility, are of primary interest for environmentally and human friendly *microelectronics for everywhere*.[118,119,155-157]

Melanin is a ubiquitous biopigment in flora and fauna. It exhibits strong broad-band UV-visible absorption, metal chelation as well as good thermal and photo-stability. Different forms of melanin perform various functions in the human body, such as photoprotection (eumelanin) and hair and eye color (eumelanin and pheomelanin). Moreover, melanin pigments are also present in unexposed regions such as the inner ear and the *substantia nigra* of the brain as neuromelanin.[110,115,158] The form of melanin most investigated by physicists and materials chemists is eumelanin (indicated henceforth as melanin for simplicity). Melanin is based on 5,6-dihydroxyindole (DHI) and 5,6-dihydroxyindole carboxylic acid (DHICA) building blocks (Scheme 4.1). The different redox forms of the building blocks, hydroxyquinone, semiquinone and quinone moieties, coexist in the macromolecular structure that results from the non-covalent interactions of nanoaggregates, which in turn ensue from the p-p stacking of planar sheets of the building blocks, of variable extent.[159-160] The macromolecular structure of melanin stabilizes the semiquinone and quinone (oxidized) redox forms of the building blocks. The quinone functionality of the molecule has the ability to store $2e^{-}/2H^{+}$ per quinone unit (Scheme 4.1).[153,161-163]

The synergy between the redox activity of the building blocks and the capability of several of their functionalities to reversibly bind cations constitutes the foundation for the use of melanin in pseudocapacitive energy storage systems. Unlike supercapacitors making use of carbon electrodes, which store energy by a purely electrostatic process, redox-active materials (pseudocapacitive materials) permit to exploit Faradaic processes to achieve higher specific capacitance. The redox processes are accompanied by ion motion from/to the electrolyte into/from the redox active material. In melanin, carboxyl, amine, hydroxyl (phenolic), quinone and semiquinone moieties can serve as potential sites for metal cation accommodation.[56] Kim et al. reported catechol-mediated reversible binding of multivalent cations in melanin half-cells and, based on different affinities for multivalent cations of catechols and quinones, proposed that these cations bind to melanin via catechols and are extracted from melanin as catechol oxidizes

into quinone. Functionalities other than catechols would likely have a minor effect on charge storage.[119,164,165] A complete picture of the potential of melanin as active material in energy storage needs also to take into account the electronic and ionic transport properties. Studies of the generation and transport of charge carriers established that the electrical response of melanin strongly depends on its hydration state through a comproportionation equilibrium. In presence of water, hydroquinone and quinone moieties form free carriers, protons and electrons (semiquinone extrinsic free radicals).[103,104] Recent studies by our groups contributed to the understanding of the proton conduction properties of melanin, under controlled humidity conditions.[113,166] Important findings on the ion transport properties of melanin have been reported in relation to its biological role in the human body, where melanin is believed to act as an ion storage and release medium.[110,56] For applications in electrochemical energy storage, the relatively low electrical conductivity of melanin (10^{-4} - 10^{-3} S/cm) points to the need for efficient current collectors, such as electrically conductive carbon-based materials.[167,168]

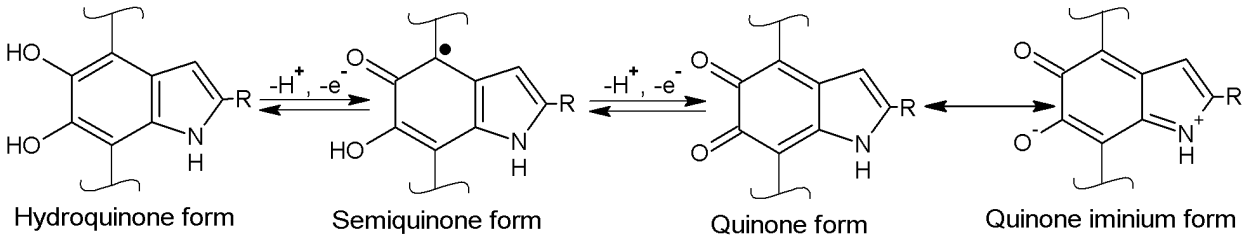

Scheme 4.1 Melanin building blocks DHI (R=H) and DHICA (R=COOH) and their redox forms hydroquinone (H_2Q), semiquinone (SQ) and quinone (Q); the quinone iminium (QI) form is the canonical form of quinone.

Here we report on the use of melanin as electrode material for supercapacitors and micro-supercapacitors. The pseudocapacitive properties of melanin were initially studied using conductive carbon paper as current collector and then exploited to demonstrate, through the use of unconventional patterning, melanin-based flexible micro-supercapacitors. The main novelty of our work is the discovery of a new natural material for supercapacitor electrodes, besides well-established materials, such as activated carbons, carbon nanotubes, graphene, metal oxides and conducting polymers. Natural materials have already been used for the fabrication of

supercapacitor electrodes. Nevertheless, in most cases, these materials have to be pyrolysed and activated to yield activated carbon electrodes, or they are mixed with conducting polymers to yield pseudocapacitive electrodes (APPENDIX A, Table S1).[169-187] Unlike these natural materials, our melanin can be simply deposited by solution processing at room temperature and does not require any thermal treatment or further mixing. The biocompatibility and biodegradability featured by melanin, together with its easy availability, make it an extremely attractive material for environmentally and human friendly energy storage solutions.[188]

4.4 Results and Discussions

4.4.1 Cyclic Voltammetry Studies on Melanin

The capability of melanin to store charge was initially assessed by cyclic voltammetry using electrodes consisting of melanin drop cast on conductive carbon paper (indicated henceforth with Mel/CP, see Experimental), exploiting the high mechanical stability of melanin on CP (Figure 4.1). As a matter of fact, we were able to run only 1-3 voltammetric cycles using melanin deposited on other types of electrodes, such as indium tin oxide (ITO). We investigated different electrolytes, in a typical three-electrode configuration, to assess the effect of the composition and pH of the electrolyte on the Mel/CP behavior. In $NH_4CH_3COO_{(aq)}$ at pH 5.5, the voltammetric response of Mel/CP electrodes with increasing melanin loadings (33.75 and 67.5 $\mu g/cm^2$, normalized with respect to the electrode footprint) shows that the current density increases with increasing loading (Figure 4.1a). Our measurements also show that bare CP does not contribute significantly to the overall capacitance. The Mel/CP voltammograms are quasi box-shaped (rectangular). The absence of easily distinguishable voltammetric peaks is likely due to the convolution of several redox processes taking place at sites characterized by different molecular environments and different affinity to the electrolyte.[189] Indeed, melanin is a mixture of chemically similar biopolymers, rather than a well-defined chemical entity.[115] This chemical heterogeneity, coupled with limited solubility, made the characterization of melanin notoriously challenging over the years[190].

The presence of melanin on CP was confirmed by Scanning Electron Microscopy (SEM) images obtained in back-scattered electron (BSE) mode (Figure 4.1b). The intensity of the BSE signal is related to the atomic number. Melanin and CP are not distinguishable in BSE SEM images since

they are constituted of carbon and other low-atomic number species. Therefore, to distinguish melanin from CP, we used staining with the salt uranyl acetate, exploiting the well-established property of melanin to chelate cationic species containing heavy metals, such as uranium.[56,191]

The voltammetric current of Mel/CP electrodes has a linear dependence on the scan rate ($i = C\frac{dV}{dt}$, Figure 4.1c, where C is the capacitance) thus suggesting that the Mel/CP electrochemical behavior is pseudocapacitive. Notably, the electrically conducting network of CP permits values of the specific current (current normalized by melanin weight), as high as 5 A/g. The specific capacitance of the Mel/CP electrodes was obtained by normalizing, over the melanin loading, the slope of the plot of the integral of the cathodic current over time *vs*. electrode potential. The gravimetric specific capacity (storable charge per unit weight) was deduced from the cathodic current integrated over time and normalized by the melanin loading (Figure 4.1d). At 5 mV/s, we obtained a specific capacitance of 167 F/g (i.e. 5.6 mF/cm^2), which well compares with values found on high surface area carbons, carbon nanotubes and graphene,[192] and a specific capacity of 24 mAh/g. The specific capacitance and capacity decrease with increasing scan rate, as expected for pseudocapacitive processes, which are affected by the rate of charge transfer/transport and mass transport (diffusion) of counter ions to/from the redox sites. However, faradaic side reactions, potentially contributing to the pseudocapacitive response, cannot be excluded at relatively low scan rates. From the comparison of the electrochemical behavior in different electrolytes, within a pH range compatible with the chemical stability of melanin (APPENDIX A, Figure S1),[193-195] we deduced that the best response is achieved for $NH_4CH_3COO_{(aq)}$ pH 5.5, in agreement with the well-established proton conduction properties of melanin.[113] At pH 5.5, the currents in $NH_4CH_3COO_{(aq)}$ are higher than in $Na_2SO_{4(aq)}$ (this holds true for different $NH_4CH_3COO_{(aq)}$ concentrations). This result suggests possible specific effects of the ions constituting the electrolyte on the electrochemical behavior.[196] NH_4CH_3COO has acido-base properties possibly assisting proton transfer associated to electron transfer. Furthermore, aqueous solutions of the organic salt NH_4CH_3COO are expected to wet the melanin surface better than $Na_2SO_{4(aq)}$, thus promoting the access of the electrolyte to the melanin redox sites. Given that the highest specific capacitance was obtained with $NH_4CH_3COO_{(aq)}$, this electrolyte was selected for further studies of supercapacitors.

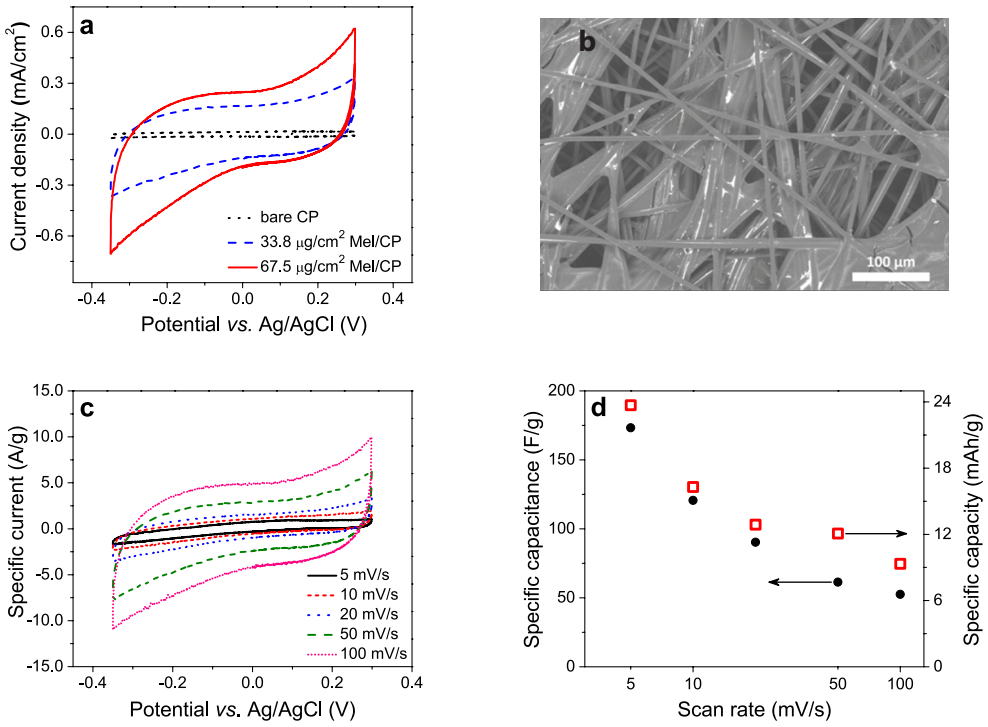

Figure 4.1 (a) Cyclic voltammetry of 33.8 µg/cm^2 and 67.5 µg/cm^2 Mel/CP electrodes and bare carbon paper (CP, control sample) in $NH_4CH_3COO_{(aq)}$ pH 5.5; scan rate 50 mV/s. (b) SEM image, acquired in BSE mode, of a sample made of melanin on carbon paper (CP, loading of ca 0.9 mg/cm^2) stained with uranyl acetate. The bright areas correspond to melanin chelating the uranyl oxycation. Acceleration voltage 10 kV. (c) Cyclic voltammetry of 33.8 µg/cm^2 Mel/CP in $NH_4CH_3COO_{(aq)}$ pH 5.5 at different scan rates. (d) Specific capacitance and capacity *vs.* scan rate of Mel/CP electrodes (33.8 µg/cm^2), in $NH_4CH_3COO_{(aq)}$ at pH 5.5. Geometric size of the samples 0.4 cm^2.

4.4.2 Melanin-based Supercapacitor

The pseudocapacitive properties of Mel/CP electrodes were exploited to demonstrate supercapacitors based on identical positive and negative Mel/CP electrodes, immersed in the electrolyte $NH_4CH_3COO_{(aq)}$ at pH 5.5. Supercapacitors with different melanin loadings were characterized by galvanostatic charge/discharge cycles (Figure 4.2). The profiles of the cell voltage and potentials of the individual electrodes during a galvanostatic charge/discharge cycle at 12.5 mA/cm^2 (i.e. 92.6 A/g, considering the melanin loading of both electrodes) have a

triangular shape. The coulombic efficiency (charge liberated during the discharge divided by charge accumulated during the charge) is 99.7% (Figure 4.2a). These results demonstrate the good reversibility of the charge/discharge process. The capacitance of the supercapacitor, evaluated from the reciprocal of the slope of the cell voltage over the charge liberated during the discharge, is of 0.48 mF/cm^2 (i.e. 3.6 F/g considering the total melanin loading on the two electrodes). The corresponding maximum energy density, E_{max}, is 0.135 mJ/cm^2 and the maximum power density, P_{max}, is 20 mW/cm^2, deduced from the relationships $E_{max} = \frac{1}{2}CV^2$ and $P_{max} = \left(\frac{V^2}{4\times \mathrm{ESR}}\right)$, where C is the cell areal capacitance, V is the cut off voltage (0.75 V) and ESR is the equivalent series resistance (6.8 Ω cm^2).[197]

The charge/discharge rate capability of supercapacitors with Mel/CP electrodes featuring different melanin loadings was investigated by galvanostatic charge/discharge cycles, run at different values of the current density (Figure 4.2b). The capacitance density increased with the increase of the melanin loading from 33.8 to 67.5 μg/cm^2, whereas at 150 μg/cm^2 the performance did not significantly improve, likely due to the relatively low melanin conductivity and to a more difficult access of the electrolyte to the electrode. The supercapacitor with the lowest melanin loading featured the highest retention of the capacitance density that decreased by only 57% by increasing the current density by more than two orders of magnitude, i.e. from 0.125 up to 50 mA/cm^2.

The analysis of the galvanostatic discharge profiles for increasing values of the current density permitted to deduce the energy density ($E = I \int V \cdot dt$, in mJ/cm^2, where I is the current density) and the average power density ($P = E/\Delta t$ in mW/cm^2, where Δt is the discharge time) delivered during a complete discharge. The E and P values were in turn used to build Ragone plots, where the energy density is plotted versus the power density (Figure 4.2c).[52,198,199] For a melanin loading of 33.8 μg/cm^2 we obtained a relatively high value of the power density, i.e. up to 13.2 mW/cm^2, and a relatively low value of the energy density (highest value 0.08 mJ/cm^2). Supercapacitors with 67.5 μg/cm^2 and 150 μg/cm^2 loadings showed similar power density (highest value ca. 9.3 mW/cm^2) and energy density (highest value ca. 0.23-0.25 mJ/cm^2). These results point to the need of efficient and stable electrical contact between the melanin and the carbon current collector, further confirmed by the cycling performance of the supercapacitor (APPENDIX A, Figure S2).

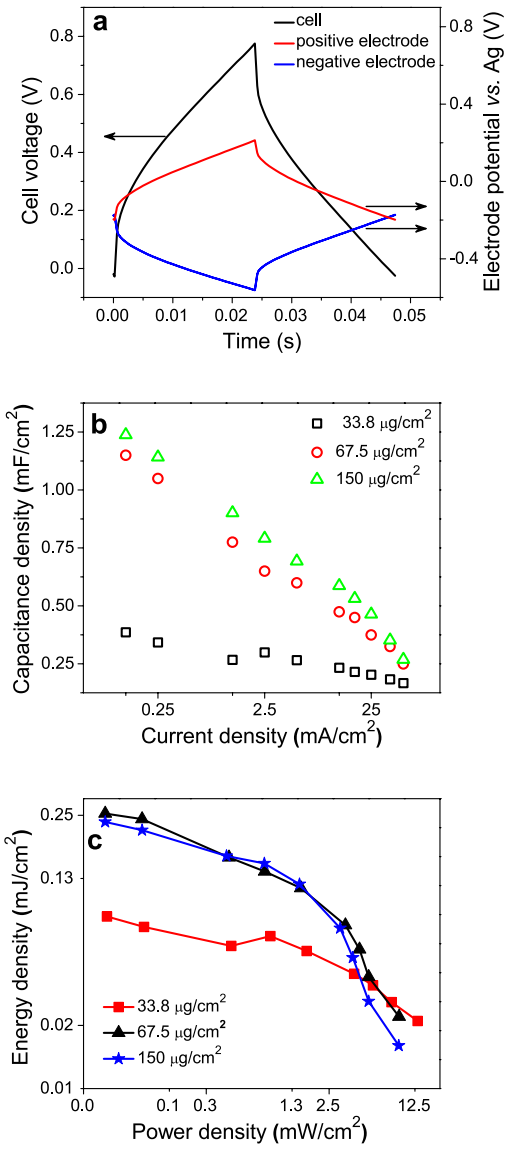

Figure 4.2 Mel/CP supercapacitors with two identical Mel/CP electrodes of equal loadings and with $NH_4CH_3COO_{(aq)}$ pH 5.5 electrolyte. (a) Cell voltage and electrode potential profiles during a charge–discharge galvanostatic cycle (20^{th} cycle) obtained at 12.5 mA/cm^2 with 67.5 μg/cm^2 Mel/CP (each electrode). (b) Capacitance density vs. current density, for three different melanin loadings. (c) Ragone plots extracted from galvanostatic discharge cycles for different melanin loadings with current density of 0.125, 0.25, 1.25, 2.5, 5, 12.5, 17.5, 25, 37.5 mA/cm^2.

We propose the following working principle for our melanin supercapacitors (Figure 4.3). At the positive electrode, during charging (Figure 4.3b), the redox active groups that are in the (semi) reduced form (semiquinone, SQ, and hydroquinone, H_2Q) are oxidized, thus leading to the increase of the concentration of quinone (Q) groups. At the same time, protons and ammonium cations are released in solution and anions (acetate) are incorporated in the electrode material. At the negative electrode, Q and SQ groups are reduced with an increase of the concentration of H_2Q groups. At the same time, anions are released in solution and protons and ammonium cations are incorporated in the electrode material. These processes are reversed during discharging (Figure 4.3c).

With the aim to shed light on the evolution of the chemical features of our melanin-based electrodes after charging and discharging processes, we performed an X-ray photoelectron spectroscopy (XPS) study on the positive electrode of our supercapacitor. Although the results of the high resolution spectra did not permit us to draw an exhaustive and detailed picture, nonetheless they permitted to deduce an increase of the C1s peak associated with the aromatic C=O bonding (binding energy of 287.4 eV), in agreement with the hypothesis of an increased concentration of quinone groups during the charging step (APPENDIX A, Table S2, Figure S3, Figure S4, Figure S5). No significant shift of the position of the N1s and O1s peaks was detected. Such a shift might have been attributed to the formation of new bonds involving O and N atoms, during the charging and discharging steps. The slight, but still significant, increase of the overall N1s concentration after charging with respect to discharging, can tentatively be attributed to the chemical affinity between melanin and NH_3.[196,200] Indeed, $NH_4^+{}_{(aq)}$ is expected to be present as NH_3 in proximity of the positive electrode during the charging step.

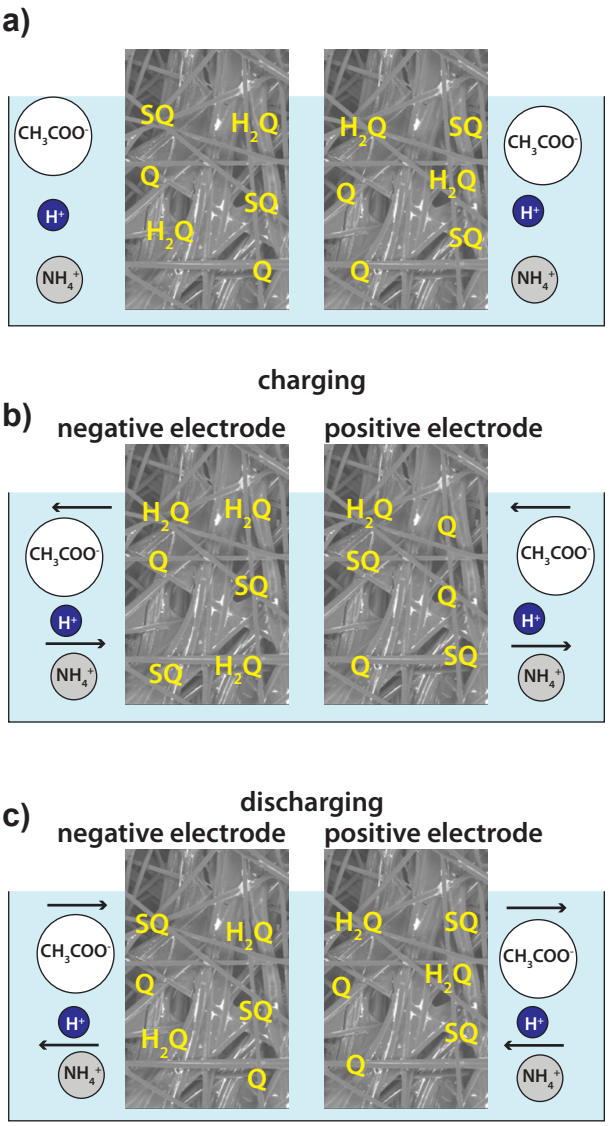

Figure 4.3 Working principle of melanin-based supercapacitors constituted by two identical negative and positive electrodes, immersed in $NH_4CH_3COO^-_{(aq)}$ pH 5.5. a) Situation before a potential is applied between the electrodes, b) situation produced during charging and c) situation produced during the discharging of the electrodes. See Scheme 1 for the chemical structure of H_2Q, SQ and Q groups.

4.4.3 Melanin-based Micro-supercapacitors

The progress in electronics *for everywhere* calls for flexible and conformable microelectromechanical systems (MEMS) with integrated power sources. Flexible supercapacitors have generated enormous interest in recent years. A wide range of devices, based on several electrode/electrolyte combinations, fabricated with lithography or direct write techniques have been reported.[201-207]

We fabricated planar and binder-free micro-supercapacitors on flexible polyethylene terephthalate (PET) substrates (Appendix A, Scheme S1) employing an unconventional and environmentally friendly microfabrication process based on parylene patterning (Figure 4.4).[157,84, 208,209] Pre-cleaned PET sheets (thickness of about 180 μm) were placed on a glass wafer pre-coated with a thin polydimethylsiloxane (PDMS) layer, to ensure flatness and rigidity during the following lithography steps. To facilitate parylene peel-off at the end of the patterning process, a cetyl trimethylammonium bromide (CTAB) solution was spin coated on PET prior to parylene coating. Successively, a 2 μm-thick ParyleneC film was deposited. A positive-tone photoresist was then spun onto parylene and a mask aligner was used to expose it through a photomask featuring the shape of the supercapacitor electrodes. After photoresist development, the unprotected parylene was etched by oxygen plasma and the unexposed photoresist was removed (see Experimental), to leave a patterned parylene layer, which acted as a mask for the patterning of the micro-supercapacitors. The electrode material of the micro-supercapacitors consisted of a slurry of melanin and carbon black (Timcal Super C65, surface area 60 m^2/g) drop-cast on evaporated Ti/Au current collectors (2 mm × 4 mm), with an electrode gap of 200 μm (see Experimental and Appendix A, Scheme S1). After a thermal treatment, the parylene film was peeled off, leaving the patterned micro-supercapacitor (Figure 4.5). A PDMS or glass well was used to confine the electrolyte ($NH_4CH_3COO_{(aq)}$ pH 5.5).

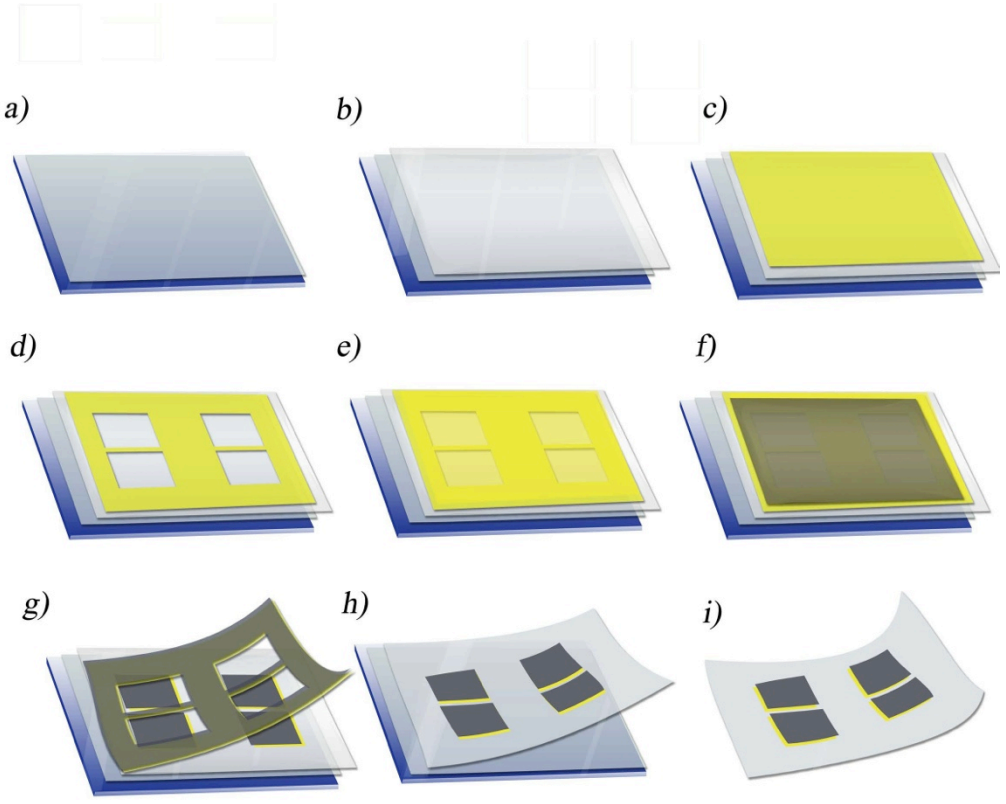

Figure 4.4 Process flow for fabrication of micro-supercapacitors on flexible PET substrates: (a) a glass slide is covered with PDMS; (b) PET is laminated on the glass slide; (c) Parylene C is deposited by chemical vapor deposition; (d) Parylene C is patterned by photolithography and oxygen RIE to generate Parylene C-free regions on PET; (e) Ti (4 nm) and Au (40 nm) are deposited by e-beam evaporation; (f); melanin/carbon black slurry is drop cast; (g) Parylene C is peeled-off; (h) and (i) PET is removed from the glass slide to achieve the final flexible device.

From the voltammograms of micro-supercapacitors on PET (APPENDIX A, Figure S6a and S6b), we deduced the areal, volumetric and gravimetric specific capacitances (APPENDIX A, Figure 4.5b and Figure S6c), at scan rates ranging from 0.01 V/s to 10 V/s. At a scan rate of 0.01 V/s, we deduced a gravimetric specific capacitance of 10.8 F/g, considering the total melanin loading on the two electrodes, and a specific capacity of 1.8 mAh/g (APPENDIX A, Figure S6c), whereas at 10 V/s corresponding values of 2.5 F/g, and 0.4 mAh/g were obtained. Areal and volumetric capacitances of 4.2 mF/cm^2 and 1.7 F/cm^3 were deduced at 0.01 V/s (Figure 4.5b).

The rate response of micro-supercapacitor was investigated by Electrochemical Impedance Spectroscopy (EIS). The Nyquist plot (APPENDIX A, Figure S7a) consists of a high frequency semicircle overlapped to a low frequency tail. The ESR estimated by the Z_r axis intercept of the plot at 100 kHz is 4.5 Ω cm^2. The high frequency semicircle is related to electron transfer processes that give rise to the capacitive response of the electrodes and to the contact resistance between melanin and carbon particles and between melanin and current collector. The areal impedance related to the high frequency semicircle is smaller than 4.5 Ω cm^2, which indicates the good electronic properties of the electrodes. The low frequency tail is almost parallel to the Z_i axis and is representative of the pseudocapacitive behavior of melanin. The Bode plot (APPENDIX A, Figure S7b), given in terms of capacitance normalized to the capacitance exhibited at 10 mHz, where capacitance is obtained at each frequency by the equation C = 1/(Zi2πf), reveals a good frequency response of the micro-supercapacitor. Indeed, the micro-supercapacitor features a pseudocapacitive behavior starting from frequencies as high as 5 kHz.

The galvanostatic charge/discharge characterization of micro-supercapacitors yielded a maximum capacitance of 2.1 mF/cm^2 (i.e. 5.25 F/g) at 0.625 mA/cm^2 (Appendix A, Figure S8 and Figure 4.5c) and an equivalent series resistance (ESR) of 6 Ω cm^2 that well compares with the value estimated by EIS. We obtained E_{max} and P_{max} of 0.6 mJ/cm^2 and 23 mW/cm^2, calculated as previously discussed. The practical energy and power values were evaluated from the galvanostatic discharges at different current densities and reported in a Ragone plot (Fig. 5d): 0.44 mJ/cm^2 and 5.24 mW/cm^2 were the highest values deduced. Ragone plots where the performance of the micro-supercapacitor is normalized with respect to the volume or the area of the micro-supercapacitor are shown in Figure S8b (APPENDIX A). Considering the typical thickness of about 12.5 μm for each of our electrodes, the volume of each electrode in the micro-supercapacitor is ca 1×10^{-4} cm^3. Hence, E_{max} and P_{max} of the flexible melanin-based micro-supercapacitors, normalized to the volume of the two electrodes, are about 0.24 J/cm^3 (68 μWh/cm^3) and 9.4 W/cm^3. In principle, our patterning process permit to microfabricate a "battery" of micro-supercapacitors on the same flexible substrate, thus enabling series/parallel connections for powering small electronics devices. As an example, the three series connected micro-supercapacitors of Figure 4.5a could deliver a maximum power of 5.5 mW at 2.25 V. Our micro-supercapacitor showed 61% retention of the capacitance between the 500^{th} and $20{,}000^{th}$ cycle (APPENDIX A, Figure S9). Within the same range, the supercapacitor showed capacitance

retention of about 40% (APPENDIX A, Figure S2). Despite the fact that a melanin-based supercapacitor is a totally new concept, and as such there is plenty of room to improve its performance, the values of the energy and power density, as well as device stability, compare reasonably well with the those of micro-supercapacitors based on more established materials.[145,210]

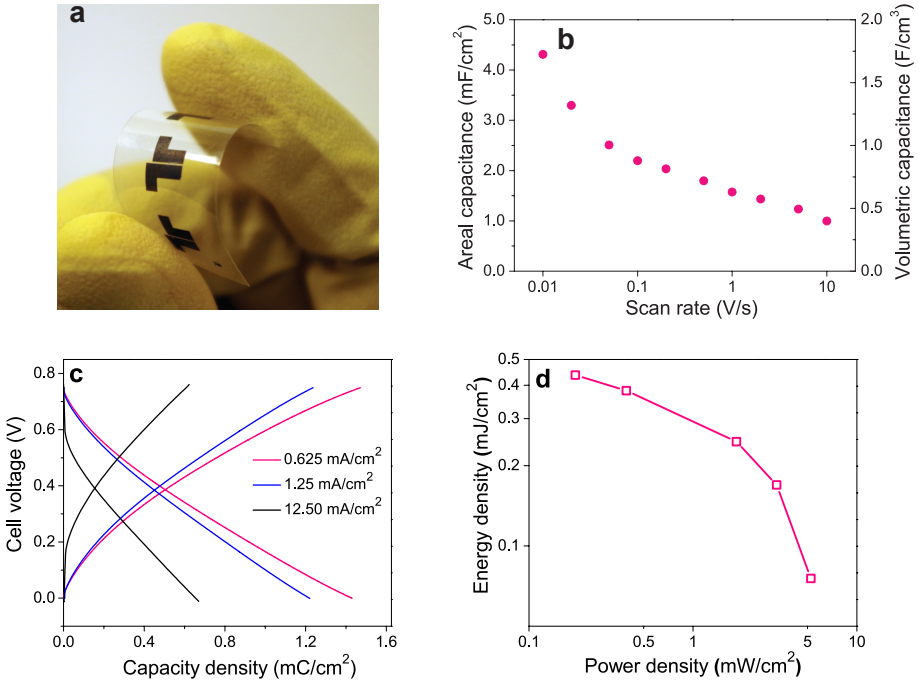

Figure 4.5 Melanin-based flexible micro-supercapacitors with ~200 µg/cm^2 melanin loading on each electrode using $NH_4CH_3COO_{(aq)}$ pH 5.5 as the electrolyte. (a) Optical image of the micro-supercapacitor (total three micro-supercapacitors) on a flexible PET substrate. (b) Areal capacitance and volumetric capacitance vs. scan rate of the cyclic voltammetry (obtained from Figures S10a and S10b) taking into account that the total area of the two electrodes is 0.16 cm^2 and that the corresponding volume is about 2×10^{-4} cm^3 (see Experimental) (c) Galvanostatic charge/discharge cycles with three different values of the current density (0.625, 1.25, and 12.5 mA/cm^2). (d) Ragone plot extracted from the galvanostatic discharge cycles at different values of the current density (0.625, 1.25, 6.25, 12.5 and 25 mA/cm^2). The area of each electrode is 0.08 cm^2.

Preliminary tests performed on the melanin micro-supercapacitors show that no significant change of the voltammetric current occurs upon bending the micro-supercapacitors up to about 50% (APPENDIX A, Figure S110, Scheme S2). The capacitance contribution of carbon Super C-65 in micro-supercapacitors was evaluated by cyclic voltammetry analysis (APPENDIX A, Figure S11). The voltammograms show the higher capacitance of melanin/carbon C-65 compared to carbon Super C-65.

4.5 Conclusions

In summary, we demonstrated supercapacitors and flexible micro-supercapacitors making use of electrodes based on the biocompatible and biodegradable pigment melanin, working in aqueous electrolytes. Melanin-based supercapacitor electrodes are fabricated at room temperature, by easy solution processing, without the need of a high-temperature treatment, unlike the large majority of supercapacitors based on biopolymer-derived electrodes reported to date. In slightly acidic media, a gravimetric specific capacitance as high as 167 F/g (specific capacity of 24 mAh/g) was observed for melanin-based electrodes on carbon paper. A maximum power density of up to 20 mW/cm^2 was deduced for the corresponding melanin supercapacitor. Capitalizing on these results, we demonstrated a binder-free micro-supercapacitor fabricated on flexible polyethylene terephthalate (PET). The microfabrication was performed by unconventional lithography based on ParyleneC patterning. Our flexible micro-supercapacitors showed a power density of 5.24 mW/cm^2 at an energy density of 0.44 mJ/cm^2 and a specific capacitance of 10.8 F/g (about 4.3 mF/cm^2, i.e. 1.7 F/cm^3). Micro-supercapacitors were operated at fast electrode potential scan rates (up to 10 V/s).

The performance of melanin micro-supercapacitors can be further improved by i) using interdigitated finger structures with tuned electrode width, length, interelectrode distance and number of fingers and ii) improving the formulation of the melanin slurry to optimize melanin loading. To achieve a better understanding about the redox sites active during the operation of the (micro-)supercapacitors, we are presently characterizing the electrochemical properties of chemically controlled melanins, e.g. obtained by the solid state polymerization of the DHI building blocks.[210] Our work paves the way to the fabrication of biodegradable/bioresorbable micro-supercapacitors using substrates such as poly(lactic-*co*-glycolic acid) (PLGA) or shellac

and current collectors based on magnesium or iron alloys. Melanin based micro-supercapacitors may serve in biocompatible and biodegradable power sources for applications such as implantable medical devices, wearable electronics and *ubiquitous* sensor networks.

4.6 Experimental Section

4.6.1 Materials

For the microfabrication process, we used glass slides (Corning), Polydimethylsiloxane (PDMS) Sylgard 184 from Dow Corning, PET sheets from Policrom Inc. (Bensalem, PA), CTAB from Sigma Aldrich and Parylene C from SCS Coatings. Photoresist SPR 220 3.0 and stripper PG 1165 were purchased from MicroChem. Developer AZ 726 was purchased from MicroChemicals. Eumelanin, phosphate buffered saline (PBS) tablets, ammonia buffer pH 10, sodium sulfate decahydrate ($Na_2SO_4 \cdot 10H_2O$) were purchased from Sigma-Aldrich. Ammonium acetate and dimethyl sulfoxide (DMSO) were purchased from Caledon Labs. All the materials were used as received. To prepare the solution of ammonium acetate $NH_4CH_3COO_{(aq)}$ pH 5.5, the salt was dissolved in water by sonication to obtain a concentration of 7.5 M and acetic acid was added to adjust the pH to 5.5 (other concentrations of ammonium acetate solutions, at pH 5.5, were also studied following an analogous procedure). The ionic conductivity of $NH_4CH_3COO_{(aq)}$ pH 5.5 was 60.5 mS/cm whereas that one of 0.5 M $Na_2SO_{4(aq)}$ pH 5.5 was 61.3 mS/cm. To prepare the PBS solution, one tablet was dissolved in 200 mL of deionized water. This yields 0.01 M phosphate, 0.0027 M potassium chloride and 0.137 M sodium chloride, pH 7.4, at 25 °C.

4.6.2 Fabrication of Melanin Electrodes on Carbon Paper (Mel/CP Electrodes)

A melanin suspension in DMSO at 3 mg/mL was prepared by mixing in a planetary mixer (Thinky ARM-310) at 2000 rpm for 30 min. Three different loadings of the aforementioned suspension (33.8 μg/cm^2, 67.5 μg/cm^2 and 150 μg/cm^2, normalized with respect to the electrode footprint) were applied by drop-casting melanin on carbon paper (CP, Spectracarb™ 2050A, 10 mils). After drop casting, the samples were dried at 50 °C under vacuum (ca. 40 mbar) for 2 hrs, to facilitate DMSO removal. Mel/CP electrode area is 0.4 cm^2.

4.6.3 Structures of the Supercapacitors and Micro-supercapacitors

For the supercapacitors, two identical electrodes of melanin on carbon paper (Mel/CP) were used as positive and negative electrodes and Ag wire was used as quasi reference electrode. For the micro-supercapacitors, the positive and negative electrodes were made of melanin/carbon black slurry (weight ratio 4/1, i.e. 16 mg of melanin and 4 mg of conductive carbon Super C-65 in 1 ml DMSO) deposited on Au electrodes (see below). The capacitive performance of carbon Super C-65 was evaluated by cyclic voltammetry in a three-electrode cell. Melanin/carbon Super C-65 (weight ratio 4/1 - 96 μg of melanin and 24 μg of carbon Super C-65) and pure carbon Super C-65 (24 μg) in DMSO were deposited on Au and used as working electrodes in the electrochemical cell. The electrode area was 0.36 cm^2.

4.6.4 Unconventional Lithography Steps for Micro-supercapacitors on Plastics

To fabricate flexible micro-supercapacitors on plastic, polyethylene terephthalate (PET) substrates were cleaned by sequential sonication in acetone, isopropanol, and de-ionized (DI) water, dried using a nitrogen flow and laminated on a cleaned glass wafer pre-covered with a polydimethylsiloxane (PDMS) adhesive layer, which was used to ensure the PET flatness and rigidity during the successive patterning steps. An aqueous solution of CTAB (10^{-3} M) was spun on PET to enable parylene delamination at the end of the process. The PET substrates were then transferred to a system for parylene-C deposition (SCS coating). After ParyleneC deposition, a positive tone photoresist (MEGAPOSIT SPR 220.3) was spin-coated on Parylene C, then exposed to the UV light of the Karl Suss MA-6/BA-6 mask aligner (wavelength 365 nm) through a photomask and developed by immersion in AZ-726 to open windows on Parylene C. The unprotected Parylene C was then etched by oxygen reactive ion etching (RIE) and the photoresist remaining on Parylene C film was removed by immersing the samples in PG 1165 remover. Subsequently, 4 nm Ti and 40 nm Au were deposited on the patterned samples by E-beam evaporation, followed by a drop casting of melanin/carbon black slurry for micro-supercapacitors (see above). After a soft baking at 40ºC under vacuum (30 mmHg for 20 minutes), the Parylene C layer on PET was slowly peeled off, leaving patterned melanin micro-supercapacitors on PET. The fabrication process was completed by peeling-off PET from the PDMS/glass substrate. The area of each electrode is 0.08 cm^2, the thickness of the coating about 12.5 μm and the inter electrode distance is 200 μm (Scheme S1).

4.6.5 Electrochemical Set-up

Cyclic voltammetry (CV) was performed using a Versa STAT 3 potentiostat (Princeton Applied Research) in a three-electrode cell, where Mel/CP was the working electrode, Pt foil the counter electrode and $Ag/AgCl_{(aq)}$ the reference electrode. Galvanostatic charge/discharge cycles in the supercapacitor and micro-supercapacitor structures were performed using a Biologic VSP 300 multichannel potentiostat.

4.6.6 X-ray Photoelectron Spectroscopy (XPS)

High-resolution XPS analysis was carried out with a VG ESCALAB 3 MKII instrument under Mg Kα radiation by applying 300W (15 kV, 20 mA) power. The pressure in the chamber during the analyses was 5.0×10^{-9} Torr. The high resolution spectra were acquired with a pass energy of 20 eV and electrons were collected at a 90 deg takeoff angle. Peak fitting was performed with symmetrical Gaussian-Laurentzian product functions after Shirley background subtraction. Wagner sensitivity factors were used to normalize the peak intensities for quantification.

4.6.7 Scanning Electron Microscopy (SEM)

SEM was performed at an acceleration voltage of 10 kV in backscattered electron (BSE) imaging mode using a FEI Quanta 450 Environmental Scanning Electron Microscope (FE-ESEM). Staining was achieved by exposing the samples (30 μL of a suspension of 12 mg/ml of melanin in DMSO poured on an area of 1 cm×0.4 cm leading to a final loading of ca 0.9 mg/cm^2) to an aqueous solution of uranyl acetate (2%) for 3 minutes followed by rinsing with deionized water for 5 minutes.

4.7 Acknowledgments

The authors are grateful to Y. Drolet, D. Pilon and C. Clement for technical assistance, to Prof. H. Vali and Dr S. K. Sears for SEM investigations and to Dr J. Lefebvre for XPS studies. Funding for this project was provided by grants *NSERC Discovery* (F. C. and C. S.), FRQNT *Équipe* (F.C. and C. S.) and FRQNT *Établissement de Nouveau Chercheur* (F.C.). S.Z. is grateful to NSERC for financial support through a Vanier Canada Graduate Scholarship. F.S. acknowledges financial support from Università di Bologna (Research Mobility Program)

and the Embassy of Canada (2015 Canada-Italy Innovation Award). This work is supported by CMC Microsystems through the MNT Financial Assistance and CMC Solutions programs.

CHAPTER 5 ACTIVATED CARBON GATE ELECTRODES FOR ORGANIC ELECTROCHEMICAL TRANSISTOR (OECT)

The chapter deals with the investigation of high specific surface area activated carbon as the gate electrode material for organic electrochemical transistors (OECTs). In order to understand the role of gate electrodes in OECT performances, we have considered one of my shared first author articles "Conducting Polymer Transistors Making Use of Activated Carbon Gate Electrodes", by Hao Tang, Prajwal Kumar, Shiming Zhang, Zhihui Yi, Gregory De Crescenzo, Clara Santato, Francesca Soavi, and Fabio Cicoira, which published in " ACS Applied Materials and Interfaces" in 2014 as a reference.

Several types of gate electrodes such as Pt, Au, Ag, Ag/AgCl and patterned PEDOT:PSS films for OECT have been reported.[84,87,91] We studied activated carbon (AC) as a gate electrode. Activated carbons are charcoal based materials with high degree of porosity and with high surface area that found many applications in wastewater treatment, solvent recovery, air purification and in different industrial processes as porous electrode material.

OECTs consist of source and drain electrodes and a channel containing the conducting polymer PEDOT:PSS in ionic contact with a gate electrode via an electrolyte solution (Figure 5.1). PEDOT:PSS, because of its high conductivity, leads to OECT working in depletion mode. The conductivity of PEDOT:PSS films ranges from a few hundreds to few thousands S cm^{-1}.[82]

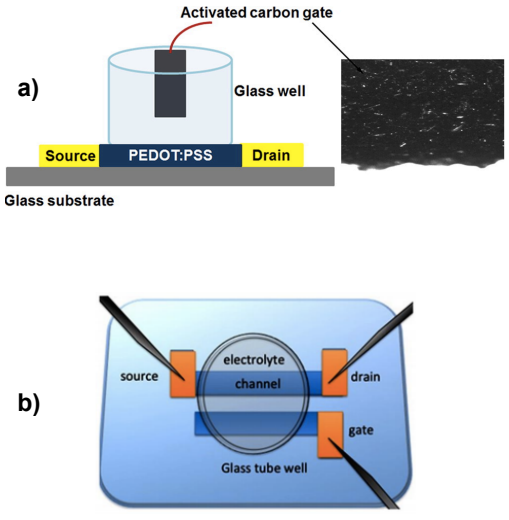

Figure 5.1 Scheme of the architecture of OECT using a conducting polymer channel made of

PEDOT:PSS with a) AC gate electrode and b) PEDOT:PSS gate.[93] Reprinted with permission.

5.1 Fabrication of Organic Electrochemical Transistors

The devices were fabricated on cleaned glass wafers as described in the literature [84,96]. "Metal contacts (4 nm of Ti and 40 nm Au) were patterned with standard photolithography (using a photoresist AZ 5214), followed by metal evaporation by e-beam and lift-off using PG remover 1163."[211] PEDOT:PSS channels were patterned using Parylene C. Parylene C was deposited by chemical vapor deposition to form a 1.2 μm thick film. To define the channel, a second layer of photolithography step was carried out on Parylene by using photoresist SPR 220 3.0. After photoresist development, parylene was etched by an oxygen reactive ion etching plasma. The PEDOT:PSS processing mixture was spin coated onto the substrate in order to achieve 100 nm PEDOT:PSS film. The electrolyte confined by using a glass ring.

In OECT, the current flowing in the channel between the drain and source electrodes (I_{ds}) is modulated by the gate-source voltage (V_{gs}). A high current modulation is essential for bioelectronic applications, which require low-voltage operation and high sensitivity.[68] In order to achieve higher current modulation, it is essential to explore the influence of gate electrode on channel current modulation. We have discussed two types of gate electrodes: i) PEDOT:PSS films ii) high surface area activated carbon electrode.

5.2 Preparation of PEDOT:PSS processing mixture

"For the preparation of the PEDOT:PSS films, 20 mL of aqueous dispersion (Clevios PH-1000 from Heraeus GmbH) were mixed with ethylene glycol (1 mL) and dodecyl benzene sulfonic acid (DBSA, 50 μL), to enhance conductivity and film forming properties, and with 1 wt% of (3-glycidyloxypropyl) trimethoxysilane (GOPS), to crosslink the films for stable operation in aqueous conditions".[211]

5.3 Preparation of the activated carbon electrodes

"The AC gate electrodes were prepared using carbon paper (Spectracarb 2050, 10 mils) coated with an ink of activated carbon (PICACHEM BP9, 28 mg/mL) and Nafion binder (2.4 mg/mL) dissolved in isopropanol (the amount of solution was about 80 µL). The coating was followed by thermal treatment at 60 °C for 1 hour to remove the solvent. For OECT gate electrodes we used carbon paper stripes having a geometric area of about 12 mm^2 when immersed into the electrolyte (similar to that of the PEDOT:PSS gate and channel)".[211]

5.4 Organic Electrochemical Transistor characterization

The performance of OECTs based on PEDOT:PSS using PEDOT:PSS and AC gate electrodes are shown in Figure 5.2. The typical output characteristics of PEDOT:PSS OECT using AC gate electrodes are shown in Figure 5.2 A and compared to those of OECTs with planar PEDOT:PSS gate electrodes in Figure 5.2 B.

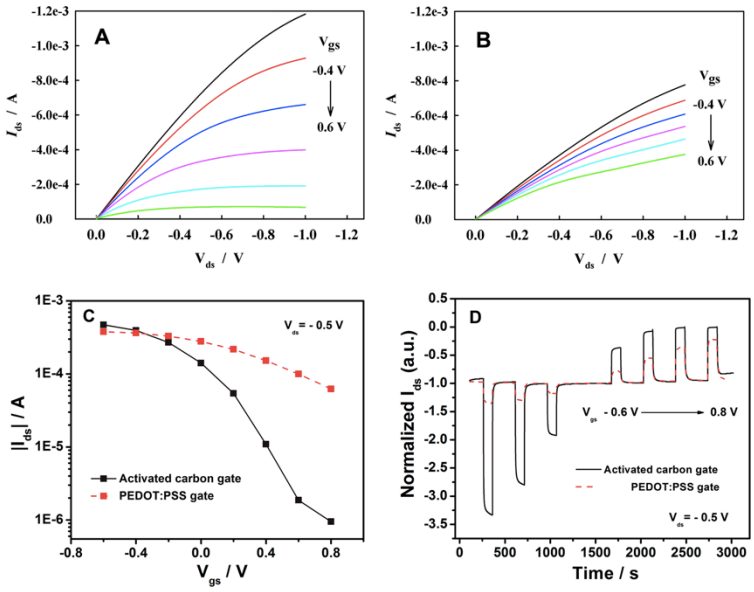

Figure 5.2 Characteristics of PEDOT:PSS based OECT using AC and PEDOT:PSS gate electrodes, employing an aqueous solution of NaCl (0.01M) as the electrolyte. Typical output characteristics obtained with an AC (A) or a PEDOT:PSS gate electrode (B). The V_{ds} scan rate is 5 mV/s and V_{gs} is varied from −0.4 to +0.6 V in steps of 0.2 V. Transfer characteristics (C) of

PEDOT:PSS OECTs using an AC (black line) and a PEDOT:PSS gate electrode (red line) at V_{ds}= −0.5 V and −0.6 V ≤ V_{gs} ≤ 0.8 V. Transient (I_{ds} vs time) responses (D) normalized with respect to the current at V_{gs}= 0 V of OECTs using AC (black solid line) and PEDOT:PSS (red dashed line) gate electrodes at V_{ds}= −0.5 V. From left to right, V_{gs} is pulsed from 0 to −0.6, −0.4, −0.2, +0.2, +0.4, +0.6 and +0.8 V with pulse duration of 100 s.[93] Reprinted with permission. Copyright © 2014 American Chemical Society.

OECTs with AC gate electrodes show larger I_{ds} modulation with respect to those using PEDOT:PSS. For instance, for the output characteristics of OECTs at V_{ds} = − 0.4 V, upon variation of V_{gs} from − 0.4 to +0.6 V with a step of 0.2 V, the I_{ds} of OECT using AC varies by about a factor of 10, while that of the devices using PEDOT:PSS gate electrodes varies by about a factor of 3. Also, devices using AC gates saturate at V_{ds} ≈ − 0.2 V, whereas devices using PEDOT:PSS gates do not show saturation even at higher |V_{ds}|. The further confirmation of higher I_{ds} modulation with AC gate electrodes was achieved through the transfer (Figure 5.2 C) and transient (I_{ds} *versus* time, Figure 5.2 D) characteristics. For AC gate electrodes the shown higher ON/OFF ratio is about 500, whereas OECT PEDOT:PSS based gate show an ON/OFF ratio of about 15. The transient characteristics reveal that, the I_{ds} during de-doping of PEDOT:PSS channel (*off current)* at given V_{gs}, is significantly higher for OECT with an AC gate (Figure 5.2 D, black solid line) than that of OECT with a PEDOT:PSS gate (Figure 4.2 D, red dashed line). The use of high specific surface area AC gate electrodes in OECTs is expected to enable to counterbalance the charge required to dedope/dope the channel within a relatively narrow electrode potential excursion, by a fast and highly reversible electrostatic process.

The current modulation exclusively depends on the electrolyte potential (V_{sol}), which is the potential acting on the OECT channel upon the application of V_{gs}, defined by $V_{sol} = \frac{V_{gs}}{1+\frac{C_{ch}\,A_{ch}}{C_g\,A_g}}$

Where C_{ch} and C_g are the channel and gate capacitance, A_{ch} and A_g are the channel and gate areas respectively.[83] In these conditions, when the area and capacitance of channel is comparative with the capacitance of gate (case of PEDOT:PSS gate), the potential drop takes place between the gate electrode and the electrolyte, which results in a weak modulation of the channel current. In the case of high area gate electrode with high capacitance (as it is the case for AC gate), the

electrolyte potential is almost equal to the bias at the gate. This implies that the drop of potential takes place close to channel, which results in a greater modulation of channel current. AC gates that feature higher specific areas than PEDOT:PSS, result in relatively high gate currents (Figure 5.3 A).

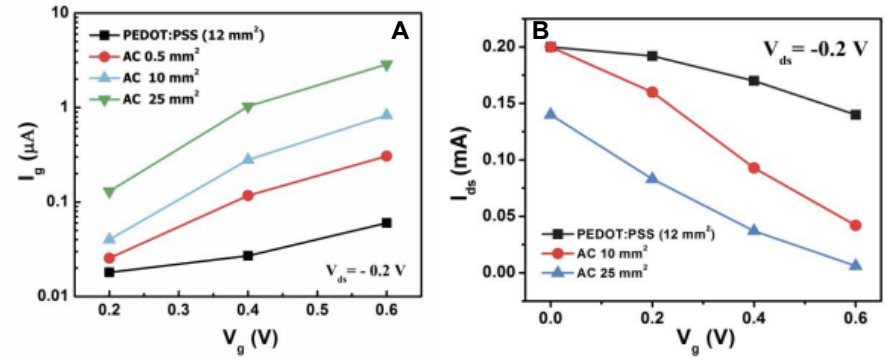

Figure 5.3 (A) Steady state gate-source current (I_{gs}) of OECTs with PEDOT:PSS (black line) and AC of different geometric areas as gate electrodes. (B) Comparison of transfer current modulations for devices using AC gate electrodes of different geometric areas and a PEDOT:PSS gate electrode. An aqueous solution of NaCl (0.01 M) is used as the electrolyte.[211] Reprinted with permission. Copyright © 2014 American Chemical Society.

Interestingly, the decrease of I_{gs} of OECT is observed with the decrease of geometric surface area of the AC gate (Figure 5.3 A). However, the current modulation is independent of geometric area of the AC electrode (Figure 5.3 B).Therefore, the AC gate area and mass loading need to be properly optimized to reduce gate currents".[211]

In summary, we investigated PEDOT:PSS OECT using high specific surface area AC gate electrodes. The use of AC gate electrodes leads to higher current modulations, at low voltage, compared to PEDOT:PSS gate electrodes. AC gate current I_{gs} of OECT increase with increasing the geometric surface area of AC but the current modulation remains same and higher for AC electrode. In order to reduce the to reduce gate currents, AC gate area and mass loading need to be optimized.

CHAPTER 6 EUMELANIN ELECTROCHEMISTRY: COMPLEMENTARY RESULTS

Chapter 6 is focuses on my research contribution to the study of electrochemical properties of melanin (from coauthored articles). In particular, this chapter is includes some parts of the recently published article (shared first author) in *Polymer International* (2016) "Novel insights on the physicochemical properties of eumelanins and their DMSO derivatives" by L .GS Albano, E. Di Mauro, P. Kumar, F. Cicoira, C. FO Graeffa, and C. Santato, some of the supplementary results of the article were published in *Journal of Materials Chemistry C* (2016) "Melanin-based flexible supercapacitors" by P. Kumar, E. Di Mauro, S. Zhang, A. Pezzella, F. Soavi, C. Santato and F. Cicoira, electrochemistry part of coauthored article was published in *Chemistry of Materials* (2015) "Protonic and electronic transport in hydrated thin films of the pigment eumelanin" J. Wünsche, Y. Deng, P. Kumar, E. Di Mauro, E. Josberger, J. Sayago, A. Pezzella, F. Soavi, F. Cicoira, M. Rolandi and C. Santato.

As we discussed in the chapter 4, biopigment eumelanin is composed of chemically heterogeneous macromolecules based on the 5,6-dihydroxyindole (DHI) and 5,6-dihydroxyindole-2-carboxylic acid (DHICA) building blocks and their various redox forms. The building blocks are randomly cross-linked to form planar sheets, stacked through aromatic π-interactions.[104,159] The molecular randomness in the arrangement of eumelanin challenges the scientific community to reveal the structure-electroactivity properties. Further, the gaining insight into the electrochemical properties of melanin-based electrodes can be beneficial to design eumelanin-based technologies for bioelectronics and sustainable electronics. In this chapter, eumelanins with three different synthetic routes were investigated. Namely, eumelanin obtained from Sigma Aldrich (which is synthesized through oxidation of tyrosine) is known as Sigma melanin, chemically controlled eumelanins,[210] obtained by the in situ polymerization of the DHI building blocks and DHICA building blocks are known as DHI melanin and DHICA melanin respectively. In addition, dimethyl sulfoxide (DMSO) functionalized DHI monomer is polymerized known as DMSO melanin has investigated. To shed light on possible redox processes at the eumelanin electrodes, cyclic voltammetry (CV) measurements were conducted on films of Sigma melanin, 5,6-dihydroxyindole (DHI) melanin and 5,6-dihydroxyindole-2-carboxylic acid (DHICA) melanin and DMSO melanin in a conventional electrochemical cell.

There are three important aspects taken into consideration while investigating melanin for electrochemistry.

i) Irreversible oxidation peaks during the first CV cycle

ii) The electrochemical study of more controlled counter part of Sigma melanin i.e., DHI and DHICA melanin

ii) The influence of reversible cationic binding property of two –OH groups of catechol (in Sigma melanin) through comparative electrochemical study of sigma melanin and DMSO melanin

6.1 Electrochemical set-up

Cyclic voltammetry (CV) was performed using a Versa STAT 3 potentiostat (Princeton Applied Research) in a three-electrode cell, where Mel/CP was the working electrode, Pt foil the counter electrode and $Ag/AgCl_{(aq)}$ the reference electrode. Galvanostatic charge/discharge cycles in the supercapacitor and micro-supercapacitor structures were performed using a Biologic VSP 300 multichannel potentiostat.

6.2 Irreversible oxidation peak

Eumelanin thin films were deposited from a suspension of synthetic eumelanin (Sigma-Aldrich) in dimethyl sulfoxide (sonicated and filtered) by spin coating (1 min at 1000 rpm for 30 s at 4000 rpm, 30 mg/mL suspension). Solutions of DHI and DHICA in methanol (30 mg/mL) were spin-coated on ITO substrates using a rotation speed 2000 rpm for 1 minute and exposed under aerial polymerization using ammonia as a catalyst.

Sigma melanin (eumelanin), and melanin with controlled chemical composition on ITO were explored as working electrodes for CV measurements in PBS buffer (0.01 M) of pH 7.4. An intense oxidation peak was observed for all the samples at about 0.5 V *versus* SCE (Figure 6.1). This peak has an irreversible character. The irreversibility of the oxidation peak likely originates from the covalent coupling (intramolecular reticulation) of the intermediate species formed at the

positive electrode. Indeed, radicals and quinone species of building blocks formed by the oxidation of DHI moieties are reactive and may undergo coupling processes with other radicals and nucleophilic counterparts.[113]

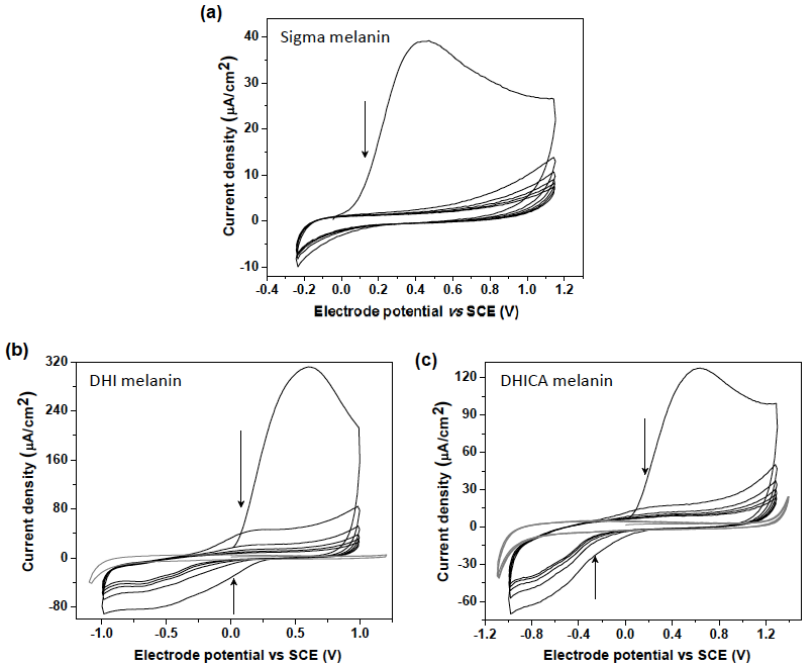

Figure 6.1 Cyclic voltammetry of (a) Sigma melanin, (b) DHI melanin, (c) DHICA melanin on ITO substrates as working electrode, platinum foil and saturated calomel electrode as the counter and the reference electrodes, respectively. Nitrogen purged PBS buffer (0.01 M) of pH 7.4 is used as the electrolyte and a 50 mV s^{-1} scan rate is maintained. The cyclic voltammogram of ITO without melanin in PBS is represented in gray. Black arrows indicate the decrease in current density as a function of the number of cycles.[113]

6.3 Melanin on carbon paper electrodes

The capability of melanin to store charge was initially assessed by cyclic voltammetry, using electrodes consisting of melanin drop cast on conductive carbon paper (indicated henceforth with Mel/CP).

6.3.1 Fabrication of melanin electrodes on carbon paper (Mel/CP electrodes)

A melanin suspension in DMSO at 3 mg/mL was prepared by mixing in a planetary mixer (Thinky ARM-310) at 2000 rpm for 30 min. Melanin with loading of 33.8 μg/cm^2, (normalized with respect to the electrode footprint) were applied by drop-casting on carbon paper (CP, Spectracarb™ 2050A, 10 mils). After drop casting, the samples were dried at 50 °C under vacuum (ca. 40 mbar) for 2 hrs, to facilitate DMSO removal. The area of electrodes Mel/CP is 0.4 cm^2.

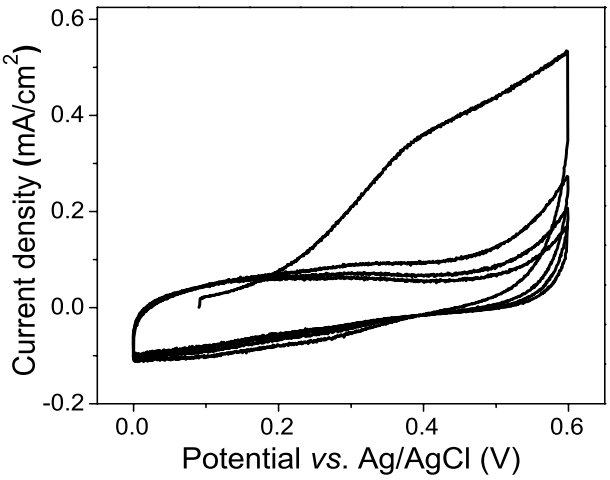

Figure 6.2 Cyclic voltammograms (first three cycles) of a Mel/CP electrode (33.8 μg/cm^2 melanin loading, normalized over the electrode footprint) in NH_4CH_3COO(aq) at pH 5.5, at 50 mV/s. A broad anodic peak, with irreversible characteristics, is observed during the first cycle of the cyclic voltammetry of Mel/CP. Pt foil used as counter electrode.

Similar to melanin on ITO electrode, the irreversible oxidation peak is observed during the first cycle. However unlike ITO electrode, CP electrodes showed significant capacitive current. This is due to the porous nature and high surface area of CP electrodes.

The voltammetric current of Mel/CP electrodes has a linear dependence on the scan rate ($i = C\frac{dV}{dt}$, Fig. 1c and Fig. S2, where C is the capacitance) thus suggesting that the Mel/CP electrochemical behavior is pseudocapacitive as shown in the Figure 6.3.

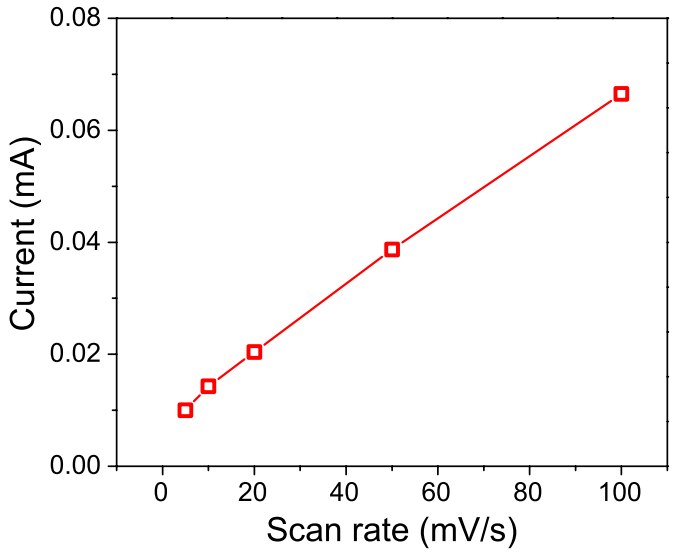

Figure 6.3 Anodic current at 0 V (*versus* Ag/AgCl) *versus* scan rate, obtained from the cyclic voltammograms of Mel/CP with 33.8 µg/cm^2 melanin loading in $NH_4CH_3COO_{(aq)}$ pH 5.5.

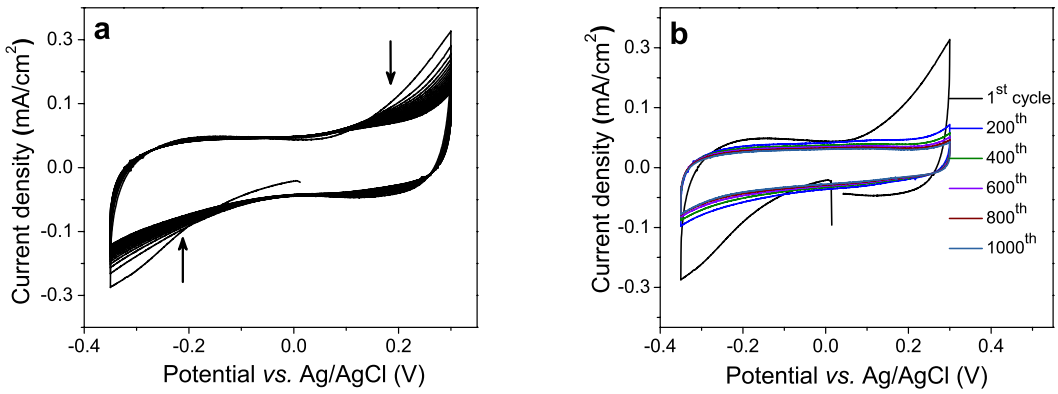

Figure 6.4 Cycling stability of 33.8 µg/cm^2 Mel/CP in $NH_4CH_3COO_{(aq)}$ pH 5.5 at 50 mV/s. (a) 1,000 voltammetric cycles and (b) cyclic voltammograms extracted from (a) every 100 cycles.

The cycling stability of Mel/CP (with 33.8 μg/cm^2 loading) in $NH_4CH_3COO_{(aq)}$ at pH 5.5 was investigated (Figure 6.4). The values of the capacitance calculated for the 2nd cycle and 1,000th cycle are 1.98 mF/cm^2 (58.7 F/g) and 1.46 mF/cm^2 (43.3 F/g), i.e. a 26 % loss in the capacitance is observed over cycling.

6.3.2 The influence of aqueous electrolytes on the performance of Mel/CP electrodes

In addition to the $NH_4CH_3COO_{(aq)}$ at pH 5.5 electrolyte, aqueous sodium sulfate at pH 5.5, phosphate buffer saline at pH 7.4 and ammonia buffer at pH 10 were investigated (Figure 6.5). From the comparison of the electrochemical behavior in different electrolytes, within a pH range compatible with the chemical stability of melanin (Figure 6.5d) we deduced that the highest response is achieved for $NH_4CH_3COO_{(aq)}$ pH 5.5, in agreement with the well-established proton conduction properties of melanin.

The cathodic wave observed below -0.2 V *vs.* Ag/AgCl in ammonia buffer pH 10 (Fig. 6.5c) can be partly attributed to the reduction of O_2 possibly present in limited amount in our N_2 degassed cell.[193, 194] The electrocatalytic effect of hydroquinone species on O_2 reduction in alkaline solutions has already been reported.[195]Therefore the measurements performed at pH 10 might lead to an overestimation of the capacitance.

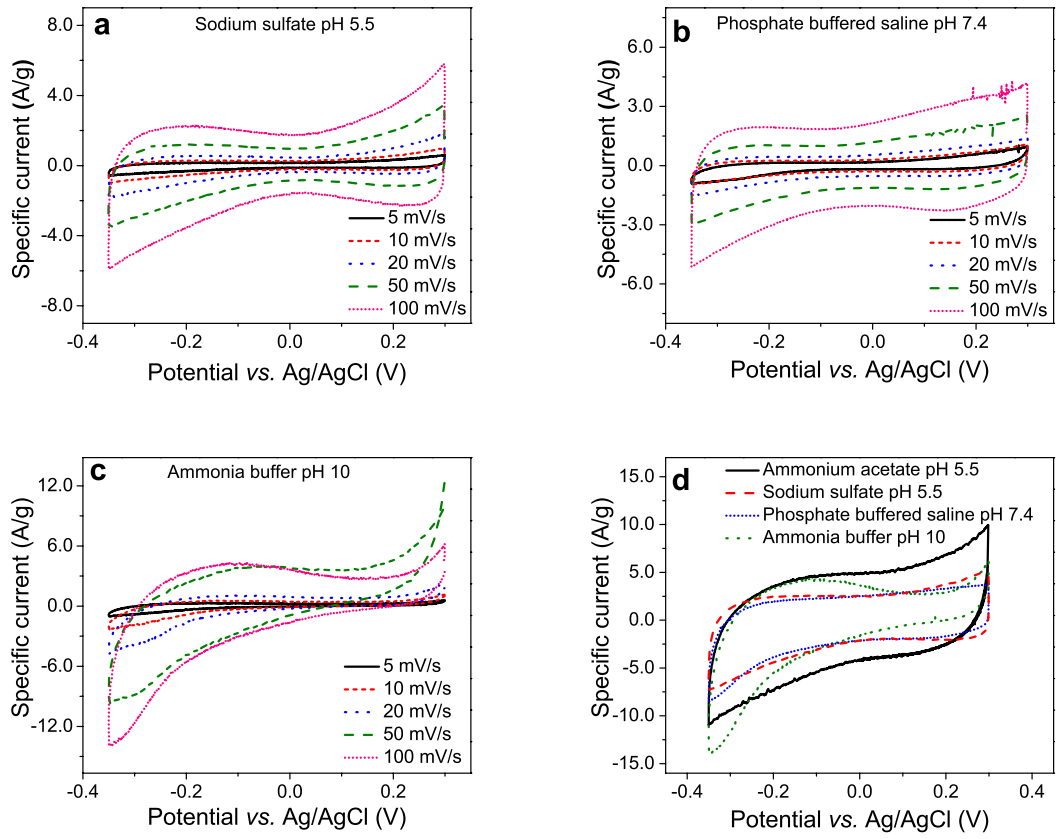

Figure 6.5 Cyclic voltammograms at different scan rates of Mel/CP electrodes (33.8 µg/cm^2 loading of melanin) in (a) sodium sulfate at pH 5.5, (b) phosphate buffered saline at pH 7.4 and (c) ammonia buffer at pH 10 (see Experimental in main text). Geometric size of samples 0.4 cm^2. (d) Cyclic voltammograms of Mel/CP electrodes (33.8 µg/cm^2 loading of melanin) at 100 mV/s.

6.4 Sigma melanin comparison with DMSO melanins

A comparative study was performed to gain insight on the electrochemical activity of DMSO melanin with respect to the commercially available, non-derivatized, Sigma melanin, prepared by oxidation of tyrosine with hydrogen peroxide. Similarly, The oxidation of L-DOPA with benzoyl peroxide in DMSO leads to the synthesis of DMSO melanin, with good solubility in DMSO, functional for the production of high quality films. Increasing the temperature during the synthesis of the DMSO melanin significantly increases the reaction rate and induces the decarboxylation of DHICA, thus increasing the number of positions available in the molecule for polymerization.

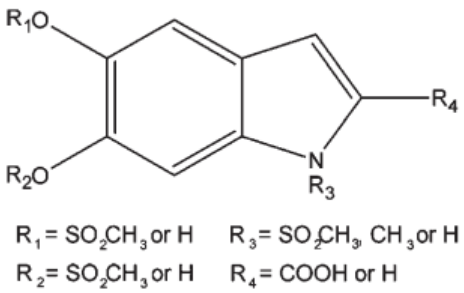

Figure 6.6 Building blocks of DMSO melanins.[212]

To gain insight into the electron transfer properties of Sigma melanin, DMSO melanin RT and DMSO melanin 100 °C, their electrochemical behavior was investigated by cyclic voltammetry. Cyclic voltammetry measurements were performed using Mel/CP working electrodes fabricated using Sigma melanin, DMSO melanin synthesized in room temperature (DMSO melanin RT) melanin synthesized at 100 °C (DMSO melanin 100 °C). Aqueous Ag/AgCl as a RE, Pt foil as CE and electrolyte $NH_4CH_3COO_{(aq)}$ pH 5.5 were considered for the investigation.

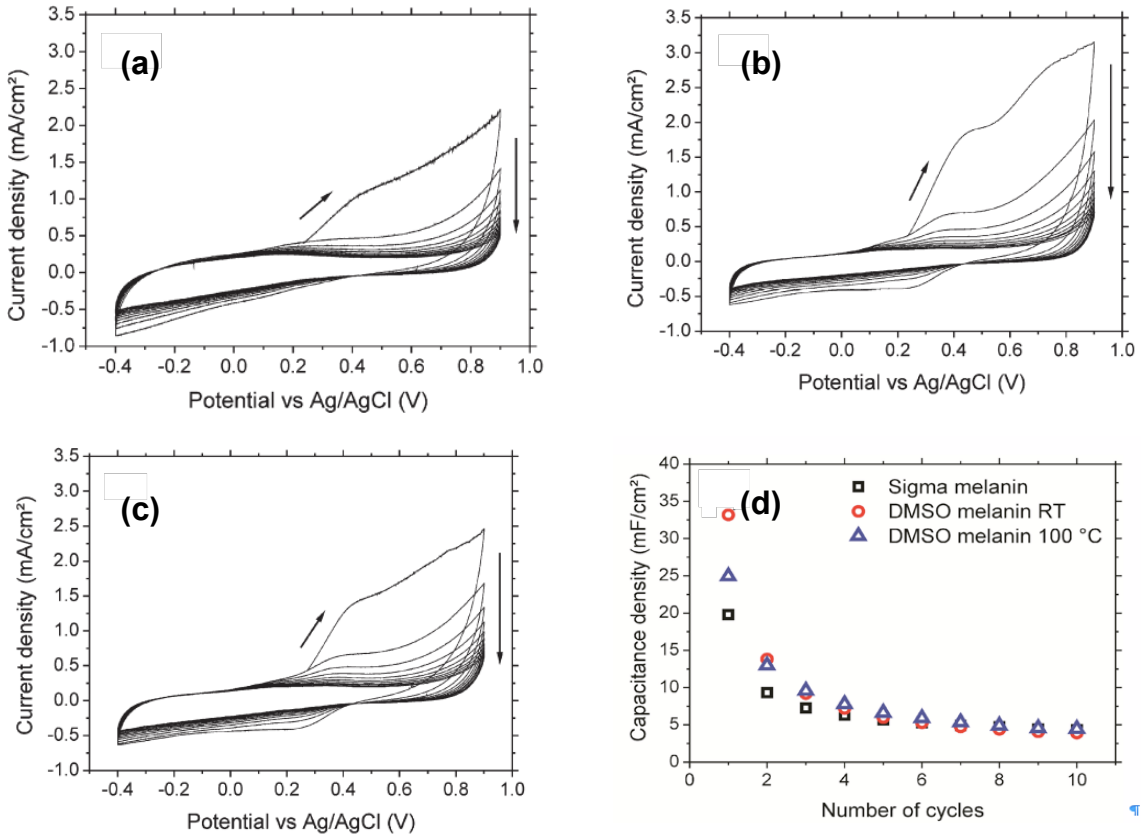

Figure 6.7 Cyclic voltammograms (total 10 cycles) of (a) Sigma melanin (b) DMSO melanin RT and (c) DMSO melanin 100 °C and (d) capacitance values evaluated from the CV. 120 µg/ cm^2 of melanin on carbon paper is the loading in the working electrode. $NH_4CH_3COO_{(aq)}$ 7.5 M (pH 5.5) was used an electrolyte, carbon paper strips were used also as counter electrode; scan rate 50 mV/s; the geometric area of the working electrode was 0.25 cm^2.

During the first two to three voltammetric cycles, a broad, irreversible anodic response has observed between 0.25 and 0.9 V *vs.* Ag/AgCl, irrespective of thee type of melanin and electrolyte (Figure 6.7). The cyclic voltammograms of DMSO melanin RT and DMSO melanin 100 °C show a shoulder (for the first three to four cycles) located at about 0.4 V *vs.* Ag/AgCl (Figure 6.7b & 6.7c). The difference in the cyclic voltammograms of DMSO melanins with respect to Sigma is probably due to the sulfonate termination. The contribution due to the possible oxidation of species susceptible to polymerization at the positive electrode, already discussed for Sigma melanin, has to be contemplated even for the DMSO melanins.

The quinone moieties present in the DHI and DHICA building blocks are known for their reversible cation binding from the electrolyte and has the ability to store $2e^{-}/2H^{+}$ per quinone, are responsible for pseudocapacitive behavior eumelanin. In DMSO melanin, the redox activity is expected to deteriorate due to functionalization of building blocks by DMSO. Interestingly, the measured capacitances of first 10 CV cycles are higher for DMSO melanins than Sigma melanin (Figure 6.7d). This may be due to fact that, sulfonate and sulfonamide groups of DMSO melanin also contributed for monovalent cation binding from the electrolyte. Further investigation will be needed to understand this phenomenon.

CHAPTER 7 GENERAL DISCUSSION

During my Ph.D., I explored the polymers PEDOT:PSS and eumelanin as materials featuring biocompatibility, for electronics and energy storage. This chapter is a general discussion of the results achieved in during the PhD.

From the point of view of their molecular structures, there are both differences and analogies between PEDOT:PSS and melanin. PEDOT:PSS is a thiophene-based conducting polymer, whereas eumelanin is made up of indole-based building blocks. PEDOT:PSS is a well-known p-type conducting polymer with electrical conductivity typically ranging from 100-1000 S/cm. On the other hand, eumelanin is believed to be a mixed electronic-ionic conductor rather than an amorphous semiconductor, and its electrical conductivity is pretty low (in the order of 10^{-11}-10^{-5} S/cm). For PEDOT:PSS, co-solvents, such as ethylene glycol, glycerol, DMSO need to be added to achieve high conductivity. The conductivity of melanin increases upon hydration of the biopolymer. The details of the molecular structure of PEDOT:PSS are well known while those of eumelanin are still under debate. PEDOT:PSS is essentially an ionomer where electrostatic interactions between PEDOT and PSS, hold PEDOT:PSS together. The intrinsic conductivity of PEDOT:PSS depends, among others, on the number of PSS polyanions electrostatically interacting with the PEDOT chain. The diethoxy substituents makes PEDOT chemically stable, due to the fact that the diethoxy substituents replace extra hydrogen atoms, likely responsible for synthetic defects. The electron donating nature of the pendant oxygen atoms of diethoxy substituents facilitate the delocalization of π conjugated system of doped state of PEDOT, which not only improves the stability of PEDOT:PSS against the atmospheric oxygen and humidity but also improves the conductivity of the polymer.

Martin et al., observed that there are certain structural similarities between PEDOT and eumelanin. The diethoxy groups present on PEDOT chains resembles the catechol groups of eumelanin building blocks. Furthermore, the delocalization of π electrons in the carbon backbone of eumelanin is similar to that featured by PEDOT. (Figure 7.1).[44, 213]

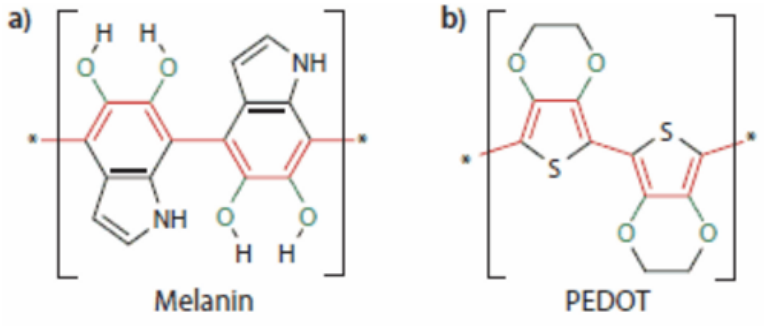

Figure 7.1 (a) The repeating unit of eumelanin, a natural conjugated polymer pigment. (b) Synthetic PEDOT polymer. Similarities between melanin and PEDOT highlighted in red and green colors.[213]

PEDOT:PSS can be doped/dedoped electrochemically, by electrolyte ions. For instance, cations will dedope PEDOT:PSS whereas anions will dope it. During my PhD, I showed that thin (50 nm) films of PEDOT:PSS can be doped more easily than thicker (500 nm) ones. This effect is more pronounced in case of unconventional micellar electrolytes, for instance cetyltrimethylammonium bromide (CTAB). Furthermore, the rate of ion diffusion into the PEDOT:PSS film depends on the film thickness and size of the electrolyte ions. I observed a slower diffusion rate for bulky ions in thick PEDOT:PSS films. Furthermore, I observed the electrocatalytical activity of PEDOT:PSS for the oxygen reduction reaction, more pronounced in the case of electrolytes containing higher concentrations of dissolved oxygen. The investigations of high surface area carbon as the gate electrode leads better OECT performance with respect to PEDOT:PSS- and metal-based gate electrodes.

The building blocks 5,6-dihydroxyindole (DHI) and 5,6-dihydroxyindole-2-carboxylic acid (DHICA) of eumelanin are known for their various reversible redox forms (hydroquinone, semiquinone, quinone). Besides ionic binding sites specific to the redox forms of eumelanin, amine and carboxylic groups (in DHICA) are also sites with pronounced ionic binding affinity. During our fundamental studies about the charge transfer (redox) properties of eumelanin, I discovered the charge storage property of eumelanin, exploited to demonstrate supercapacitors based on eumelanin electrodes.

CHAPTER 8 CONCLUSION AND PERSPECTIVES

This Ph.D. thesis in the field of organic electronic polymers with mixed electronic/ionic conduction led to a number of successful advancements on: i) the influence of the thickness of PEDOT:PSS channel films and electrolyte ions on the performance of organic electrochemical transistors (OECTs); ii) the influence of high specific surface area activated carbon (AC) as a gate material on OECT performance; iii) the discovery of the ion storage properties of the biopolymer melanin (that permitted the fabrication of supercapacitors (SCs) and micro-supercapacitors (μSCs) based on melanin electrodes). The work presented in this Ph.D. thesis contributes to demonstrate the high performance OECT and to identify the suitable biopolymers for electrochemical energy storage.

Going through the key results collected during this Ph.D. work on the effect of influence of the thickness of the PEDOT:PSS channel, electrolyte ions (NaCl and CTAB) and dissolved O_2 on the performance of OECTs, we could organize the finding as follows:

(i) higher ON/OFF ratios are achieved when CTAB is used as the electrolyte;

(ii) thin PEDOT:PSS films have superior performance as OECT channels, in terms of current modulation, compared to their thicker counterpart, despite their lower electrical conductivity;

(iii) the effect of the thickness on the modulation of the current is more pronounced when CTAB is used as an electrolyte.

Using the cyclic voltammetry (CV) electrochemical technique, we detected a significant effect of dissolved O_2 on the voltammetric current of PEDOT:PSS, particularly in the presence of a NaCl electrolyte. The dissolved oxygen might oxidize PEDOT:PSS during the electrochemical dedoping process, thus leading to lower ON/OFF ratios. On the other hand, using electrochemical impedance spectroscopy, we found that the doping/dedoping process in PEDOT:PSS becomes slower at higher film thicknesses and in the presence of bulky ions.

Furthermore, the investigation of PEDOT:PSS OECT using high specific surface area of 1000-2000 m^2/g AC gate electrodes revealed that higher current modulations can be achieved at relatively low electrical biases (0.6 V), compared to PEDOT:PSS gate electrodes of comparable geometric area. The gate current observed using AC in OECT increases with increasing the

geometric surface area of the AC gate, but the current modulation stays the same.

In melanin supercapacitors, we demonstrated supercapacitors and flexible micro-supercapacitors working in aqueous electrolytes. The melanin electrodes were fabricated at room temperature, by facile solution processing, without the need for high-temperature treatment, unlike the large majority of supercapacitors based on biopolymer-derived electrodes reported to date. In slightly acidic media, a gravimetric specific capacitance as high as 167 F/g (specific capacity of 24 mAh/g) was observed for melanin-based electrodes on carbon paper. A maximum power density of up to 20 mW/cm^2 was deduced for the corresponding melanin supercapacitors. Capitalizing on these results, we demonstrated binder-free micro-supercapacitors fabricated on flexible polyethylene terephthalate (PET). The microfabrication was performed by unconventional lithography based on Parylene C patterning. Our flexible micro-supercapacitors showed a power density of 5.24 mW/cm^2 at an energy density of 0.44 mJ/cm^2 and a specific capacitance of 10.8 F/g (about 4.3 mF/cm^2, i.e. 1.7 F/cm^3). Micro-supercapacitors were operated at fast electrode potential scan rates (up to 10 V/s). Melanin-based micro-supercapacitors may serve in biocompatible and biodegradable power sources for applications such as implantable medical devices, wearable electronics and ubiquitous sensor networks.

The results generated by this PhD thesis permits to conceive a number of potential developments. To further understand the doping/dedoping mechanism of OECT, we could explore PEDOT making use of the non-polymeric dopant tosylate, through the in-situ Vapor Phase Polymerization (VPP) technique. Furthermore, by the combination of VPP and the versatile electrosopinning technique we could fabricate OECT based on PEDOT:Tosylate nanofibers. High surface area nanofiber channels are expected to lead to better OECT modulation and mechanical stability on various substrates, with respect to spin-coated film channels.

Several possibilities are foreseen to further improve the capacitance and cyclic stability of the melanin supercapacitors. In future work, the performance of melanin micro-supercapacitors could be improved by: i) using interdigitated finger structures with tuned electrode width, length, interelectrode distance and number of fingers and, ii) improving the formulation of the melanin slurry, to optimize eumelanin loading. To achieve a better understanding about the redox sites

active during the operation of the micro- supercapacitors, characterizing the electrochemical properties of chemically controlled melanins, e.g. obtained by the solid state polymerization of the DHI building blocks is a future perspective. Our work in supercapacitors paves the way to the fabrication of biodegradable/bioresorbable micro-supercapacitors using substrates such as poly(lactic-co-glycolic acid) (PLGA) or shellac and current collectors based on magnesium or iron alloys.

BIBLIOGRAPHY

[1]. H. Shirakawa, E. J. Louis, A. G. Macdiarmid, C. K. Chiang and A. J. Heeger, “Synthesis of electrically conducting organic polymers: halogen derivatives of polyacetylene, $(CH)_X$”, Journal of the Chemical Society, *Chemical Communications*, 16, 578-580, 1977.

[2]. G. G. Malliaras and R. H. Friend, “An organic electronics primer”, *Physics Today*, 58, 53–58, 2005.

[3]. M. Pope and C. E. Swenberg, “Electronic Processes in Organic Crystals and Polymers” (Oxford University Press, NY, 1999).

[4]. C. W. Tang and S. A. VanSlyke, "Organic electroluminescent diodes," *Applied Physics Letters,* 51, 913-915, *1987*.

[5]. J. H. Burroughes, D. D. C. Bradley, A. R. Brown, R. N. Marks, K. Mackay, R. H. Friend, P. L. Burns and A. B. Holmes, “Light-emitting diodes based on conjugated polymers”, Nature, 347, 539–541, 1990.

[6]. H. Koezuka, A. Tsumura, and T. Ando, "Field-effect transistor with polythiophene thin film," *Synthetic Metals,* 18, 699-704, 1987.

[7]. A. Tsumura, H. Koezuka, and T. Ando, "Macromolecular electronic device: Field-effect transistor with a polythiophene thin film," *Applied Physics Letters,* 49, 1210-1212, 1986.

[8]. M. Muccini, “A bright future for organic field-effect transistors”, *Nature Materials*, 5, 605-613, 2016.

[9]. H. Klauk, “Organic thin-film transistors”, *Chemical Society Reviews*, 39, 2643– 2666, 2010.

[10]. R. H. Friend, R. W. Gymer, A. B. Holmes, J. H. Burroughes, R. N. Marks, C. Taliani, D. D. C. Bradley, D. A. Dos Santos, J. L. Brédas, M. Lögdlund and W. R. Salaneck, “Electroluminescence in conjugated polymers”, *Nature*, 397, 121–128, 1999.

[11]. R. Coehoorn, H. van Eersel, P. A. Bobbert and R. A. J. Janssen, “Kinetic Monte Carlo Study of the Sensitivity of OLED Efficiency and Lifetime to Materials Parameters”, *Advanced Functional Materials*, 25, 2024–2037, 2015.

[12]. C. R. Newman, C. D. Frisbie, D. A. da Silva Filho, J.-L. Brédas, P. C. Ewbank, and K. R. Mann, "Introduction to Organic Thin Film Transistors and Design of n-Channel Organic Semiconductors," *Chemistry of Materials,* 16, 4436-4451, 2004.

[13]. M. Grätzel, “Photoelectrochemical cells”, *Nature*, 414, 338–344, 2001.

[14]. S. Burns, C. Kuhn, N. Stone, D. Wilson, A. C. Arias, T. Brown*, et al.*, "43.1: Invited Paper: Inkjet Printed Polymer Thin Film Transistors for Active-Matrix Display Applications," *SID Symposium Digest of Technical Papers,* 33, 1193-1195, 2002.

[15]. C. K. Chiang, S. C. Gau, C. R. Fincher, Y. W. Park, A. G. MacDiarmid, and A. J. Heeger, "Polyacetylene, (CH)x: n-type and p-type doping and compensation," *Applied Physics Letters,* 33, 18-20, 1978.

[16]. H. Shirakawa, "Synthesis and characterization of highly conducting polyacetylene," *Synthetic Metals,* 69, 3-8, 1995.

[17]. A. A. Nardes, "On the conductivity of PEDOT:PSS thin films," Technische Universiteit Eindhoven, Eindhoven, 2007.

[18]. M. Gross, D. C. Muller, H.-G. Nothofer, U. Scherf, D. Neher, C. Brauchle*, et al.*, "Improving the performance of doped [pi]-conjugated polymers for use in organic light-emitting diodes," *Nature,* 405, 661-665, 2000.

[19]. C. D. Muller, A. Falcou, N. Reckefuss, M. Rojahn, V. Wiederhirn, P. Rudati, et al., "Multi-colour organic light-emitting displays by solution processing," *Nature*, 421, 829-833, 2003.

[20]. H. Kallmann and M. Pope, “Photovoltaic effect in organic crystals”, *Journal of Chemical Physics*, 30, 585–586, 1959.

[21]. C. W. Tang, S. A. VanSlyke, and C. H. Chen, "Electroluminescence of doped organic thin films," *Journal of Applied Physics,* 1989, 65, 3610.

[22]. E. Bequerel, “Recherches sur les effets de la radiation chimique de la lumière solaire, au moyen des courants électriques”, *Comptes Rendus de L´Academie des Sciences,* 9, 145–149, 1839.

[23]. C. E. Fritts, "On a New Form of Selenium Photocell," *American Journal of Science,* 26, 1883.

[24]. D. M. Chapin, C. S. Fuller, and G. L. Pearson, "A New Silicon p-n Junction Photocell for Converting Solar Radiation into Electrical Power," *Journal of Applied Physics,* 25, 676-677, 1954.

[25]. S. Ryuzaki and J. Onoe, "Basic aspects for improving the energy conversion efficiency of hetero-junction organic photovoltaic cells," *Nano Reviews,* 4, 1-12, 2013.

[26]. G. E. Moore, "Cramming more components onto integrated circuits," *Electronics,* 38, (4 pages), 1965.

[27]. G. Horowitz, "Organic Field-Effect Transistors," *Advanced Materials,* 10, 365-377, 1998.

[28]. Z. Bao, A. Dodabalapur, and A. J. Lovinger, "Soluble and processable regioregular poly(3-hexylthiophene) for thin film field-effect transistor applications with high mobility," *Applied Physics Letters,* 69, 4108-4110, 1996.

[29]. S. H. Kim, K. Hong, W. Xie, K. H. Lee, S. Zhang, T. P. Lodge, C. D. Frisbie, "Electrolyte-gated transistors for organic and printed electronics", *Advanced Material*, 25, 1822–1846, 2013.

[30]. G. Tarabella, F. M. Mohammadi, N. Coppede, F. Barbero, S. Iannotta, C. Santato and F. Cicoira, "New opportunities for organic electronics and bioelectronics: ions in action", *Chemical Science*, 4, 1395–1409, 2013.

[31]. H. Letaw and J. Bardeen, "Electrolytic Analog Transistor", *Journal of Applied Phys*ics, 1954, 25, 600.

[32]. J. O. M. Bockris and A. K. N. Reddy, "The Electrified Interface," in *Volume 2 Modern Electrochemistry: An Introduction to an Interdisciplinary Area*, ed Boston, MA: Springer US, 623-843, 1970.

[33]. B. Nasr, D. Wang, R. Kruk, H. Rösner, H. Hahn, S. Dasgupta, "High-Speed, Low-Voltage, and Environmentally Stable Operation of Electrochemically Gated Zinc Oxide Nanowire Field-Effect Transistors", *Advanced Functional Materials,* 23, 1750–1758, 2013.

[34]. H. Yuan, H. Shimotani, A. Tsukazaki, A. Ohtomo, M. Kawasaki, and Y. Iwasa, "High-Density Carrier Accumulation in ZnO Field-Effect Transistors Gated by Electric Double Layers of Ionic Liquids," *Advanced Functional Materials,* 19, 1046-1053, 2009.

[35]. H. Yoon, J. Jang, "Conducting-Polymer Nanomaterials for High-Performance Sensor Applications: Issues and Challenges", *Advanced Functional Materials,* 19, 1567–1576, 2009.

[36]. J. Lee, L. G. Kaake, J. H. Cho, X.-Y. Zhu, T. P. Lodge, and C. D. Frisbie, "Ion Gel-Gated Polymer Thin-Film Transistors: Operating Mechanism and Characterization of Gate Dielectric Capacitance, Switching Speed, and Stability", *The Journal of Physical Chemistry C*, 113, 8972–8981, 2009.

[37]. S. Rosenblatt, Y. Yaish, J. Park, J. Gore, V. Sazonova, and P. L. McEuen, "High Performance Electrolyte Gated Carbon Nanotube Transistors," *Nano Letters,* 2, 869-872, 2002.

[38]. E. Penzo, M. Palma, D. A. Chenet, G. Ao, M. Zheng, J. C. Hone, and S. J. Wind, “Directed Assembly of Single Wall Carbon Nanotube Field Effect Transistors”, *ACS Nano*, 10, 2975−2981, 2016.

[39]. J. Rivnay, R. M. Owens, and G. G. Malliaras, "The Rise of Organic Bioelectronics," *Chemistry of Materials,* 26, 679-685, 2014.

[40]. L. Kergoat, B. Piro, M. Berggren, G. Horowitz, and M.-C. Pham, "Advances in organic transistor-based biosensors: from organic electrochemical transistors to electrolyte-gated organic field-effect transistors," *Analytical and Bioanalytical Chemistry,* 402, 1813-1826, 2012.

[41]. R. M. Owens, G. G. Malliaras, "Organic Electronics at the Interface with Biology," *MRS Bulletin,* 35, 449-456, 2010.

[42]. E. Smela, "Conjugated Polymer Actuators for Biomedical Applications," *Advanced Materials,* 15, 481-494, 2003.

[43]. Y. Wenrong, T. Pall, J. J. Gooding, P. R. Simon, and B. Filip, "Carbon nanotubes for biological and biomedical applications," *Nanotechnology,* 18, 412001, 2007.

[44]. D. C. Martin, "Organic electronics: Polymers manipulate cells," *Nature Materials,* 6, 626-627, 2007.

[45]. M. Berggren and A. Richter-Dahlfors, “Organic bioelectronics”, *Advanced Materials.*, 19, 3201–3213, 2007.

[46]. K. Svennersten, K. C. Larsson, M. Berggren, and A. Richter-Dahlfors, "Organic bioelectronics in nanomedicine," *Biochimica et Biophysica Acta,* 1810, 276-85, 2011.

[47]. R. Kötz and M. Carlen, "Principles and applications of electrochemical capacitors," *Electrochimica Acta,* 45, 2483-2498, 2000.

[48]. H. I. Becker, "Low voltage electrolytic capacitor," US Patents, US 2800616 A, 1957.

[49]. A. Yoshida, K. Imoto, A. Nishino, and H. Yoneda, "An electric doublelayer capacitor with high capacitance and low resistance," *41st Electronic Components and Technology Conference*, Atlanta, GA, USA, 1991.

[50]. G. L. Bullard, H. B. Sierra-Alcazar, H. L. Lee, and J.L. Morris,"Operating principles of the ultracapacitor," *IEEE Transactions on Magnetics,* 25, 102-106, 1988.

[51]. B. E. Conway," Transition from “Supercapacitor” to “Battery” Behavior in Electrochemical Energy Storage", *Journal of Electrochemical Society,* 138, 1539-1548, 1991.

[52]. B. E Conway, "Electrochemical supercapacitors: Scientific fundamentals and technological applications", Kluwer Academic Plenum Publishers, New York, 1999.

[53]. T. Chen and L. Dai, "Flexible supercapacitors based on carbon nanomaterials," *Journal of Materials Chemistry A,* 2, 10756, 2014.

[54]. C. C. Felix, J. S. Hyde, T. Sarna, and R. C. Sealy, "Interactions of melanin with metal ions. Electron spin resonance evidence for chelate complexes of metal ions with free radicals," *Journal of the American Chemical Society,* 100, 3922-3926, 1978.

[55]. L. Hong and J. D. Simon, "Insight into the binding of divalent cations to Sepia eumelanin from IR absorption spectroscopy," *Photochemistry and Photobiology,* 82, 1265-1269, 2006.

[56]. L. Hong and J. D. Simon, "Current Understanding of the Binding Sites, Capacity, Affinity, and Biological Significance of Metals in Melanin," *The Journal of Physical Chemistry B, ,*111, 7938-7947, *2007*.

[57]. F.Jonas, G. Heywang, W. Schmidtberg, (Bayer AG), "Novel polythiophenes, process for their preparation, and their use", DE 3813589 A1, April 22, 1988.

[58]. L. Groenendaal, F. Jonas, D. Freitag, H. Pielartzik, and J. R. Reynolds, "Poly(3,4-ethylenedioxythiophene) and Its Derivatives: Past, Present, and Future," *Advanced Materials,* 12, 481-494, 2000.

[59]. S. Kirchmeyer and K. Reuter, "Scientific importance, properties and growing applications of poly(3,4-ethylenedioxythiophene)," *Journal of Materials Chemistry,* 15, 2077-2088, 2005.

[60]. L. Groenendaal, G. Zotti, P. H. Aubert, S. M. Waybright, and J. R. Reynolds, "Electrochemistry of Poly(3,4-alkylenedioxythiophene) Derivatives," *Advanced Materials,* 15, 855-879, 2003.

[61]. A. Elschner, A. Eiling, J. Bayley, "ITO Alternative: solution deposited Clevios™PEDOT:PSS for transparent conductive applications.pdf," *Trade article,* 11 pages, 2012.

[62]. Y. Yang, G. Yu, J. J. Cha, H. Wu, M. Vosgueritchian, Y. Yao*, et al.*, "Improving the Performance of Lithium–Sulfur Batteries by Conductive Polymer Coating," *ACS Nano,* 5, 9187-9193, 2011.

[63]. Y. Xuan, M. Sandberg, M. Berggren, and X. Crispin, "An all-polymer-air PEDOT battery," *Organic Electronics,* 13, 632-637, 2012.

[64]. L. Ran, C. Seung Il, and L. Sang Bok, "Poly(3,4-ethylenedioxythiophene) nanotubes as electrode materials for a high-powered supercapacitor," *Nanotechnology,* 19, 215710, 2008.

[65]. E. Frackowiak, V. Khomenko, K. Jurewicz, K. Lota, and F. Béguin, "Supercapacitors based on conducting polymers/nanotubes composites," *Journal of Power Sources,* 153, 413-418, 2006.

[66]. F. Jonas, W. Krafft, and B. Muys, "Poly(3, 4-ethylenedioxythiophene): Conductive coatings, technical applications and properties," *Macromolecular Symposia,* 100, 169-173, 1995.

[67]. D. Nilsson, "An Organic Electrochemical Transistor for Printed Sensors and Logic, *Ph.D.thesis*, Dept. of Science and Technology, Linköpings Universitet, , Linköpings Universitet, Sweden, 2005.

[68]. D. Khodagholy, J. Rivnay, M. Sessolo, M. Gurfinkel, P. Leleux, L. H. Jimison*, et al.*, "High transconductance organic electrochemical transistors," *Nature Communications,* 4, 2133, 2013.

[69]. J. Huang, P. F. Miller, J. S. Wilson, A. J. de Mello, J. C. de Mello, and D. D. C. Bradley, "Investigation of the Effects of Doping and Post-Deposition Treatments on the Conductivity, Morphology, and Work Function of Poly(3,4-ethylenedioxythiophene)/Poly(styrene sulfonate) Films," *Advanced Functional Materials,* 15, 290-296, 2005.

[70]. Y. H. Kim, C. Sachse, M. L. Machala, C. May, L. Müller-Meskamp, and K. Leo, "Highly Conductive PEDOT:PSS Electrode with Optimized Solvent and Thermal Post-Treatment for ITO-Free Organic Solar Cells," *Advanced Functional Materials,* 21, 1076-1081, 2011.

[71]. Q. Wei, M. Mukaida, Y. Naitoh, and T. Ishida, "Morphological change and mobility enhancement in PEDOT:PSS by adding co-solvents," *Advanced Materials,* 25, 2831-2836, May 28 2013.

[72]. D. Alemu, H.-Y. Wei, K.-C. Ho, and C.-W. Chu, "Highly conductive PEDOT:PSS electrode by simple film treatment with methanol for ITO-free polymer solar cells," *Energy & Environmental Science,* 5, 9662, 2012.

[73]. J. Y. Kim, J. H. Jung, D. E. Lee, and J. Joo, "Enhancement of electrical conductivity of poly(3,4-ethylenedioxythiophene)/poly(4-styrenesulfonate) by a change of solvents," *Synthetic Metals,* 126, 311-316, 2002.

[74]. A. M. Nardes, M. Kemerink, M. M. de Kok, E. Vinken, K. Maturova, and R. A. J. Janssen, "Conductivity, work function, and environmental stability of PEDOT:PSS thin films treated with sorbitol," *Organic Electronics,* 9, 727-734, 2008.

[75]. J. Ouyang, C. W. Chu, F. C. Chen, Q. Xu, and Y. Yang, "High-Conductivity Poly(3,4-ethylenedioxythiophene):Poly(styrene sulfonate) Film and Its Application in Polymer Optoelectronic Devices," *Advanced Functional Materials,* 15, 203-208, 2005.

[76]. L. A. A. Pettersson, S. Ghosh, and O. Inganäs, "Optical anisotropy in thin films of poly(3,4-ethylenedioxythiophene)–poly(4-styrenesulfonate)," *Organic Electronics,* 3, 143-148, 2002.

[77]. S. K. M. Jönsson, J. Birgerson, X. Crispin, G. Greczynski, W. Osikowicz, A. W. Denier van der Gon*, et al.*, "The effects of solvents on the morphology and sheet resistance in poly(3,4-ethylenedioxythiophene)–polystyrenesulfonic acid (PEDOT–PSS) films," *Synthetic Metals,* 139, 1-10, 2003.

[78]. L. Ouyang, C. Musumeci, M. J. Jafari, T. Ederth, and O. Inganäs, "Imaging the Phase Separation Between PEDOT and Polyelectrolytes During Processing of Highly Conductive PEDOT:PSS Films," *ACS Applied Materials & Interfaces,* 7, 19764-19773, 2015.

[79]. H. S. White, G. P. Kittlesen and M. S. Wrighton, “Chemical derivatization of an array of three gold microelectrodes with polypyrrole: fabrication of a molecule-based transistor”, *Journal of American Chemical Society*, 106, 5375–5377, 1984.

[80]. H. Tang, P. Lin, H. L. W. Chan and F. Yan, “Highly sensitive dopamine biosensors based on organic electrochemical transistors”, *Biosensors and Bioelectronics*, 26, 4559–4563, 2011.

[81]. D. A. Bernards, G. G. Malliaras, G. E. S. Toombes, and S. M. Gruner, "Gating of an organic transistor through a bilayer lipid membrane with ion channels," *Applied Physics Letters,* 89, 053505, 2006.

[82]. P. Lin, F. Yan, J. Yu, H. L. Chan, and M. Yang, "The application of organic electrochemical transistors in cell-based biosensors," *Advanced Materials,* 22, pp. 3655-60, 2010.

[83]. D. A. Bernards, D. J. Macaya, M. Nikolou, J. A. DeFranco, S. Takamatsu and G. G. Malliaras, “Enzymatic sensing with organic electrochemical transistors”, *Journal of Materials Chemistry*, 18, 116–120, 2008.

[84]. F. Cicoira, M. Sessolo, O. Yaghmazadeh, J. A. DeFranco, S. Y. Yang and G. G. Malliaras, “Influence of device geometry on sensor characteristics of planar organic electrochemical transistors”, *Advanced Materials,* 22, 1012–1016, 2010.

[85]. O. Yaghmazadeh, F. Cicoira, D. A. Bernards, S. Y. Yang, Y. Bonnassieux and G. G. Malliaras, “Optimization of Organic Electrochemical Transistors for Sensor Applications”, *Journal of Polymer Science Polymer Physics,* 49, 34–39, 2011.

[86]. S. Y. Yang, F. Cicoira, R. Byrne, F. Benito-Lopez, D. Diamond, R. M. Owens and G. G. Malliaras, “Electrochemical transistors with ionic liquids for enzymatic sensing”, *Chemical Communications,* 46, 7972–7974, 2010.

[87]. H. Tang, F. Yan, P. Lin, J. B. Xu and H. L. W. Chan, “Highly sensitive glucose biosensors based on organic electrochemical transistors using platinum gate electrodes modified with enzyme and nanomaterials”, *Advanced Functional Materials*, 21, 2264–2272, 2011.

[88]. M. Demelas, E. Scavetta, L. Basiricò, R. Rogani and A. Bonfiglio, “A deeper insight into the operation regime of all-polymeric electrochemical transistors”, *Applied Physics Letters*, 102, 193301, 2013.

[89]. G. Tarabella, G. Nanda, M. Villani, N. Coppedè, R. Mosca, G. G. Malliaras*, et al.*, "Organic electrochemical transistors monitoring micelle formation," *Chemical Science,* 3, 3432, 2012.

[90]. J. Rivnay, P. Leleux, M. Ferro, M. Sessolo, A. Williamson, D. A. Koutsouras*, et al.*, "High-performance transistors for bioelectronics through tuning of channel thickness," *Science Advances,* 1, 2015.

[91]. G. Tarabella, C. Santato, S. Y. Yang, S. Iannotta, G. G. Malliaras, and F. Cicoira, "Effect of the gate electrode on the response of organic electrochemical transistors," *Applied Physics Letters,* 97, 123304, 2010.

[92]. D. A. Bernards and G. G. Malliaras, “Steady-State and Transient Behavior of Organic Electrochemical Transistors”, *Advanced Functional Materials*, 17, 3538–3544, 2007.

[93]. H. Tang, P. Kumar, S. Zhang, Z. Yi, G. D. Crescenzo, C. Santato, F. Soavi and F. Cicoira, “Conducting Polymer Transistors Making Use of Activated Carbon Gate Electrodes”, *ACS Applied Materials and Interfaces*, 7, 969−973, 2015.

[94]. Z. Yi, G. Natale, P. Kumar, E. Di Mauro, M. Heuzey, F. Soavi, I. I. Perepichka, S. K. Varshney, C. Santato and F. Cicoira, “Ionic liquid–water mixtures and ion gels as electrolytes for organic electrochemical transistors”, *Journal of Materials Chemistry C*, 3, 6549–6553, 2015.

[95]. S. H. Kim, K. Hong, W. Xie, K. H. Lee, S. Zhang, T. P. Lodge*, et al.*, "Electrolyte-Gated Transistors for Organic and Printed Electronics," *Advanced Materials,* 25, 1822-1846, 2013.

[96]. J. Rivnay, P. Leleux, M. Sessolo, D. Khodagholy, T. Herve, M. Fiocchi*, et al.*, "Organic electrochemical transistors with maximum transconductance at zero gate bias," *Advanced Materials,* 25, 7010-7014, 2013.

[97]. M. Asplund, T. Nyberg, and O. Inganäs, "Electroactive polymers for neural interfaces," *Polymer Chemistry,* 1, 1374, 2010.

[98]. N. K. Guimard, N. Gomez, and C. E. Schmidt, "Conducting polymers in biomedical engineering," *Progress in Polymer Science,* 32, 876-921, 2007.

[99]. A. Campana, T. Cramer, D. T. Simon, M. Berggren, and F. Biscarini, "Electrocardiographic Recording with Conformable Organic Electrochemical Transistor Fabricated on Resorbable Bioscaffold," *Advanced Materials,* 26, 3874–3878, 2014.

[100]. P. Leleux, J. Rivnay, T. Lonjaret, J.-M. Badier, C. Bénar, T. Hervé*, et al.*, "Organic Electrochemical Transistors for Clinical Applications," *Advanced Healthcare Materials,* 4,142-147, 2015.

[101]. D. Khodagholy, T. Doublet, P. Quilichini, M. Gurfinkel, P. Leleux, A. Ghestem*, et al.*, "In vivo recordings of brain activity using organic transistors," *Nature Communications,* 4, 1575, 2013.

[102]. R. Owens, P. Kjall, A. Richter-Dahlfors, and F. Cicoira, " Organic bioelectronics - novel applications in biomedicine. Preface," *Biochimica et Biophysica Acta,* 1830, pp. 4283-5, 2013.

[103]. S. B. Rienecker, A. B. Mostert, G. Schenk, G. R. Hanson, and P. Meredith, "Heavy Water as a Probe of the Free Radical Nature and Electrical Conductivity of Melanin," *The Journal of Physical Chemistry B,* 119, 14994-5000, 2015.

[104]. A. B. Mostert, B. J. Powell, F. L. Pratt, G. R. Hanson, T. Sarna, I. R. Gentle*, et al.*, "Role of semiconductivity and ion transport in the electrical conduction of melanin," *Proceedings of the National Academy of Sciences U S A,* 109, 8943-8947, 2012.

[105]. J. Borovansky, “History of melanosome research,” in Melanins and Melanosomes: Biosynthesis, Biogenesis, Physiological, and Pathological Functions, J. Borovanský and P. A. Riley, Eds., pp. 1–19, Wiley-VCH Verlag GmbH & Co. KGaA, 1st edition, 2011.

[106]. N. Kollias, “The spectroscopy of human melanin pigmentation,” in Melanin: Its Role in Human Photoprotection, 31–38, Valdenmar Publishing, 1995.

[107]. P. R. Crippa, "Oxygen adsorption and photoreduction on fractal melanin particles," *Colloids and Surfaces B: Biointerfaces,* 20, 315-319, 2001.

[108]. S. Colombo, I. Berlin, V. Delmas, and L. Larue, "Classical and Nonclassical Melanocytes in Vertebrates," in *Melanins and Melanosomes*, ed: Wiley-VCH Verlag GmbH & Co. KGaA, 21-61, 2011.

[109]. A. M. Meyer zum Gottesberge-Orsulakova, “Melanin in the inner ear: micromorphological and microanalytical investigations,” Acta Histochemica. Supplementband, 32, 245–253, 1986.

[110]. P. Meredith and T. Sarna, "The physical and chemical properties of eumelanin," *Pigment Cell Res,* 19, 572-94, 2006.

[111]. D. Stuart-Fox and A. Moussalli, “Camouflage, communication and thermoregulation: lessons from colour changing organisms,” Philosophical Transactions of the Royal Society B, 364, 463–470, 2009.

[112]. J. McGinness, P. Corry, and P. Proctor, "Amorphous Semiconductor Switching in Melanins," *Science,* 183, 853, 1974.

[113]. J. Wünsche, Y. Deng, P. Kumar, E. Di Mauro, E. Josberger, J. Sayago*, et al.*, "Protonic and Electronic Transport in Hydrated Thin Films of the Pigment Eumelanin," *Chemistry of Materials,* 27, 436-442, 2015.

[114]. Z. Wang, J. Dillon, and E. R. Gaillard, “Antioxidant properties of melanin in retinal pigment epithelial cells,” *Photochemistry and Photobiology*, 82, 474–479, 2006.

[115]. M. d'Ischia, A. Napolitano, A. Pezzella, P. Meredith, and T. Sarna, "Chemical and Structural Diversity in Eumelanins: Unexplored Bio-Optoelectronic Materials," *Angewandte Chemie International Edition,* 48, 3914-3921, 2009.

[116]. V. Horak, and G. Weeks, "Poly(5,6-dihydroxyindole) melanin film electrode Bioorganic Chemistry", 21, 24–33, 1993.

[117]. S. Gidanian and P. J. Farmer, "Redox behavior of melanins: direct electrochemistry of dihydroxyindole-melanin and its Cu and Zn adducts," *Journal of Inorganic Biochemistry,* 89, 54-60, 2002.

[118]. Y. J. Kim, W. Wu, S. E. Chun, J. F. Whitacre, and C. J. Bettinger, "Biologically derived melanin electrodes in aqueous sodium-ion energy storage devices," *Proceedings of the National Academy of Sciences U S A,* 110, 20912-20917, 2013.

[119]. Y. J. Kim, W. Wu, S. E. Chun, J. F. Whitacre, and C. J. Bettinger, "Catechol-Mediated Reversible Binding of Multivalent Cations in Eumelanin Half-Cells," *Advanced Materials,* 26, 6572–6579, 2014.

[120]. Y. J. Kim, A. Khetan, W. Wu, S.-E. Chun, V. Viswanathan, J. F. Whitacre*, et al.*, "Evidence of Porphyrin-Like Structures in Natural Melanin Pigments Using Electrochemical Fingerprinting," *Advanced Materials,* 28, 3173–3180*,* 2016.

[121]. J. M. Leger, "Organic Electronics: The Ions Have It," *Advanced Materials,* 20, 837-841, 2008.

[122]. J. Isaksson, P. Kjall, D. Nilsson, N. D. Robinson, M. Berggren, and A. Richter-Dahlfors, "Electronic control of Ca^{2+} signalling in neuronal cells using an organic electronic ion pump," *Nature Materials,* 6, 673-679, 2007.

[123]. Z. T. Zhu, J. T. Mabeck, C. Zhu, N. C. Cady, C. A. Batt, and G. G. Malliaras, "A simple poly(3,4-ethylene dioxythiophene)/poly(styrene sulfonic acid) transistor for glucose sensing at neutral pH," *Chemical Communications,* 1556-1557, 2004.

[124]. M. M. de Kok, M. Buechel, S. I. E. Vulto, P. van de Weijer, E. A. Meulenkamp, S. H. P. M. de Winter*, et al.*, "Modification of PEDOT:PSS as hole injection layer in polymer LEDs," *physica status solidi (a),* 201, 1342-1359, 2004.

[125]. D. J. Kim, N. E. Lee, J. S. Park, I. J. Park, J. G. Kim, and H. J. Cho, "Organic electrochemical transistor based immunosensor for prostate specific antigen (PSA) detection using gold nanoparticles for signal amplification," *Biosensors and Bioelectronics,* 25, 2477-2482, 2010.

[126]. P. Lin and F. Yan, "Organic thin-film transistors for chemical and biological sensing," *Advanced Materials,* 24, 34-51, 2012.

[127]. S. Zhang, P. Kumar, A. S. Nouas, L. Fontaine, H. Tang, and F. Cicoira, "Solvent-induced changes in PEDOT:PSS films for organic electrochemical transistors," *APL Materials,* 3, 014911, 2015.

[128]. P. C. Hütter, T. Rothländer, A. Haase, G. Trimmel, and B. Stadlober, "Influence of geometry variations on the response of organic electrochemical transistors," *Applied Physics Letters,* 103, 043308, 2013.

[129]. G. Tarabella, C. Santato, S. Y. Yang, S. Iannotta, G. G. Malliaras, and F. Cicoira, "Effect of the gate electrode on the response of organic electrochemical transistors," *Applied Physics Letters,* 97, 123304, 2010.

[130]. G. Tarabella, A. G. Balducci, N. Coppede, S. Marasso, P. D'Angelo, S. Barbieri*, et al.*, "Liposome sensing and monitoring by organic electrochemical transistors integrated in microfluidics," *Biochimica et Biophysica Acta,,* 1830, 4374-80, 2013.

[131]. F. Dinelli, M. Murgia, P. Levy, M. Cavallini, F. Biscarini, and D. de Leeuw, "Spatially Correlated Charge Transport in Organic Thin Film Transistors," *Physical Review Letters*. 92, 2004.

[132]. S. Y. Yang, J. A. Defranco, Y. A. Sylvester, T. J. Gobert, D. J. Macaya, R. M. Owens*, et al.*, "Integration of a surface-directed microfluidic system with an organic electrochemical transistor array for multi-analyte biosensors," *Lab on a Chip,* 9, 704-708, 2009.

[133]. M. Smits, "Measurement of Sheet Resistivities by Four point -probe," *The Bell System Technical Journal,* 37, 711–718, 1958.

[134]. S. De and J. N. Coleman, "The effects of percolation in nanostructured transparent conductors," *MRS Bulletin,* 36, 774-781, 2011.

[135]. V. G. Rao, C. Ghatak, S. Ghosh, R. Pramanik, S. Sarkar, S. Mandal*, et al.*, "Ionic liquid-induced changes in properties of aqueous cetyltrimethylammonium bromide: a comparative study of two protic ionic liquids with different anions," *The Journal of Physical Chemistry B,* 115, 3828-37, 2011.

[136]. T. Johansson, L. A. A. Pettersson, and O. Inganäs, "Conductivity of de-doped poly(3,4-ethylenedioxythiophene)," *Synthetic Metals,* 129, 269-274, 2002.

[137]. B. Winther-Jensen, O. Winther-Jensen, M. Forsyth, and D. R. Macfarlane, "High rates of oxygen reduction over a vapor phase-polymerized PEDOT electrode," *Science,* 321, 671-4, 2008.

[138]. M. Zhang, W. Yuan, B. Yao, C. Li, and G. Shi, "Solution-processed PEDOT:PSS/graphene composites as the electrocatalyst for oxygen reduction reaction," *ACS Applied Materials & Interfaces,* 6, 3587-93, 2014.

[139]. R. Kerr, C. Pozo-Gonzalo, M. Forsyth, and B. Winther-Jensen, "The Reduction of Oxygen on Iron(II) Oxide/Poly(3,4-ethylenedioxythiophene) Composite Thin Film Electrodes," *Electrochimica Acta,* 154, 142-148, 2015.

[140]. R. Kerr, C. Pozo-Gonzalo, M. Forsyth, and B. Winther-Jensen, "Influence of the Polymerization Method on the Oxygen Reduction Reaction Pathway on PEDOT," *ECS Electrochemistry Letters,* 2, F29-F31, 2013.

[141]. K. K. Tintula, A. K. Sahu, A. Shahid, S. Pitchumani, P. Sridhar, and A. K. Shukla, "Mesoporous Carbon and Poly(3,4-ethylenedioxythiophene) Composite as Catalyst Support for Polymer Electrolyte Fuel Cells," *Journal of The Electrochemical Society,* 157, B1679, 2010.

[142]. S. Bubel, M. S. Menyo, T. E. Mates, J. H. Waite, and M. L. Chabinyc, "Schmitt Trigger Using a Self-Healing Ionic Liquid Gated Transistor," *Advanced Materials,* 27, 3331-3335, 2015.

[143]. M. Irimia-Vladu, ""Green" electronics: biodegradable and biocompatible materials and devices for sustainable future," *Chemical Society Reviews,* 43, 588-610, 2014.

[144]. P. Meredith, C. J. Bettinger, M. Irimia-Vladu, A. B. Mostert, and P. E. Schwenn, "Electronic and optoelectronic materials and devices inspired by nature," *Reports on Progress in Physics,* 76, 034501, 2013.

[145]. M. Beidaghi and Y. Gogotsi, "Capacitive energy storage in micro-scale devices: recent advances in design and fabrication of micro-supercapacitors," *Energy & Environmental Science,* 7, 867, 2014.

[146]. T. M. Dinh, K. Armstrong, D. Guay, and D. Pech, "High-resolution on-chip supercapacitors with ultra-high scan rate ability," *Journal of Materials Chemistry A,* 2, 7170, 2014.

[147]. A. Ferris, S. Garbarino, D. Guay, and D. Pech, "3D RuO2 Microsupercapacitors with Remarkable Areal Energy," *Advanced Materials,* 27, 6625-9, 2015.

[148]. D. Pech, M. Brunet, H. Durou, P. Huang, V. Mochalin, Y. Gogotsi*, et al.*, "Ultrahigh-power micrometre-sized supercapacitors based on onion-like carbon," *Nature Nanotechnology,* 5, 651-4, 2010.

[149]. J. Chmiola, C. Largeot, P.-L. Taberna, P. Simon, and Y. Gogotsi, "Monolithic Carbide-Derived Carbon Films for Micro-Supercapacitors," *Science,* 328, 480-483, 2010.

[150]. J. Maeng, C. Meng, and P. P. Irazoqui, "Wafer-scale integrated micro-supercapacitors on an ultrathin and highly flexible biomedical platform," *Biomedical Microdevices,* 17, 7, 2015.

[151]. K. Wang, W. Zou, B. Quan, A. Yu, H. Wu, P. Jiang*, et al.*, "An All-Solid-State Flexible Micro-supercapacitor on a Chip," *Advanced Energy Materials,* 1, 1068-1072, 2011.

[152]. C. Meng, J. Maeng, S. W. M. John, and P. P. Irazoqui, "Ultrasmall Integrated 3D Micro-Supercapacitors Solve Energy Storage for Miniature Devices," *Advanced Energy Materials,* 4, 1301269, 2014.

[153]. D. Vonlanthen, P. Lazarev, K. A. See, F. Wudl, and A. J. Heeger, "A stable polyaniline-benzoquinone-hydroquinone supercapacitor," *Advanced Materials,* 26, 5095-5100, 2014.

[154]. A. González, E. Goikolea, J. A. Barrena, and R. Mysyk, "Review on supercapacitors: Technologies and materials," *Renewable and Sustainable Energy Reviews,* 58, 1189-1206, 2016.

[155]. G. Milczarek and O. Inganas, "Renewable cathode materials from biopolymer / conjugated polymer interpenetrating networks," *Scienc,e* 335, 1468-1471, 2012.

[156]. C. Dagdeviren, B. D. Yang, Y. Su, P. L. Tran, P. Joe, E. Anderson*, et al.*, "Conformal piezoelectric energy harvesting and storage from motions of the heart, lung, and diaphragm," *P Proceedings of the National Academy of Sciences U S A,* 111, 1927-32, 2014.

[157]. S. Zhang, E. Hubis, C. Girard, P. Kumar, J. DeFranco, and F. Cicoira, "Water stability and orthogonal patterning of flexible micro-electrochemical transistors on plastic," *Journal of Materials Chemistry C,* 4, 1382-1385, 2016.

[158]. L. Zecca, C. Bellei, P. Costi, A. Albertini, E. Monzani, L. Casella*, et al.*, "New melanic pigments in the human brain that accumulate in aging and block environmental toxic metals," *Proceedings of the National Academy of Sciences U S A,*105, 17567-17572, 2008.

[159]. A. A. R. Watt, J. P. Bothma, and P. Meredith, "The supramolecular structure of melanin," *Soft Matter,* vol. 5, pp. 3754-3760, 2009.

[160]. C. T. Chen, C. Chuang, J. Cao, V. Ball, D. Ruch, and M. J. Buehler, "Excitonic effects from geometric order and disorder explain broadband optical absorption in eumelanin," *Natrure Communications,* 5, 3859, 2014.

[161]. E. Frackowiak, M. Meller, J. Menzel, D. Gastol, and K. Fic, "Redox-active electrolyte for supercapacitor application," *Faraday Discuss,* 172, 179-98, 2014.

[162]. B. Huskinson, M. P. Marshak, C. Suh, S. Er, M. R. Gerhardt, C. J. Galvin*, et al.*, "A metal-free organic-inorganic aqueous flow battery," *Nature,* 505, 195-8, 2014.

[163]. Y. Ding and G. Yu, "A Bio-Inspired, Heavy-Metal-Free, Dual-Electrolyte Liquid Battery towards Sustainable Energy Storage," *Angewandte Chemie International Edition,* 55, 4772-4776, 2016.

[164]. H. Lee, N. F. Scherer, and P. B. Messersmith, "Single-molecule mechanics of mussel adhesion," *Proceedings of the National Academy of Sciences U S A,* 103, 12999-13003, 2006.

[165]. N. Holten-Andersen, M. J. Harrington, H. Birkedal, B. P. Lee, P. B. Messersmith, K. Y. Lee*, et al.*, "pH-induced metal-ligand cross-links inspired by mussel yield self-healing polymer

networks with near-covalent elastic moduli," *Proceedings of the National Academy of Sciences U S A,* 108, 2651-2655, 2011.

[166]. J. Wünsche, F. Cicoira, C. F. O. Graeff, and C. Santato, "Eumelanin thin films: solution-processing, growth, and charge transport properties," *Journal of Materials Chemistry B,* 1, 3836, 2013.

[167]. M. Lazzari, C. Arbizzani, F. Soavi, and M. Mastragostino, "EDLCs Based on Solvent-Free Ionic Liquids," in *Supercapacitors*, ed: Wiley-VCH Verlag GmbH & Co. KGaA, 2013, 289-306.

[168]. M. Lazzari, M. Mastragostino, and F. Soavi, "Capacitance response of carbons in solvent-free ionic liquid electrolytes," *Electrochemistry Communications,* 9, 1567-1572, 2007.

[169]. F. N. Ajjan, N. Casado, T. Rebis, A. Elfwing, N. Solin, D. Mecerreyes*, et al.*, "High performance PEDOT/lignin biopolymer composites for electrochemical supercapacitors," *Journal of Materials Chemistry A,* 4, 1838-1847, 2016.

[170]. L. Jiang, G. W. Nelson, S. O. Han, H. Kim, I. N. Sim, and J. S. Foord, "Natural Cellulose Materials for Supercapacitors," *Electrochimica Acta,* 192, 251-258, 2016.

[171]. Y. Lv, L. Gan, M. Liu, W. Xiong, Z. Xu, D. Zhu*, et al.*, "A self-template synthesis of hierarchical porous carbon foams based on banana peel for supercapacitor electrodes," *Journal of Power Sources,* 209, 152-157, 2012.

[172]. M. Genovese, J. Jiang, K. Lian, and N. Holm, "High capacitive performance of exfoliated biochar nanosheets from biomass waste corn cob," *Journal of Materials Chemistry A,* 3, 2903-2913, 2015.

[173]. J. Hur, K. Im, S. W. Kim, U. J. Kim, J. Lee, S. Hwang*, et al.*, "DNA hydrogel templated carbon nanotube and polyaniline assembly and its applications for electrochemical energy storage devices," *Journal of Materials Chemistry A,* 1, 14460-14466, 2013.

[174]. Q. Wang, Q. Cao, X. Wang, B. Jing, H. Kuang, and L. Zhou, "A high-capacity carbon prepared from renewable chicken feather biopolymer for supercapacitors," *Journal of Power Sources,* 225, 101-107, 2013.

[175]. M. Biswal, A. Banerjee, M. Deo, and S. Ogale, "From dead leaves to high energy density supercapacitors," *Energy & Environmental Science,* 6, 1249, 2013.

[176]. C. Wang, M. J. O'Connell, and C. K. Chan, "Facile One-Pot Synthesis of Highly Porous Carbon Foams for High-Performance Supercapacitors Using Template-Free Direct Pyrolysis," *ACS Applied Materials & Interfaces,* 7, 8952-8960, 2015.

[177]. L. Zhu, F. Shen, R. L. Smith, and X. Qi, "High-Performance Supercapacitor Electrode Materials from Chitosan via Hydrothermal Carbonization and Potassium Hydroxide Activation," *Energy Technology,* 4, 1-10 2016.

[178]. X. Wang, D. Kong, Y. Zhang, B. Wang, X. Li, T. Qiu*, et al.*, "All-biomaterial supercapacitor derived from bacterial cellulose," *Nanoscale,* 8, 9146-9150, 2016.

[179]. D. H. Nagaraju, T. Rebis, R. Gabrielsson, A. Elfwing, G. Milczarek, and O. Inganäs, "Charge Storage Capacity of Renewable Biopolymer/Conjugated Polymer Interpenetrating Networks Enhanced by Electroactive Dopants," *Advanced Energy Materials,* 4, 1300443, 2014.

[180]. L. Wei, M. Sevilla, A. B. Fuertes, R. Mokaya, and G. Yushin, "Hydrothermal Carbonization of Abundant Renewable Natural Organic Chemicals for High-Performance Supercapacitor Electrodes," *Advanced Energy Materials,* 1, 356-361, 2011.

[181]. S.-K. Kim, Y. K. Kim, H. Lee, S. B. Lee, and H. S. Park, "Superior Pseudocapacitive Behavior of Confined Lignin Nanocrystals for Renewable Energy-Storage Materials," *ChemSusChem,* 7, 1094-1101, 2014.

[182]. C. Falco, J. M. Sieben, N. Brun, M. Sevilla, T. van der Mauelen, E. Morallón*, et al.*, "Hydrothermal Carbons from Hemicellulose-Derived Aqueous Hydrolysis Products as Electrode Materials for Supercapacitors," *ChemSusChem,* 6, 374-382, 2013.

[183]. E. Raymundo-Piñero, F. Leroux, and F. Béguin, "A High-Performance Carbon for Supercapacitors Obtained by Carbonization of a Seaweed Biopolymer," *Advanced Materials,* 18, 1877-1882, 2006.

[184]. E. Raymundo-Piñero, M. Cadek, and F. Béguin, "Tuning Carbon Materials for Supercapacitors by Direct Pyrolysis of Seaweeds," *Advanced Functional Materials,* 19, 1032-1039, 2009.

[185]. L. Yuan, C. Feng, C. Wang, Z. Fu, X. Yang, and Y. Tang, "Facile fabrication of activated carbonized horseweed-based biomaterials and their application in supercapacitors," *Journal of Materials Science,* 51, 3880-3887, 2016.

[186]. B. Xu, S. Hou, F. Zhang, G. Cao, M. Chu, and Y. Yang, "Nitrogen-doped mesoporous carbon derived from biopolymer as electrode material for supercapacitors," *Journal of Electroanalytical Chemistry,* 712, 146-150, 2014.

[187]. K. Wang, R. Yan, N. Zhao, X. Tian, X. Li, S. Lei*, et al.*, "Bio-inspired hollow activated carbon microtubes derived from willow catkins for supercapacitors with high volumetric performance," *Materials Letters,* 174, 249-252, 2016.

[188]. B. J. Bettinger CJ, Misra A, Borenstein JT and Langer R., "Biocompatibility of biodegradable semiconducting melanin films for nerve tissue engineering," *Biomaterials,* 17, 3050-7, 2009.

[189]. S. Gidanian and P. J. Farmer, "Redox behavior of melanins: direct electrochemistry of dihydroxyindole-melanin and its Cu and Zn adducts," *Journal of Inorganic Biochemistry,* 89, 54-60, 2002.

[190]. M. d'Ischia, K. Wakamatsu, F. Cicoira, E. Di Mauro, J. C. Garcia-Borron, S. Commo*, et al.*, "Melanins and melanogenesis: from pigment cells to human health and technological applications," *Pigment Cell Melanoma Research,* 28, 520-544, 2015.

[191]. T. Sakaguchi and A. Nakajima, "Accumulation of uranium by biopigments," *Journal of Chemical Technology & Biotechnology,* 40, 133-141, 1987.

[192]. G. Xiong, C. Meng, R. G. Reifenberger, P. P. Irazoqui, and T. S. Fisher, "A Review of Graphene-Based Electrochemical Microsupercapacitors," *Electroanalysis,* 26, 30-51, 2014.

[193]. A. J. Bard and L. R. Faulkner, *Electrochemical Methods: Fundamentals and Applications, 2nd Edition*: Wiley Global Education, 2000.

[194]. P. Kumar, Z. Yi, S. Zhang, A. Sekar, F. Soavi, and F. Cicoira, "Effect of channel thickness, electrolyte ions, and dissolved oxygen on the performance of organic electrochemical transistors," *Applied Physics Letters,* 107, 053303, 2015.

[195]. A. Sarapuu, K. Vaik, D. J. Schiffrin, and K. Tammeveski, "Electrochemical reduction of oxygen on anthraquinone-modified glassy carbon electrodes in alkaline solution," *Journal of Electroanalytical Chemistry,* 541, 23-29, 2003.

[196]. P. Prem, K. J. Dube, S. A. Madison, and J. Bartolone, "New insights into the physicochemical effects of ammonia/peroxide bleaching of hair and Sepia melanins," *J Cosmet Sci,* 54, 395-409, 2003.

[197]. The maximum power is deduced from $P_{max} = \left(\frac{V^2}{4 \times ESR}\right)$ where the equivalent series resistance (ESR) is ESR=ΔV/2I, with ΔV the initial drop in voltage upon switching from charging to discharging and I the current.

[198]. H. D. Abruna, Y. Kiya and J. C. Henderson, "Batteries and electrochemical capacitors," *Physics Today,* 61, 43-47, 2008.

[199]. T. Brousse, D. Belanger, and J. W. Long, "To Be or Not To Be Pseudocapacitive?," *Journal of the Electrochemical Society,* 162, A5185-A5189, 2015.

[200]. J. P. Bothma, J. de Boor, U. Divakar, P. E. Schwenn, and P. Meredith, "Device-Quality Electrically Conducting Melanin Thin Films," *Advanced Materials,* 20, 3539-3542, 2008.

[201]. W. Liu, C. Lu, X. Wang, R. Y. Tay, and B. K. Tay, "High-Performance Microsupercapacitors Based on Two-Dimensional Graphene/Manganese Dioxide/Silver Nanowire Ternary Hybrid Film," *ACS Nano,* 9, 1528-1542, 2015.

[202]. Y. Lim, J. Yoon, J. Yun, D. Kim, S. Y. Hong, S.-J. Lee*, et al.*, "Biaxially Stretchable, Integrated Array of High Performance Microsupercapacitors," *ACS Nano,* 8, 11639-11650, 2014.

[203]. Q. Jiang, N. Kurra, and H. N. Alshareef, "Marker Pen Lithography for Flexible and Curvilinear On-Chip Energy Storage," *Advanced Functional Materials,* 25, 4976-4984, 2015.

[204]. D. Kim, G. Lee, D. Kim, and J. S. Ha, "Air-stable, high-performance, flexible microsupercapacitor with patterned ionogel electrolyte," *ACS Applied Materials & Interfaces,* 7, 4608-4615, 2015.

[205]. D. Qi, Z. Liu, Y. Liu, W. R. Leow, B. Zhu, H. Yang*, et al.*, "Suspended Wavy Graphene Microribbons for Highly Stretchable Microsupercapacitors," *Advanced Materials,* 27, 5559–5566, 2015.

[206]. J. Liu, L. Zhang, H. B. Wu, J. Lin, Z. Shen, and X. W. Lou, "High-performance flexible asymmetric supercapacitors based on a new graphene foam/carbon nanotube hybrid film," *Energy & Environmental Science,* 7, 3709-3719, 2014.

[207]. J. Liu, J. Sun, and L. Gao, "A Promising Way To Enhance the Electrochemical Behavior of Flexible Single-Walled Carbon Nanotube/Polyaniline Composite Films," *The Journal of Physical Chemistry C,* 114, 19614-19620, 2010.

[208]. I. Kymissis, C. D. Dimitrakopoulos, and S. Purushothaman, "Patterning pentacene organic thin film transistors," *Journal of Vacuum Science & Technology B,* 20, 956-959, 2002.

[209]. J. D. Slinker, J. A. DeFranco, M. J. Jaquith, W. R. Silveira, Y.-W. Zhong, J. M. Moran-Mirabal*, et al.*, "Direct measurement of the electric-field distribution in a light-emitting electrochemical cell," *Nature Materials,* 6, 894-899, 2007.

[210]. A. Pezzella, M. Barra, A. Musto, A. Navarra, M. Alfe, P. Manini*, et al.*, "Stem cell-compatible eumelanin biointerface fabricated by chemically controlled solid state polymerization," *Materials Horizons,* 2, 212-220, 2015.

[211]. H. Tang, P. Kumar, S. Zhang, Z. Yi, G. D. Crescenzo, C. Santato, F. Soavi and F. Cicoira, "Supporting Information-Conducting Polymer Transistors Making Use of Activated Carbon Gate Electrodes", find the link at: https://www.google.ca/webhp?sourceid=chrome-instant&ion=1&espv=2&ie=UTF8#q=Additional+contributions+to+the+gate+current+can+be+side+faradaic, *ACS Applied Materials and Interfaces*, 7, (6 pages), 2015.

[212]. L. G. S. Albano, E. Di Mauro, P. Kumar, F. Cicoira, C. F. O. Graeff, and C. Santato, "Novel insights on the physicochemical properties of eumelanins and their DMSO derivatives," *Polymer International,* 65, 1315-1322, 2016.

[213]. D. C. Martin, L. K. Povlich and K. E. Feldman, Material Matters 2010, 5.3, 68. " Conjugated Polymers for the Engineering of Device/Tissue Interface," Material Matters, (Sigma Aldrich Trade Article) 2010.

APPENDIX A –SUPPORTING INFORMATION FOR ARTICLE MELANIN-BASED FLEXIBLE SUPERCAPACITORS

Prajwal Kumar, Eduardo Di Mauro, Shiming Zhang, Alessandro Pezzella, Francesca Soavi, Clara Santato and Fabio Cicoira**

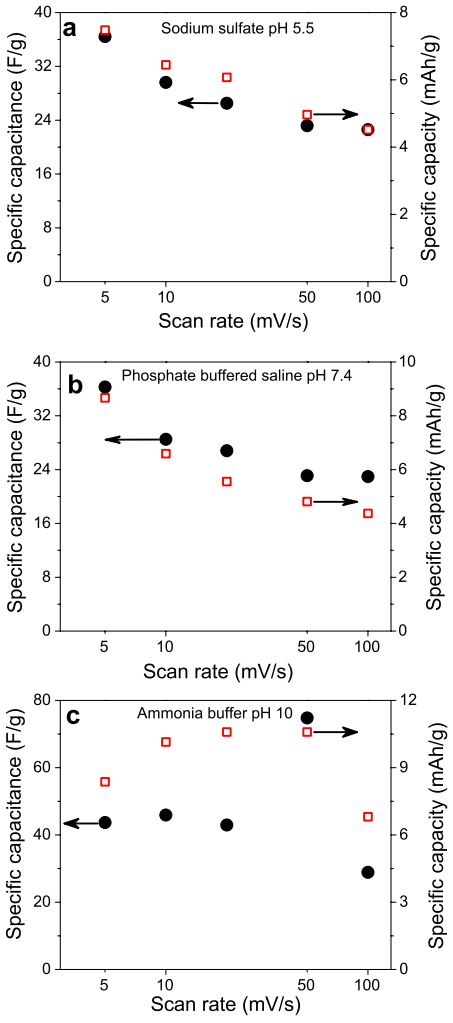

Figure S1 Specific capacitance and specific capacity *vs.* scan rate extracted from the cyclic voltammograms for Mel/CP electrodes (33.8 μg/cm^2 melanin loading) in (a) sodium sulfate pH 5.5, (b) phosphate buffer saline at pH 7.4 and (c) ammonia buffer at pH 10.

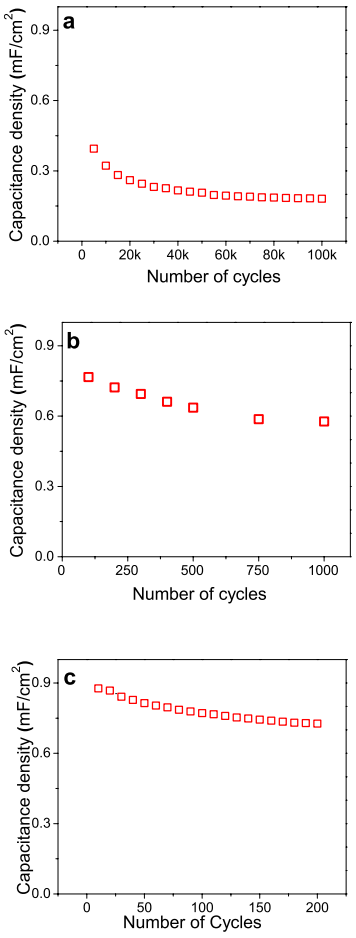

Figure S2 Trend of the capacitance density of the Mel/CP supercapacitor (67.5 µg/cm^2 Mel/CP) at 2.5 mA/cm^2 (a) during 100,000 cycles (b) during the first 1000 cycles, (c) during the first 200 cycles. Cut off voltages: 0 V to 0.75 V.

The cycling stability of a supercapacitor using electrodes with 67.5 µg/cm^2 loading was tested at 2.5 mA/cm^2. A capacitance retention of 75% was observed during the first 1,000 cycles; afterwards, the capacitance did not dramatically change over the following 10^5 cycles. The results point to the need of a stable and efficient electrical contact between the melanin and the current collector. These results are partly attributable to an aging process in the melanin.[5,6]

5. A. Pezzella, A. Napolitano, M. d'Ischia, G. Prota, R. Seraglia and P. Traldi, *Rapid Commun. Mass Spectrom.,* 1997, 11, 368-372.

6. H. Okuda, K.Yoshino, K. Wakamatsu, S. Ito and T. Sota, *Pigment Cell Melanoma Res.,* 2014, 27 664-667.

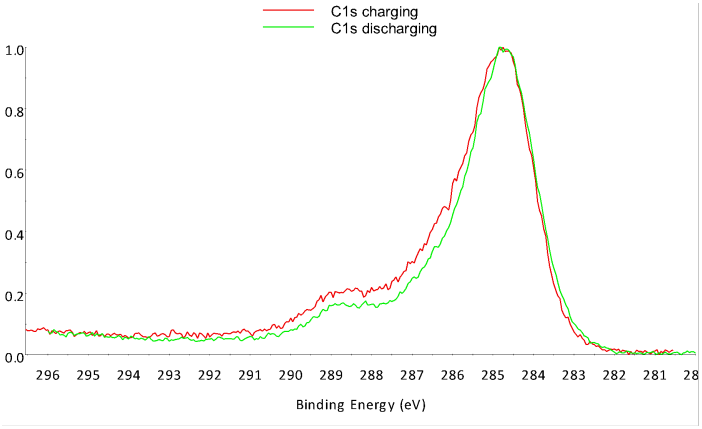

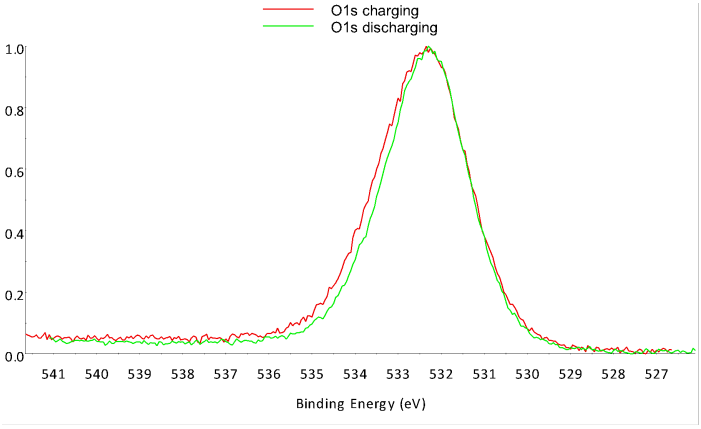

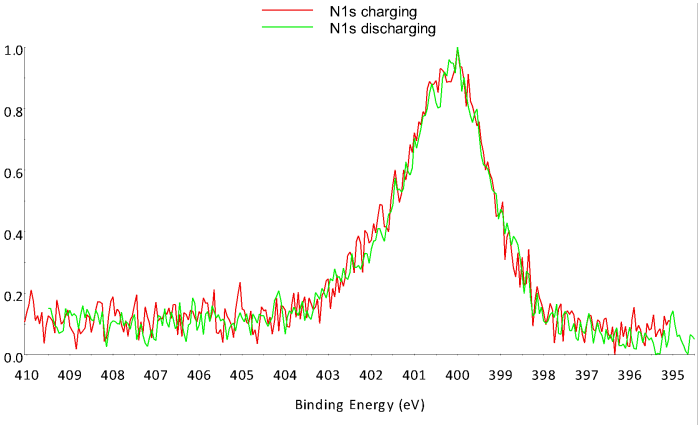

Figure S3 Overlay XPS spectra after charging and discharging steps carried out at the melanin-based positive electrode in micro-supercapacitor configuration, for C1s, O1s and N1s. For experimental details on sample preparation and charging and discharging steps please refer to Table S1 and Experimental section in the Chapter 4.

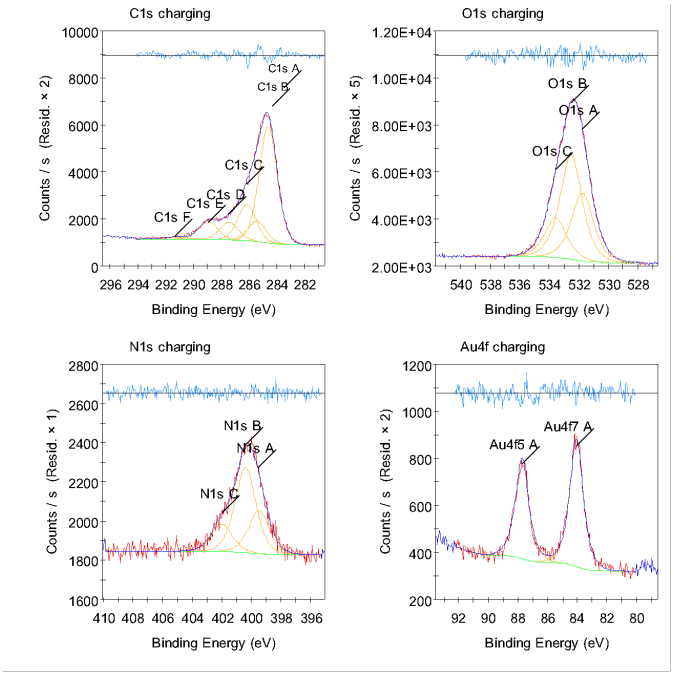

Figure S4. XPS spectra of the melanin-based positive electrode in micro-supercapacitor configuration, for C1s, O1s, N1s and Au4f after the charging step. For experimental details on sample preparation and the charging step please refer to Table S1 and Experimental section in the Chapter 4. The assignment of the individual components used for peak fitting can be found in Table S1.

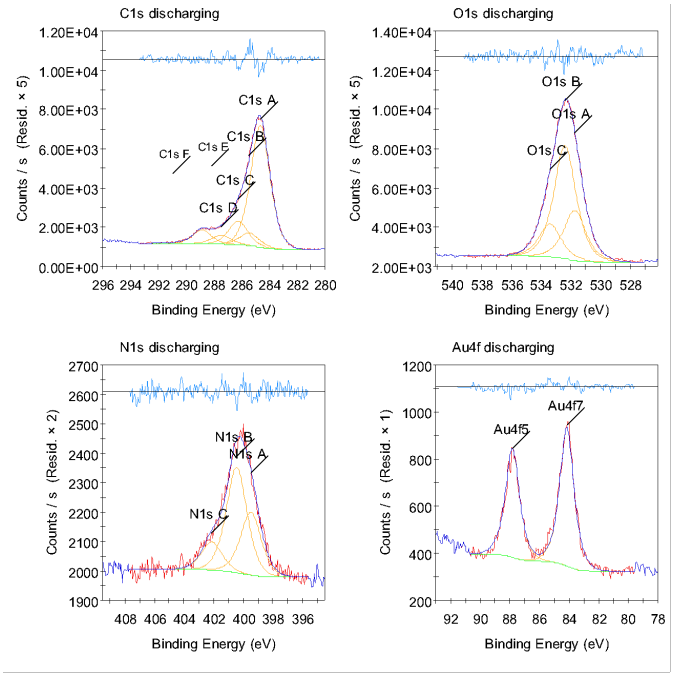

Figure S5 XPS spectra of the melanin-based positive electrode in micro-supercapacitor configuration, for C1s, O1s, N1s and Au4f after the discharging step. For experimental details on sample preparation and the charging step please refer to Table S1 and Experimental section of chapter 4. The assignment of the individual components used for peak fitting can be found in Table S1.

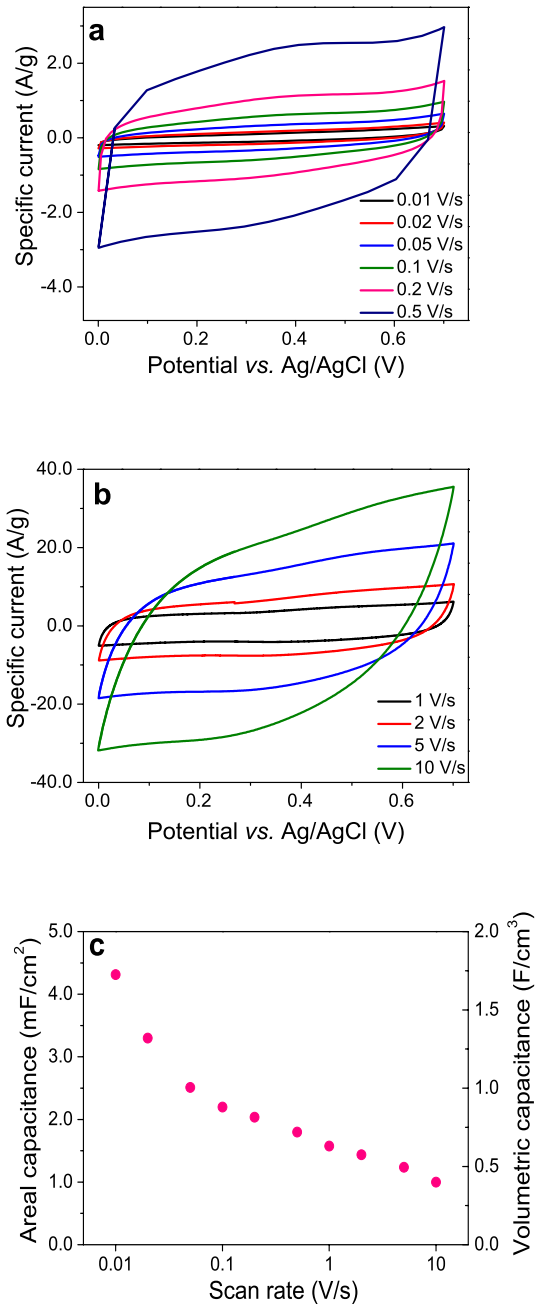

Figure S6 Cyclic voltammograms of melanin micro-supercapacitors (200 μg/cm^2 melanin loading on each electrode) in $NH_4CH_3COO_{(aq)}$ at pH 5.5: (a) at relatively slow and (b) fast scan rates. (c) Areal capacitance and volumetric capacitance vs. scan rate obtained from Figures S10a and S10b taking into account that the total area of the two electrodes is 0.16 cm^2 and the corresponding volume is about 2×10^{-4} cm^3 (see Experimental).

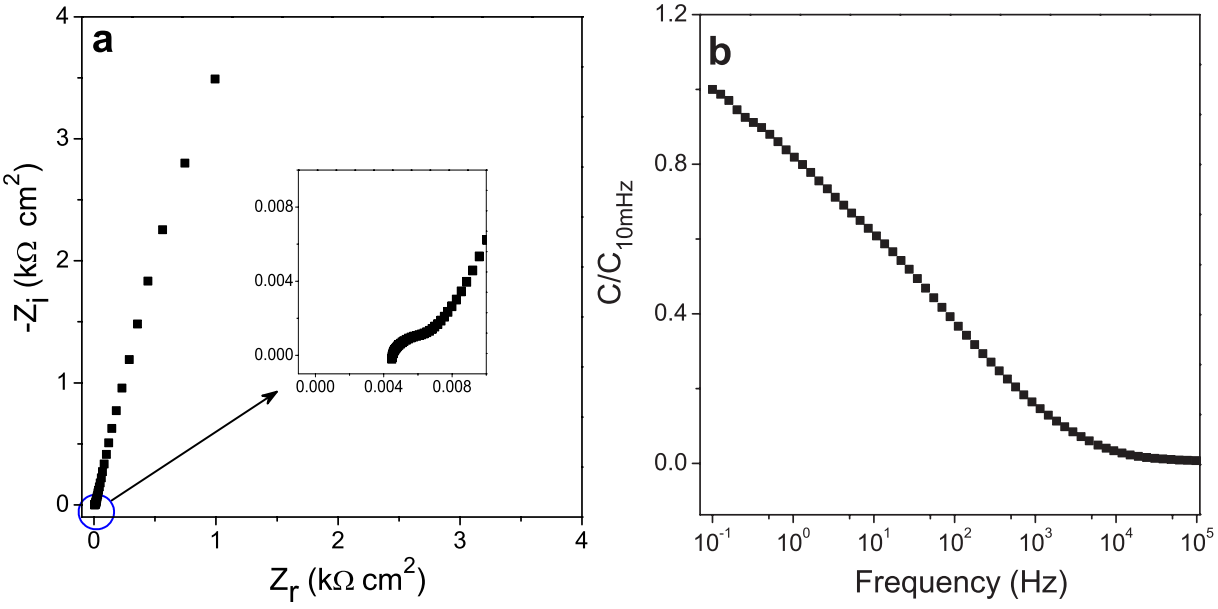

Figure S7 Electrochemical Impedance Spectroscopy (EIS) of melanin micro-supercapacitors: (a) Nyquist plots and (b) Bode plots in terms of capacitance normalized to the value obtained at 10 mHz (C/C_{10mHz}) from EIS measurements in the frequency range 100 kHz - 10^{-4} kHz with an AC amplitude of 10 mV, at open circuit potential. The loading at each electrode of area 0.08 cm^2 is ~200 μg/cm^2. The supercapacitor ESR evaluated by the Z_r intercept of the Nyquist plot at 100 kHz is 4.5 Ω cm^2.

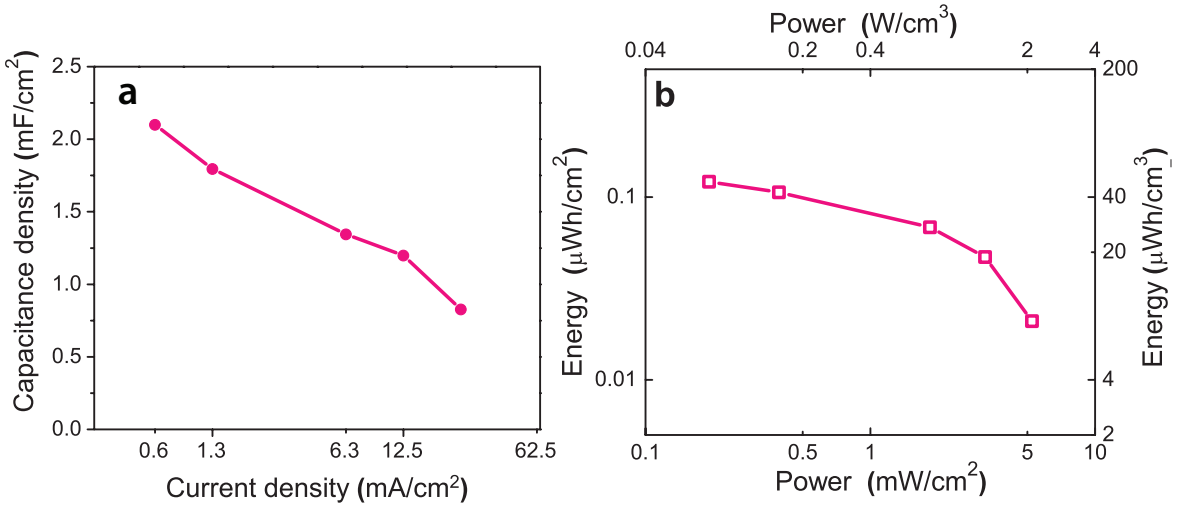

Figure S8 (a) Capacitance of melanin micro-supercapacitors (200 μg/cm^2 loading at each electrode, $NH_4CH_3COO_{(aq)}$ pH 5.5) from galvanostatic discharges at 0.625, 1.25, 6.25, 12.50 and 25 mA/cm^2. Cut off voltages of 0 V to 0.75 V. (b) Ragone plot extracted from the galvanostatic discharge cycles at the above mentioned current densities taking into account that the total area of the two electrodes is 0.16 cm^2 and the corresponding total volume is about 2×10^{-4} cm^3.

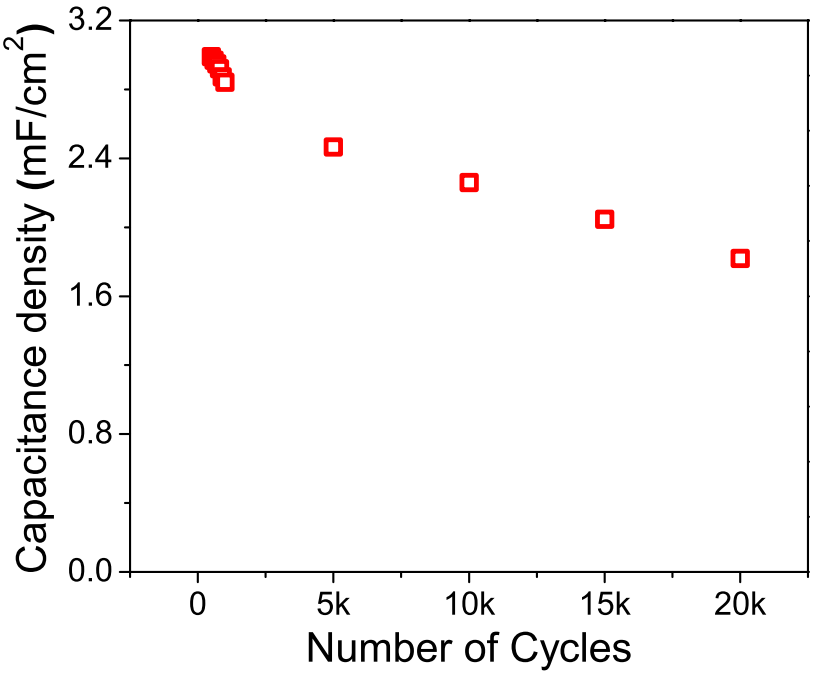

Figure S9 Trend of the capacitance density of the melanin micro-supercapacitors (200 μg/cm^2 loading at each electrode, $NH_4CH_3COO_{(aq)}$ pH 5.5 electrolyte) during the first 20,000 galvanostatic charge–discharge cycles at 1.25 mA/cm^2. Cut off voltages: 0 V to 0.75 V; area of each electrode: 0.08 cm^2. We observed 61% retention in the capacitance from the 500th cycle to the 20,000th cycle.

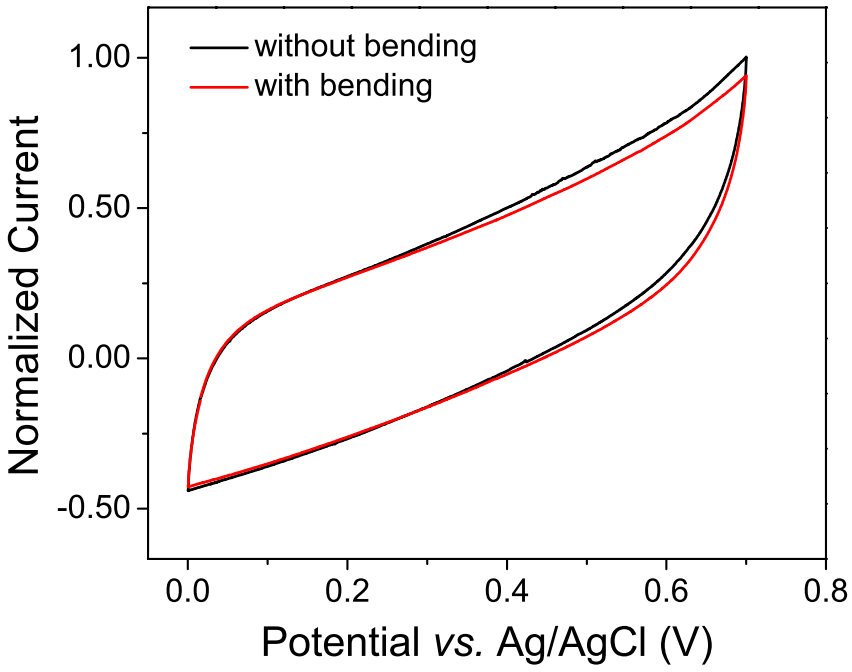

Figure S10 Cyclic voltammograms of flexible melanin micro-supercapacitors in $NH_4CH_3COO_{(aq)}$ pH 5.5, at a scan rate of 50 mV/s, without bending (black curve) and with 50% bending (red curve). The voltammograms indicate that the micro-supercapacitor is significantly stable at least up to 50% bending (as defined in the figure caption of Scheme S2).

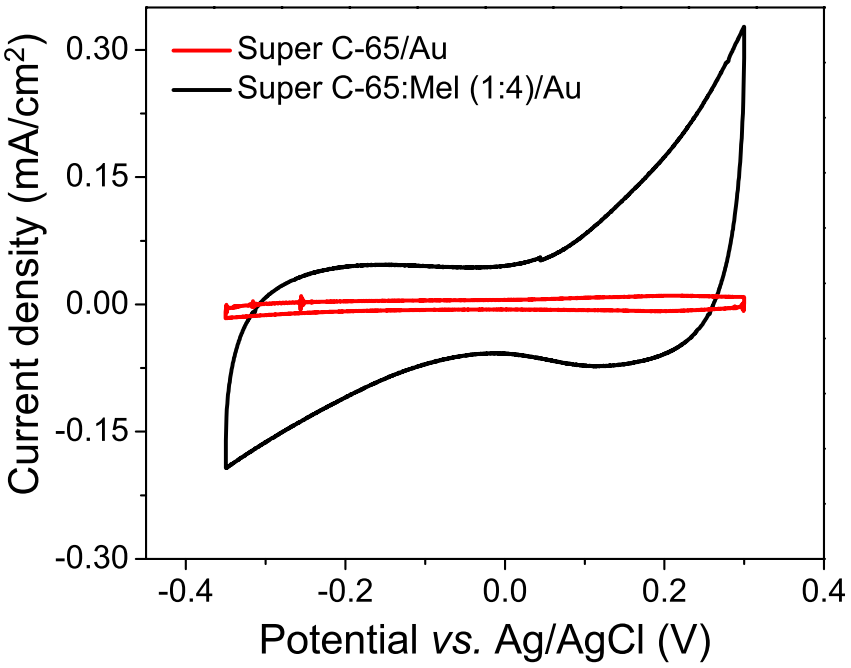

Figure S11 Cyclic voltammograms of carbon Super C-65 and melanin/ Super C-65 (4/1 weight ratio) electrodes in $NH_4CH_3COO_{(aq)}$ pH 5.5, at a scan rate of 50 mV/s. Pt foil and $Ag/AgCl_{(aq)}$ were used as counter and reference electrodes. The voltammograms show the higher capacitance of melanin/ Super C-65 compared to carbon Super C-65.

Table S1 Electrode materials derived from natural sources for supercapacitors (please refer to references cited right below this Table).

Electrode material	Surface area (m^2/g)	Highest Processing Temperature (˚C)	Electrolyte	Electrode capacitance (F/g)	Stability (Capacitance retention over cycling)	Ref
PEDOT/Lignin	NA	RT	0.1 M $HClO_4$/ acetonitrile	170 (GCD) [a]	83% after 1000 cycles	7
Ppy/Lignin-sulfonate	NA	RT	0.1 $HClO_4$	1000 (GCD)	NA	8
Ppy/Lignosulfo-nate, anthra-quinone sulfonate	NA	RT (electro-polymerization)	0.1 M $HClO_4$	250-500 (GCD)	88-98% after 200 cycles	9
Carbon derived from cellulose, potato starch, eucalyptus wood saw starch	2100 - 2900	Hydrothermal carbonization at 250-300 and activation 700-800	1 M $TEABF_4$ in acetonitrile	236 (CV) [b]	NA	10
Lignin confined	NA	RT	0.1 M $HClO_4$	432 (CV) 203 (GCD)	96% after 3000 cycles	11

on reduced graphene oxide						
Carbon-derived from cellulose	346	1000	5 M KCl	89 (CV) 107 (GCD)	90% after 2000 cycles	12
Porous carbon foams (from banana peel)	1650	1000	6 M KOH	206 (GCD)	98% after 1000 cycles	13
Biochar derived from corn cob (wrapped in a Au wire)	543.7	900	0.5M H_2SO_4	221 (GCD)	97% after 5000 cycles	14
CNTs/DNA hydrogel/ PANI	NA	RT	1M Na_2SO_4, 1M H_2SO_4	146[c] (CGD)	90% after 1000 cycles	15
Carbon derived from chicken feathers	1839	800	1M H_2SO_4	302 (GCD)	84% after 5000 cycles	16

Carbon derived from dead neem and Ashoka leaves	1230	1000	1 M H_2SO_4	400 (GCD)	NA	17
Carbon derived from chitosan	2200	800	0.5 M K_2SO_4	231 (GCD)	99% after 3000 cycles	18
Carbon derived from bacterial cellulose (BC)	491	900	BC–H_3PO_4, PVA–H_3PO_4 gel	241 (GCD)	93% after 10000 cycles	19
Carbon from spruce and corn cob hydrolyzed, PTFE and acetylene black	2300	Hydrothermal carbonization at 250-300 activation at 700	0.5 M H_2SO_4	291 (CV)	NA	20
Carbon from sodium alginate, PVDF	273	600	1 M H_2SO_4	198 (CV)	85% after 10000 cycles	21

Carbon from Lessonia Nigrescens seaweed	800	600 -900	1 M H_2SO_4	264 (GCD)	capacitance loss 11% after 10000 cycles	22
Carbon from horseweed	1500	1050	6 M KOH	184 (GCD)	97.6 % after 1000 cycles	23
Carbon from gelatin	440	700	6 M KOH	220 (GCD)	NA	24
Carbon microtubes from willow catkins	1000	700	6 M KOH	306 (GCD)	NA	25
Carbon from rice husks	1886	850	3 M KCl	210 (GCD)	NA	26
Carbon from firewood	1100	900	0.5 M H_2SO_4	140 (CV)	NA	27
Carbon from pistachio shells	1100	780	0.5 M H_2SO_4	120 (CV)	NA	28
Carbon from firewood	1064	780	0.5 M H_2SO_4	180 (CV)	NA	28
Carbon from	1100	800	1 M Na_2SO_4	75 (GCD)	95% after 500 cycles	29

banana fibers						
Carbon from waste coffee beans	1000	900	1 M H_2SO_4	368 (GCD)	95% after 10000 cycles	30
Carbon from sugar cane bagasse	1800	900	1 M H_2SO_4	300 (GCD)	77-83% after 5000 cycles	31
Carbon from cassava peel waste	1350	800	0.5 M H_2SO_4	264 (GCD)	NA	32
Carbon from sunflower seed shell	2500	900	30 wt% KOH	311 (GCD)	NA	33
Carbon from argan seed shell	2100	800	0.5 M H_2SO_4	358 (CV)	NA	34
Carbon from sucrose	2340	1200	1 M H_2SO_4	280 (GCD)	100% after 10000 cycles	35
Melanin	NA	RT	7.5 M NH_4CH_3COO pH 5.5	167 (CV)	75% after 1000 cycles (GCD)	This study

[a] GCD, Galvanostatic charge discharge. [b] CV, Cyclic Voltammetry. The two acronyms indicate the techniques used to deduce the electrode capacitance. [c] The capacitance value is for the

supercapacitor and not the electrode.

Table S1 includes a number of reports on supercapacitors making use of electrodes obtained from natural materials. It is clear from Table S1 that, quite often, the natural materials are pyrolyzed or are mixed to conducting polymers to obtain the "real" electrode material. The natural materials, the surface area of the electrode material (when available), the highest processing temperature, the electrolyte where the supercapacitor behavior was characterized and the value of the electrode capacitance (obtained by cyclic voltammetry, CV, or galvanostatic charge discharge, GCD) are reported.

Table S1 shows that natural materials have already been used for the fabrication of supercapacitor electrodes. *Nevertheless, unlike these natural materials, our melanin can be simply deposited by solution processing at room temperature and does not require any thermal treatment or further mixing*. Consequently, our melanin exhibits a great advantage over natural materials investigated to date. All in all, the biocompatibility and biodegradability featured by melanin, together with its easy availability, make it an extremely attractive material for environmentally and human friendly energy storage solutions. The main novelty of our work is the discovery of a new *natural* material for supercapacitor electrodes, besides well-established materials, such as activated carbons, carbon nanotubes, graphene, metal oxides and conducting polymers.

7. F. N. Ajjan, N. Casado, T. Rebis, A. Elfwing, N. Solin, D. Mecerreyes and O. Inganäs, *J. Mater. Chem. A*, 2016, 4, 1838–1847.

8. G. Milczarek and O. Inganas, *Science,* 2012, 335, 1468-1471

9. D. H. Nagaraju, T. Rebis, R. Gabrielsson, A. Elfwing, G. Milczarek and O. Inganäs, *Adv. Energy Mater.,* 2014, 4, 1300443(1-7).

10. L. Wei, M. Sevilla, A. B. Fuertes, R. Mokaya and G. Yushin, *Adv. Energy Mater.* 2011, 1, 356–361.

11. S-K. Kim, Y. K. Kim, H. Lee, S.B. Lee and H.S Park, *ChemSusChem* 2014, 7, 1094 – 1101.

12. L. Jiang, G.W. Nelson, S.O. Han, H. Kim, I.N. Sim and J.S. Foord, *Electrochim. Acta,* 2016, 192, 251–258.

13. Y. Lva, L. Ga, M. Liu, W. Xiong, Z. Xu, D. Zhu and D.S. Wright, *J. Power Sources* 2012, 209, 152– 157.

14. M. Genovese, J. Jiang, K. Lian and N. Holm, *J. Mater. Chem*. A, 2015, 3, 2903–2913.

15. J. Hur, K. Im, S. W. Kim, U. J. Kim, J. Lee, S. Hwang, J. Song, S. Kim, S. Hwang and N. Park, *J. Mater. Chem. A*, 2013, 1, 14460–14466.

16. Q. Wang, Q. Cao, X. Wang, B. Jing, H. Kuang and L. Zhou, *J. Power Sources*, 2013, 225, 101-107.

17. M. Biswal, A. Banerjee, M. Deo and S. Ogale, *Energy Environ. Sci.,* 2013, 6, 1249–1259.

18. L. Zhu, F. Shen, R. L. Smith, Jr. and X. Qi, *Energy Technol*. 2016, 4, 1 – 10.

19. X. Wang, D. Kong, Y. Zhang, B. Wang, X. Li, T. Qiu, Q. Song, J. Ning, Y. Song and L. Zhi, *Nanoscale*, 2016, 8, 9146–9150.

20. C. Falco, J. M. Sieben, N. Brun, M. Sevilla, T. Mauelen, E. Morallon, D.Cazorla-Amoros and M-M. Titirici, *ChemSusChem* 2013, 6, 374 – 382.

21. E. Raymundo-Piñero, F. Leroux and F. Béguin, *Adv. Mater.* 2006, 18, 1877–1882.

22. E. Raymundo-Piñero, M. Cadek and F. Béguin, *Adv. Funct. Mater*. 2009, 19, 1032–1039.

23. L. Yuan, C. Feng, C. Wang, Z. Fu, X. Yang and Y. Tang, *J. Mater. Sci*., 2016, 51, 3880–3887.

24. B. Xu, S. Hou, F. Zhang, G. Cao, M. Chu and Y. Yang, *J. Electroanal. Chem.* 2014, 712, 146–150.

25. K. Wang, R. Yan, N. Zhao, X.Tian, X. Li, S. Lei, Y. Song, Q. Guo and L. Liu, *Mater. Lett*, 2016, 174, 249–252.

26. Y. Guo, J. Qi, Y. Jiang, S. Yang, Z. Wang and H. Xu, Mater. Chem. Phys., 2003, 80, 704-709.

27. F. Wu, R. Tseng, C. Hu and C. Wang, J. Power Sources, 2004, 138, 351-359.

28. F. Wu, R. Tseng, C. Hu and C. Wang, J. Power Sources, 2005, 144, 302-309.

29. V. Subramanian, C. Luo, A. M. Stephan, K. S. Nahm, S. Thomas and B. Wei, J. Phys. Chem. C, 2007, 111, 7527-7531.

30. T. E. Rufford, D. Hulicova-Jurcakova, Z. Zhu and G. Q. Lu, Electrochem. Commun., 2008,

10, 1594-1597.

31. T. E. Rufford, D. Hulicova-Jurcakova, K. Khosla, Z. Zhu and G. Q. Lu, J. Power Sources, 2010, 195, 912-918.

32. A. E. Ismanto, S. Wang, F. E. Soetaredjo and S. Ismadji, Bioresour. Technol., 2010, 101, 3534-3540.

33. X. Li, W. Xing, S. Zhuo, J. Zhou, F. Li, S. Qiao and G. Lu, Bioresour. Technol., 2011, 102, 1118-1123.

34. Elmouwahidi, Z. Zapata-Benabithe, F. Carrasco-Marin and C. Moreno-Castilla, Bioresour. Technol., 2012, 111, 185-190.

35. C. Wang, M. J. O. Connell, C. K. Chan, ACS Appl. Mater. Interfaces 2015, 7, 8952 –8960.

Table S2 Identification of chemical bonding from high resolution XPS scans in melanin-based electrodes after charging and discharging steps, in micro-supercapacitor configuration.

	BE (eV)	Identification	Atomic %			
			Charging		Discharging	
			Total over 100%	Each element	Total over 100%	Each element
Au(4f7/2)	84.1 84.2	Au^0	0.2	100.0	0.2	100.0
C(1s)	284.6	C=C and C-C	34.4	54.8	42.2	66.5
	285.4	C-N	6.0	9.6	4.5	7.1
	286.2	C-O	10.8	17.2	8.3	13.1
	287.4	C=O	5.2	8.3	3.2	5.1
	288.9	O-C=O	5.4	8.7	4.9	7.6
	291.3	$\pi \rightarrow \pi^*$ of C=C	0.8	1.3	0.4	0.6
N(1s)	399.5	Amine N-H	1.1	27.7	0.9	32.1
	400.4	Aromatic C-N	2.1	54.8	1.6	53.6
	402.0	$C\text{-}N^+$ and/or N^+	0.7	17.5	0.4	14.4
O(1s)	531.7	C=O (aromatic)	10.6	32.0	8.5	25.4
	532.5	C-O (aliphatic), C=O (aliphatic), Si-O, O**-C=O	16.4	49.3	19.3	57.7
	533.5	(aliphatic and aromatic), C-O aromatic	6.2	18.7	5.6	16.9

**indicates that the identification pertains to this atom

Samples were prepared by initially drop casting a mixture of conductive carbon Super C-65 with a melanin suspension in DMSO, with a weight ratio 1/4. The electrode area was 0.08 cm^2. We prepared two types of samples, i.e. after charging and discharging steps carried out galvanostatically in the electrolyte $NH_4CH_3COO_{(aq)}$ pH 5.5. To prepare the samples after charging, a micro-supercapacitor pre-oxidized by cyclic voltammetry was galvanostatically charged at 0.25 mA/cm^2 for 15 minutes. To prepare the samples after discharging, a micro-

supercapacitor pre-oxidized by cyclic voltammetry was galvanostatically charged at 0.25 mA/cm^2 for 15 minutes, followed by galvanostatic discharge at -0.25 mA/cm^2 for 15 minutes. Samples were rinsed gently in water and placed under vacuum (at 30 mbar) for 1 hr prior to the XPS analysis.

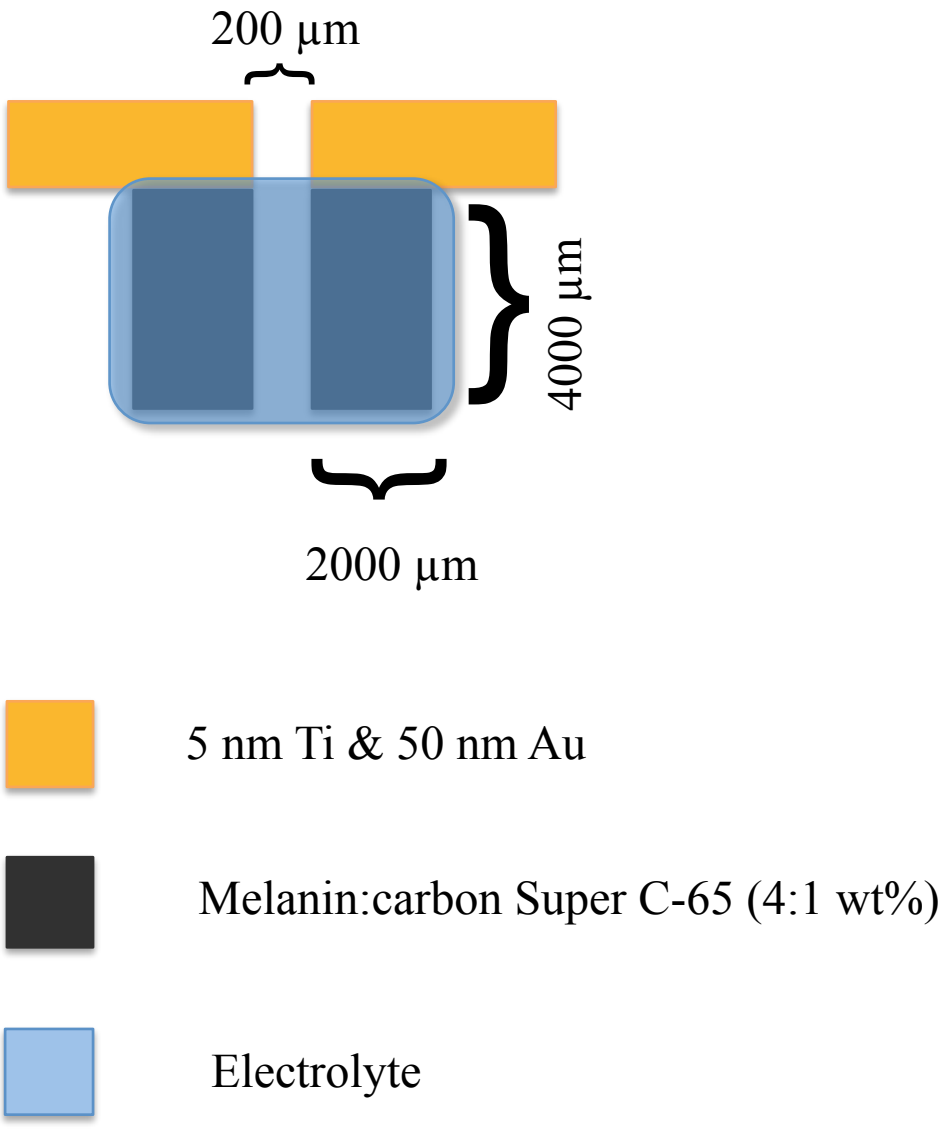

Scheme S1 Micro-supercapacitor geometry.

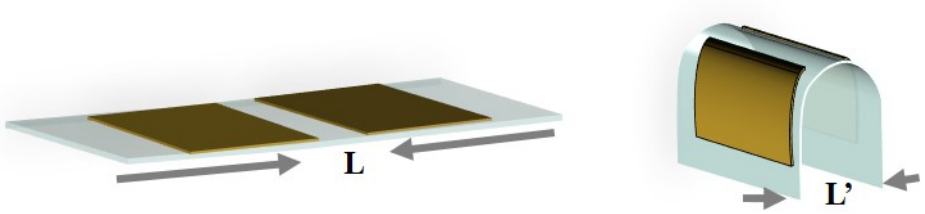

Scheme S2 Micro-supercapacitor bending. The bending percentage is defined as [(L-L')/L]×100%.

L and L' are the initial length and the length under bending, respectively.

APPENDIX B – LIST OF PUBLICATIONS IN POLYTECHNIQUE MONTREAL NOT INCLUDED IN THE THESIS

Articles

1. H. Tang,* P. Kumar,* S. Zhang,* Z. Yi, G. D. Crescenzo, C. Santato*, et al.*, "Conducting polymer transistors making use of activated carbon gate electrodes," *ACS Applied Materials & Interfaces,* 7, 969-73, 2015.

2. L. G. S. Albano,* E. Di Mauro,* P. Kumar,* F. Cicoira, C. F. O. Graeff, and C. Santato, "Novel insights on the physicochemical properties of eumelanins and their DMSO derivatives," *Polymer International,* 65, 1315-1322, 2016.

3. J. Wünsche, Y. Deng, P. Kumar, E. Di Mauro, E. Josberger, J. Sayago*, et al.*, "Protonic and Electronic Transport in Hydrated Thin Films of the Pigment Eumelanin," *Chemistry of Materials,* 27, 436-442, 2015.

4. S. Zhang, P. Kumar, A. S. Nouas, L. Fontaine, H. Tang, and F. Cicoira, "Solvent-induced changes in PEDOT:PSS films for organic electrochemical transistors," *APL Materials,* 3, 014911, 2015.

5. Z. Yi, G. Natale, P. Kumar, E. D. Mauro, M.-C. Heuzey, F. Soavi*, et al.*, "Ionic liquid-water mixtures and ion gels as electrolytes for organic electrochemical transistors," *Journal of Materials Chemistry C,* 3, 6549-6553, 2015.

6. S. Zhang, E. Hubis, C. Girard, P. Kumar, J. DeFranco, and F. Cicoira, "Water stability and orthogonal patterning of flexible micro-electrochemical transistors on plastic," *Journal of Materials Chemistry C,* 1382-1385, 2016.

7. I. Valitova, P. Kumar, X. Meng, F. Soavi, C. Santato, and F. Cicoira, "Photolithographically Patterned TiO2 Films for Electrolyte-Gated Transistors," *ACS Applied Materials & Interfaces,* 8, 14855-62, 2016.

8. Z. Yi, L. G. Bettini, G. Tomasello, P. Kumar, P. Piseri, I. Valitova*, et al.*, "Flexible conducting polymer transistors with supercapacitor function," *Journal of Polymer Science Part B: Polymer Physics,* 2016. (in press)

* Authors are equally contributed

Book Chapter

G. Tarabella, N. Coppedè, S. Iannotta, F. Cicoira, P. Kumar, and C. Santato, "Organic bioelectronics" in *Handbook of Organic Materials for Optical and (Opto)electronic Devices*, O. Osteoverkova, ed: Woodhead Publishing, 2013, 597-617.

APPENDIX C – PARTICIPATION IN THE CONFERENCES

1. “Eumelanin for Flexible, Bio-Micro-Supercapacitors” Materials Research Society (MRS) Fall Meeting and Exhibit, 2015, Boston (2015), Oral presentation.

2. “Eumelanin-based Supercapacitors” Materials Research Society (MRS) Fall Meeting and Exhibit, 2015, Boston (2016), Oral presentation.

3. “Processing of PEDOT:PSS films and devices for organic bioelectronics” International Material Research Congress (IMRC), Cancun, Mexico (2015), Oral presentation.

4. “Exploring the functional properties of the pigment eumelanin” International Material Research Congress (IMRC), Cancun, Mexico (2015), Oral presentation.